UNIVERSITI TEKNOLOGI MARA

PHOTODEGRADATION OF TETRACYCLINE ANTIBIOTICS (TC) WITH TUNGSTEN DISULPHIDE-GRAPHENE OXIDE BY LIGHT EMITTING DIODE (LED)

ZULHATIQAH BINTI ZOLEKAFELI

MSc

June 2026

UNIVERSITI TEKNOLOGI MARA

PHOTODEGRADATION OF TETRACYCLINE ANTIBIOTICS (TC) WITH TUNGSTEN DISULPHIDE-GRAPHENE OXIDE BY LIGHT EMITTING DIODE (LED)

ZULHATIQAH BINTI ZOLEKAFELI

Thesis submitted in fulfilment
of the requirements for the degree of
Master of Applied Science
(Chemistry)

Faculty of Applied Science

June 2026

CONFIRMATION BY PANEL OF EXAMINERS

I certify that a Panel of Examiners has met on 22 January 2026 to conduct the final examination of Zulhatiqah Binti Zolekafeli on her Masters of Science thesis entitled "Photodegradation of Tetracycline Antibiotics (TC) with Tungsten Disulphide-Graphene Oxide by Light Emitting Diode (LED)" in accordance with Universiti Teknologi MARA Act 1976 (Akta 173). The Panel of Examiners recommends that the student be awarded the relevant degree. The Panel of Examiners was as follows:

Norizan Ahmat @ Abdul Hamid, PhD
Professor
Faculty of Applied Sciences
Universiti Teknologi MARA
(Chairman)

Nur Hazirah Rozali Annuar, PhD
Senior Lecturer
Faculty of Applied Sciences
Universiti Teknologi MARA
(Internal Examiner)

Saliza Asman, PhD
Senior Lecturer
Faculty of Applied Sciences Technology
Universiti Tun Hussein Onn
(External Examiner)

PROFESSOR DR HJH ZURAEDA IBRAHIM
Dean
Institute of Postgraduates Studies
Universiti Teknologi MARA
Date: 16 June 2026

AUTHOR'S DECLARATION

I declare that the work in this thesis was carried out in accordance with the regulations of Universiti Teknologi MARA. It is original and is the results of my own work, unless otherwise indicated or acknowledged as referenced work. This thesis has not been submitted to any other academic institution or non-academic institution for any degree or qualification.

I, hereby, acknowledge that I have been supplied with the Academic Rules and Regulations for Postgraduate, Universiti Teknologi MARA, regulating the conduct of my study and research.

Name of Student	:	Zulhatiqah binti Zolekafeli
Student ID. No.	:	2022674844
Programme	:	Master of Applied Science (Chemistry) – AS756
Faculty	:	Applied Sciences
Thesis Title	:	Photodegradation of Tetracycline Antibiotics (TC) with Tungsten Disulphide-Graphene Oxide by Light Emitting Diode (LED)
Signature of Student	:	……
Date	:	June 2026

ABSTRACT

The adding presence of antibiotic remainders, particularly tetracycline (TC), in water environment poses significant environmental and public health threat. Hence, this study aimed to explores the conflation, characterization, and photocatalytic performance of a tungsten disulfide/graphene oxide (WS_2/GO) nanocomposite for the degradation of TC under light-emitting diode (LED) irradiation due to a good visible-light photocatalytic properties by WS_2 and excellent in electron transport ability by GO. GO was synthesized using a modified hummers' method, while WS_2 was set via a hydrothermal approach with ratio of 1%, 5%, and 15% of WS_2, these composites were comprehensively characterized through Fourier Transform Infrared Spectroscopy (FTIR), X-ray Diffraction (XRD), Brunauer-Emmett-Teller (BET), Field Emission Scanning Electron Microscopy (FESEM), UV-Visible Spectroscopy (UV-Vis), and Photoluminescence (PL) spectroscopy, to interpret the physicochemical properties of the composites.

FTIR and XRD analyses verified the successful integration of WS_2 with GO, with substantiation of reduced WS_2 crystallite size upon GO objectification. FESEM images revealed that WS_2 nanosheets were slightly distributed across the wrinkled GO wastes, indicating strong interfacial contact. BET results demonstrated a mesoporous structure with a severance size of 5.6977 nm. UV-Vis spectroscopy indicated a reduction in the optic band gap to 3.19 eV, signifying bettered visible light immersion. Likewise, PL analysis supported enhanced charge carrier separation within the compound. Among the tested samples, the WS_2/GO-15 compound displayed the highest photocatalytic degradation, removing 95.67% of TC under LED irradiation. Response Surface Methodology (RSM) is an optimization linked original photocatalyst attention as the most influential factor in achieving advanced degradation effectiveness. pH also played a pivotal part, with pH 5 yielding the maximum declination of 95.7%, suggesting that acidic conditions favour TC photodegradation. Real sample analysis revealed that saltwater samples achieved the highest degradation of TC, indicating the synergistic goods of pH and ionic strength. Next, scavenger study indicated that $K_2Cr_2O_7$ (superoxide radicals ($O_2^{\bullet-}$)), significantly enhanced the degradation of TC, emphasizing the critical part of photogenerated electrons and reactive oxygen species (ROS) in the degradation of TC. Moreover, the kinetic studies using the Langmuir-Hinshelwood (L-H) model demonstrated that the photodegradation followed the first-order kinetics under all light sources. The LED source handed the stylish fit ($R^2 = 0.986$), the highest rate constant ($k = 0.4658\ min^{-1}$), and the shortest half-life (1.4878 min), emphasizing its superior performance. In terms of stability, the compound able to recycle up to six cycles with degradation percentage at retained substantial photocatalytic exertion over six cycles with 75.34%.

Overall, WS_2/GO-15 showed as a promising visible-light-driven photocatalyst, by offering enhanced photocatalytic degradation, bettered optic parcels, and structural stability, which therefore holding strong eventuality for operation in wastewater treatment technologies.

ACKNOWLEDGEMENT

Upon completion of this project, I would like to praise to the Almighty Allah S.W.T for His blessing and guidance, I was able to complete this thesis.

Next, I would like to express my deepest gratitude to my supervisor Dr Siti Nor Atika Baharin for her patience, continues guidance, dedication, and encouragement, throughout the journey of completing my Master journey. Her insightful feedback, patience, efforts, and time spent helped me to explore new things from different point of view and brought my work to a higher level. Also, I wish to show my gratitude my co-supervisors Associate Professor Dr Kavirajaa Pandian Sambasevam and Associate Professor Dr Ali H. Jawad that together helping me in to discover new insight and seek solution with different angel of solutions. Furthermore, I would like to show my gratitude to our Head of Postgraduate School, Dr. Nur Rahimah Said for all the hard work spent to prepare and guide us, arranging programs to increase our knowledge regarding the project and exposing us to new experiences.

A special thanks to my father, Zolekafeli Abd Ghani, my mother, , my family members Zulhaqqim, Zulhanis, Zulhazuwanah, Zulhaleeshah, Siti Syarah Danian, Muhammad 'Izzat Azfar Muhd Tajudin and my best friend Nur Fateha Kamaruddin for all their prayers, supports, and love upon to complete this thesis. Thank you for always be by my side and always pushed me to be better each and everytime.

Finally, I want to thank to all postgraduate members at Universiti Teknologi Mara Kampus Kuala Pilah who offered guidance and support throughout these wonderful years of studies.

TABLE OF CONTENTS

LIST OF TABLES

LIST OF FIGURES

LIST OF SYMBOLS

Symbols

A	Constant in Tauc Equation
α	Absorption Coefficient
$(\alpha h\nu)^2$	Tauc Plot Expression for Direct Bandgap
C_o	Initial Concentration of Tetracycline
C_t	Concentration of Tetracycline at Time *t*
Eg	Optical Band Gap Energy
h	Planck's Constant
hν	Photon Energy
k	Apparent Rate Constant
n	Power Factor in Tauc Plot (n = 2 for Direct Bandgap)
η	Photodegradation Efficiency
R^2	Regression Coefficient
t	Reaction Time
ν (nu)	Frequency of Incident Light
λ	Wavelength of Incident Light

LIST OF ABBREVIATIONS

Abbreviations

BET	Brunauer–Emmett–Teller (Surface Area Analysis)
˚C	Degree Celsius
Eg	Band Gap Energy
eV	Electron Volt
FESEM	Field Emission Scanning Electron Microscopy
FTIR	Fourier Transform Infrared Spectroscopy
GO	Graphene Oxide
LED	Light Emitting Diode
mg/L	Milligrams per Litre
m^2/g	Square Metres per Gram
min	Minute
nm	Nanometre
PL	Photoluminescence
rpm	Revolutions Per Minute
TC	Tetracycline
TMDs	Transition Metal Dichalcogenides
WS_2	Tungsten Disulfide
WS_2/GO	Tungsten Disulfide–Graphene Oxide Composite
UV-Vis	Ultraviolet–Visible Spectroscopy

XRD	X-ray Diffraction

CHAPTER 1
INTRODUCTION

1.1 Research Background

The contamination of water bodies by pharmaceutical residues, particularly antibiotics, has become a significant environmental concern. Tetracycline (TC), a broad-spectrum antibiotic commonly used in both human and veterinary medicine, is one of the most persistent pharmaceutical pollutants. Its incomplete metabolism in the body, improper disposal, and agricultural runoff contribute to its widespread occurrence in natural water systems. The presence of such antibiotics not only poses ecological risks but also contributes to the development of antibiotic-resistant bacteria, which is a growing global health challenge.

To address this issue, advanced oxidation processes (AOPs), particularly photocatalysis, have emerged as promising methods for the degradation of recalcitrant organic pollutants like TC. Among various photocatalysts, tungsten disulfide (WS_2), combined with graphene oxide (GO), has garnered attention due to its unique physicochemical properties and superior performance under visible light irradiation.

Tungsten disulfide (WS_2) is a two-dimensional (2D) transition metal dichalcogenide (TMD) that has attracted significant interest in photocatalytic applications due to its distinct structural and electronic properties. WS_2 possesses a layered structure like graphene, with weak van der Waals forces between the layers, which allows for exfoliation into monolayers. This characteristic enhances its surface area, providing abundant active sites for catalytic reactions. Additionally, WS_2 has a relatively narrow bandgap (1.3-1.6 eV) (C. Li *et al.,* 2024), making it effective in absorbing visible light, a desirable feature for energy-efficient photocatalytic applications.

However, the photocatalytic efficiency of WS_2 can be limited by the rapid recombination of photogenerated electron-hole pairs. To overcome this challenge, it is often combined with other materials, such as graphene oxide, to improve its charge separation efficiency and enhance overall photocatalytic performance.

Graphene oxide (GO) is a derivative of graphene, functionalized with oxygen-containing groups such as hydroxyl, carboxyl, and epoxide groups. These groups render

GO hydrophilic, allowing for better dispersion in aqueous media, which is essential for environmental applications like water purification. GO also exhibits excellent electron mobility, large surface area, and strong adsorption capabilities, making it an ideal material for coupling with semiconductors like WS_2.

The combination of WS_2 and GO creates a heterostructure that facilitates efficient separation of photogenerated electron-hole pairs, thereby minimizing recombination losses. This synergistic effect enhances the photocatalytic degradation of organic pollutants like TC under visible light irradiation. Furthermore, GO can serve as an adsorbent, concentrating TC molecules on its surface, making them more accessible for photodegradation. Traditional photocatalysis has relied on ultraviolet (UV) light sources due to the wide bandgap of many semiconductor photocatalysts. However, UV light represents only a small fraction of the solar spectrum, making such systems inefficient in utilizing natural sunlight. In contrast, visible light accounts for nearly half of the solar spectrum, making it a more sustainable and cost-effective energy source for photocatalytic applications.

Light Emitting Diode (LED) irradiation has emerged as an efficient alternative light source in photocatalytic processes due to its high energy efficiency, tunable wavelength, and long operational life. LEDs can be tailored to emit light in the visible range, aligning with the bandgap of WS_2, thus maximizing its photocatalytic efficiency under visible light conditions. Moreover, LED-based systems are environmentally friendly and scalable, making them suitable for large-scale water treatment applications.

The photodegradation of TC using a WS_2/GO composite under LED irradiation presents a promising approach to address the environmental challenges posed by antibiotic contamination. The synergy between WS_2 and GO, combined with the energy-efficient visible light provided by LEDs, creates a highly effective system for degrading TC. Under LED light, the photogenerated electrons in WS_2 are transferred to GO, preventing electron-hole recombination and allowing the formation of reactive oxygen species (ROS) such as hydroxyl radicals ($^{\bullet}OH$) and superoxide anions ($O_2^{\bullet-}$). These ROS are highly reactive and can break down complex TC molecules into simpler, less harmful by-products.

Preliminary studies have demonstrated that WS_2/GO composites exhibit enhanced photocatalytic activity compared to pure WS_2 or GO alone, particularly in the degradation of organic pollutants under visible light. The development of this composite material under LED irradiation offers a novel and energy-efficient solution for tackling

antibiotic pollution in water systems. The rising concerns about pharmaceutical pollutants in water systems necessitate the development of innovative and sustainable remediation technologies. Photocatalysis using WS_2/GO composites under LED irradiation represents a cutting-edge approach to degrade TC antibiotics, leveraging the unique properties of WS_2, the electron mobility of GO, and the energy efficiency of LEDs. This study contributes to the growing body of research aimed at developing advanced materials and processes for environmental remediation, with potential applications in large-scale water purification systems.

A good charge carrier for semiconductors may be found in the molecularly thick, 2D nanomaterials known as graphene, which are composed of sp2 carbon atoms arranged in a honeycomb structure (Ding *et al.,* 2015). WS_2 nanocomposites were synthesized in this work using GO as a precursor. Graphene has been employed as a remarkable electron-acceptor or transport material in photocatalysis because of its capacity to lower photogenerated electron-hole recombination and increase light adsorption (Li *et al.,* 2014). Graphene has also been demonstrated to be an excellent co-catalyst for photocatalytic activity due to its huge specific surface area and efficient electron transport characteristics (K. Chang *et al.,* 2014). Therefore, in this study, WS_2/GO will be utilised as a material photocatalyst to degrade TC under LED irradiation.

1.2 Problem Statements

The contamination of water bodies by pharmaceutical compounds, particularly antibiotics like TC, has become a pressing environmental issue. A recent study by Thiang *et al.* (2022) stated that the highest concentration of TC detected from marine aquacultural farms in Peninsular Malaysia is 25.6 ng/L. TC is a commonly used antibiotic in human and veterinary medicine, but its persistence in aquatic environments poses significant risks, including the development of antibiotic-resistant bacteria and adverse effects on aquatic ecosystems. Conventional water treatment methods such as activated sludge and sedimentation are often ineffective in fully degrading such contaminants because it is often relies on biodegradation which is slow and limited for TC that is high biotoxicity and stability, and cannot degrade the dissolves antibiotics that binds to suspended solids, highlighting the need for advanced techniques to address the presence of TC in wastewater.

Photocatalysis offers a promising solution for the degradation of persistent organic pollutants like TC, but most traditional photocatalysts, such as titanium dioxide (TiO_2), are limited by their reliance on UV light, which represents a small portion of the solar spectrum. This limitation necessitates the development of visible-light-driven photocatalysts that can efficiently harness natural sunlight for environmental applications. WS_2 has emerged as a potential candidate due to its ability to absorb visible light; however, it suffers from the rapid recombination of photogenerated electron-hole pairs, reducing its overall photocatalytic efficiency.

To overcome these challenges, combining WS_2 with GO offers a strategy to enhance photocatalytic performance. GO's excellent electron mobility and large surface area can improve the charge separation efficiency in WS_2, thereby reducing electron-hole recombination and enhancing the overall degradation of TC under visible light. Despite these advantages, there is limited research exploring the use of WS_2/GO composites specifically for the degradation of TC, making it a crucial area for investigation.

Furthermore, traditional light sources used in photocatalytic systems, such as UV lamps, are energy-intensive and costly. The use of Light Emitting Diodes (LEDs), which can emit visible light efficiently, presents an energy-saving alternative. However, the application of LEDs for visible-light-driven photocatalysis, especially in conjunction with WS_2/GO composites, remains underexplored. Developing an energy-efficient photocatalytic system using LED irradiation for the degradation of TC could provide a sustainable and effective solution to this environmental problem. This research aims to address these gaps by investigating the photodegradation of TC using WS_2/GO composites under LED light, providing insights into more efficient water treatment methods.

Metal sulphides and oxides have garnered the greatest interest among all the semiconductors employed as photocatalysts. Although metal oxides have a good stability, eco-friendly and availability, it is however only responded well to UV and in certain situations of visible light (Tahir *et al.,* 2020). As an alternative, metal sulphides can be utilised as photocatalysts because they have a bandgap that is relatively less than oxides, and it is available in a wide range of useful forms and exhibit effective reactions towards large range of lights. Thus, additional metal sulphides based photocatalyst can improve and modify the lacks in the photocatalytic degradation process since the metal sulphides based such as WS_2 structures helps in improving a single photocatalyst found

it challenging to destroy the substance in the presence of visible light. Nevertheless, a single photocatalyst was difficult to degrade the TC due to rapid recombination of photogenerated electron-hole pair and tend to agglomerate between the nanosheets. Therefore, a semiconductor heterojunction is formed where WS_2 is modified by adding GO to enhance the photocatalytic activity which the incorporation of WS_2/GO can improve each element and chemical properties to degrade TC.

1.3 Significance of Study

One of the green chemical ideas is photocatalysis since it is safe, energy-efficient, and has no influence on the environment (Wang *et al.,* 2016). The use of visible light as an irradiation source is particularly appealing because it is more abundant and energy-efficient than UV light. This allows for sustainable and economical photocatalytic degradation process that are appropriate for real-world applications.

The significance of this study lies in the development of an efficient, visible-light-driven photocatalytic system that utilizes LED light, an energy-efficient and environmentally friendly alternative to traditional UV-based systems. By exploring the synergistic effects of WS_2 and graphene oxide, this research aims to enhance the photocatalytic performance of WS_2, overcoming limitations such as rapid electron-hole recombination, which commonly hampers photocatalysts. The study will contribute to a better understanding of how GO improves charge separation and electron mobility in the composite, potentially leading to improved degradation rates for TC and other organic pollutants. This work sheds fresh information on the light-photocatalyst interaction and charge transfer process in WS_2/GO composites under visible LED irradiation. The findings show that adding WS_2 to GO creates an effective heterostructure where GO serves as a transport channel and electron acceptor, hence preventing photogenerated electron-hole pairs from recombining. This work also shows that under LED irradiation, the energy supplied is enough to excite electrons in WS_2, and GO promotes rapid electron migration, which increases the production of reactive species that degrade pollutants. Furthermore, the work emphasizes that the enhanced photocatalytic activity is significantly controlled by the interfacial charge transfer dynamics between WS_2 and GO rather than being only attributable to increased surface area or light absorption. To maximize charge separation and photocatalytic efficiency,

this study extends our understanding of how visible-light-driven LED sources interact with WS_2/GO composites. This knowledge serves as a foundation for the development of more efficient photocatalysts for environmental applications.

Furthermore, this research has practical implications for water treatment technologies. The use of LED light sources (approximately 20,000 until 50,000 hours) compared with conventional UV lamps, which typically operate for 1,000 until 5,000 hours are more cost-effective and sustainable, makes the proposed system scalable for real-world applications. By optimizing the conditions for LED irradiation and WS_2/GO photocatalysis, this study can offer insights into more energy-efficient solutions for large-scale water purification. Ultimately, the outcomes of this research will advance the field of environmental remediation, providing a promising new method to combat the persistence of hazardous pharmaceutical compounds in water bodies while contributing to global efforts to reduce energy consumption in environmental technologies.

The photocatalytic investigation on the degradation of TC by WS_2/GO will also contribute to the achievement of United Nation Sustainable Development Goal SDG 6 (Clean Water and Sanitation) and SDG 7 (Affordable and Clean Energy).

1.4 Research Objectives

The study containing three objectives:

a) To synthesize and characterize tungsten disulphide (WS_2), graphene oxide (GO), and tungsten disulphide/graphene oxide (WS_2/GO) composites (1%, 5%, and 15%) physicochemical properties using Fourier Transform Infrared (FTIR), Ultraviolet-Visible (UV-Vis), Field Emission Scanning Electron Microscope (FESEM), X-ray Powder Diffraction (XRD), Raman spectroscopy, surface area analysis (BET), and Photoluminescence Spectroscopy.
b) To optimize photodegradation efficiency of the synthesize nanocomposites to the degradation of TC in an aqueous solution using Box Behnken Response Surface Methodology.
c) To investigate the performance (kinetic study), recyclability and the degradation efficiency of WS_2/GO in real samples such as sea water, lake water, tap water, and river water.

CHAPTER 2
LITERATURE REVIEW

2.1 Photocatalysis

In photocatalysis, a photocatalyst is activated by light and changes or accelerates the kinetics of a molecule without being impacted by it (Fagan *et al.,* 2016). Recently, the redox method has drawn a lot of attention from researchers who are trying to decompose organic pollutants. The photocatalytic technology to remove the pollutants is characterised as a cheaper, convenient, and advanced oxidation process. Baryne *et al.,* 2018 said, to trigger the photocatalytic reaction, a photocatalyst, such as a semiconductor, is bombarded with photons from UV light. If the energy of these photons surpasses the band gap, this creates the electrons (e^-) on the surface of the photocatalyst to move up into the conducting band and become excited in the valence band (Lui *et al.,* 2017). After the e^- is absorbed into the conduction band (e^-_{CB}), a positive hole develops on the valence band (h^+_{VB}) (Eq 2.1). The excited electrons will react with oxygen in the conduction band (e^-_{CB}) to create superoxide radicals (O_2) or hydroperoxide radicals (HO_2). This reaction is depicted in Equation 2.2. (Banerjee *et al.,* 2014). Equation 2.3's representation of the degradation of pollutants into water (H_2O) and carbon dioxide (CO_2) is followed using these reactive oxygen molecules to enhance the degradation of the toxic elements. A complete representation of the mechanism is shown in Figure 2.1.

$$TiO_2 + hv \rightarrow h^+_{VB} + e^-_{CB} \quad (2.1)$$

$$e^-_{CB} + O_2 \rightarrow O_2^- \quad (2.2)$$

$$h^+_{VB} + H_2O \rightarrow OH + H^+ \quad (2.3)$$

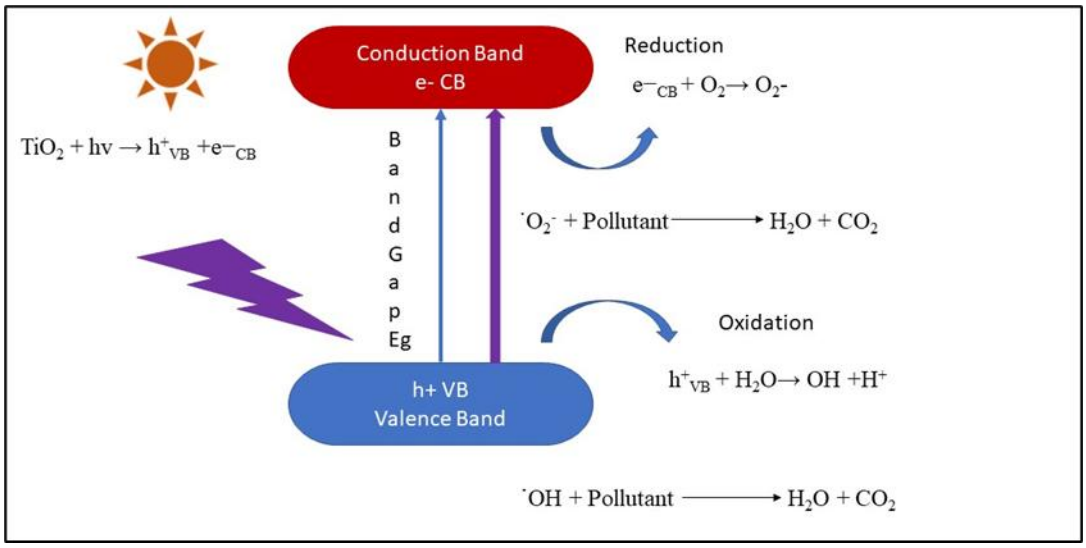

Figure 2.1 Mechanism of the Photocatalysis of Semiconductor TiO_2 (Baryne *et al.,* 2018).

It is important to emphasise certain measures in order to manage the way the photocatalysis process operates. According to the study by San Martn *et al.,* on 2020, the photocatalyzed activity must be maintained by preventing the recombination of the electron and the hole. Organic compounds that come into touch with the hole will promptly oxidise, typically to carbon dioxide, because the hole is strongly oxidising. The excited electron can then interact with photons to produce hydrogen or be foraged by the surrounding oxygen. Targeted molecules will reintegrate if their electron and hole states are not quickly recovered, preventing the desired reaction from taking place.

2.2 Photocatalyst

A material known as a photocatalyst is one that can absorb light to boost its energy level and afterwards transmit that energy to a substance that is reacting to trigger a chemical reaction (Yang & Wang, 2018). The photocatalysts might even recreate its chemical arrangement following each set of contacts (Hisatomi *et al.,* 2014). There are a variety of different types of photocatalyst, as well as those based on carbon, conductive polymers, and semiconductors (You *et al.,* 2019).

However, there are certain disadvantages to single-based photocatalysts, such as a large band gap, poorly mobile charge carriers, and easily aggregate nanosheets. Photocatalysts are used to breakdown organic pollutants by a variety of techniques, such

as doping conventional photocatalysts, making hetero-structures or compounds, and interacting with conjugated designs. Numerous studies have demonstrated that nanostructured photocatalysts (NPCs) are more energetic than bulk materials due to their higher surface area and aspect ratio. Better light absorption, efficient charge separation, and greater photostability are just a few advantages that photocatalysts may offer in general (You *et al.,* 2019).

2.2.1 Semiconductor as Photocatalyst

Recently, environmental deterioration and energy issues have captured the interest of the entire globe. Semiconductor photocatalysis has attracted a lot of interest as one of the most practical solutions for these problems since it is an environmentally friendly process for turning water into hydrogen and oxygen, which completely inactivates viruses of all varieties (Wang *et al.,* 2014). Semiconductors are being used in electrochemistry for a very long period. In electrochemistry, semiconductors use physical concepts such as charge transfer, band structure, and catalysis. Semiconductors are extensively used in a range of applications, including solar technology, photolysis of water, pollutants, and organic compounds, according to Siva Ramkumar *et al.,* (2022), Arunachalam *et al.,* (2021), and Zhang *et al.,* (2019).

The photocatalytic effectiveness of photocatalysts has been improved during the past 10 years using a variety of techniques. These techniques consist of looking for a suitable morphological design, doping, and putting them together into a semiconductor heterojunction (Wang *et al.,* 2014). Z-scheme heterojunction semiconductors are favourable because of their improved physical and chemical properties, which increase their ability to produce light and facilitate charge carriers' efficient movement, which improves photocatalytic reaction. Doping two or more semiconductors has been shown to enhance the photocatalytic efficiency of the photocatalyst, the capability of the charge carrier to dissociate during photocatalysis, and the visible light absorption (Vattikuti *et al.,* 2017). It may be found in many different forms, including oxides and sulphides in semiconductors. Semiconductors consisting of sulphides and oxides have long been employed as photocatalysts for water cure because of their suitable band gaps and characteristics (Jin *et al.,* 2015, and Vattikuti *et al.,* 2016).

2.3 Metal Sulphide

Due to their unique physical and chemical properties, metal sulphide-based photocatalysts are the subject of much investigation. Metal sulphide nanoparticles have drawn a lot of interest due to their exceptional qualities and fascinating prospects for use in electrically, optically, and optoelectronic devices. Metal sulphides are a prominent group of minerals that provide crystal chemists with a rich field of research due to their enhanced properties and cutting-edge capabilities, and well-aligned nanomaterials patterns on substrates that occur in various structural forms (Lai *et al.,* 2012). Furthermore, because metal sulphide has a lower band gap than metal oxide, it is perfectly applied to be employed as a photocatalyst (Lee and Chang, 2019). Numerous methods have been employed, including solution-phase reaction, chemical vapour deposition (CVD), high pressure autoclave methods, hydrothermal synthesis, and physical vapour deposition (PVD). Metal sulphide nanoparticles may occur when employing a high-pressure autoclave at reduced temperatures with no catalyst (Lai *et al.,* 2012). As demonstrated in Table 2.1, extensive study has been done on metal sulphides and how they may be used as photocatalysts. Material composition, morphology, and sacrificial agent selection are the main factors influencing the notable differences in hydrogen evolution activity among hybrid photocatalysts produced by hydrothermal techniques.

For instance, a study by Wang *et al.* (2016), employing lactic acid as a sacrificial agent, a MoS_2/graphene/CdS nanorod photocatalyst produced by the hydrothermal technique attained a hydrogen evolution rate of 2320 mmol h^{-1} g^{-1}. While the integration of graphene and CdS with MoS_2 improves interfacial electron transfer and inhibits recombination, the nanorod shape facilitates directed charge transport. The composite is a productive system for solar-driven hydrogen synthesis because graphene offers a high-conductivity platform for electron migration and CdS aids in the absorption of visible light.

Next, a moderate hydrogen evolution rate of 1262 mmol h^{-1} g^{-1} was also obtained by hydrothermally synthesizing CuS-TiO_2 nanocomposites and testing them under the same sacrificial circumstances (Wang *et al.,* 2013). Although TiO_2 has exceptional chemical stability, light absorption is restricted to the ultraviolet spectrum because to its large band gap. By forming a heterojunction with TiO_2 and expanding the light absorption spectrum into the visible range, CuS improves charge carrier dynamics.

However, less effective charge separation or interfacial contact might be the cause of the decreased activity when compared to the MoS_2/graphene/CdS system.

In contrast, a study by Lee and Chang (2019), a graphene/ZnS nanocomposite evaluated with a mixed sacrificial system of Na_2S, Na_2SO_3, and NaCl showed an exceptionally high photocatalytic activity of 11,600 mmol h^{-1} g^{-1}. The excellent suppression of charge recombination and the efficient electron mobility of graphene are responsible for this noticeably better performance. It is possible that the utilization of many sacrificial agents improved the reaction kinetics by preserving an ideal redox environment and encouraging ongoing hole scavenging.

These examples demonstrate how important material design is for improving photocatalytic hydrogen production, especially when mixing metal sulphides with carbon-based or metal oxide materials. Overall photocatalytic effectiveness is largely determined by factors including heterojunction formation, shape like nanorods against nanocomposites, and sacrificial agent selection. Therefore, hybrid systems based on metal sulphide remain a potential avenue for creating next generation photocatalysts.

Table 2.1
Synthesis Methods of Metal Sulphides

Photocatalyst	**Morphology**	**Synthetic Method**	**Sacrificial Agent**	**Activity (µmol h-1g-1)**	**Reference**
CuS/ZnS	Nanofiber	Solvothermal	Na_2S Na_2SO_3	1233.5	(Wang *et al.,* 2016)
MoS_2/graphene/CdS	Nanorods	Hydrothermal	Lactic acid	2320	(Liu *et al.,* 2014)
ZnS/Ag_2S	Porous Nanosheets	Thermal Decomposition	Na_2S Na_2SO_3	104.9	(Yang *et al.,* 2014)
MoS_2/CdS	Heterostructures	Precipitation	Lactic acid	-540	(Mingce *et al.,* 2008)
CuS/TiO_2	Nanocomposites	Hydrothermal	Na_2S Na_2SO_3	1262	(Wang *et al.,* 2013)
Graphene/ZnO-ZnS	Particle on sheet	Two-step heating	Glycerol	1070	(Chang *et al.,* 2018)
Graphene/ZnS	Nanocomposites	Hydrothermal	Na_2S, Na_2SO_3, NaCl	11600	(Lee and Chang, 2019)

In addition, owing to their significance in interpreting quantum size effects and applications in a range of devices, including solar panels, light-emitting diodes, detectors, thermoelectric devices, rechargeable batteries, fuel cells, and non-volatile memory devices, nanostructured metal sulphides have received a great deal of research attention. Since they typically appear in nature as crystals like heazlewoodite (Ni_3S_2), chalcocite (Cu_2S), pyrite (FeS_2), and others, metal sulphides are a significant category of minerals that provide the crystal chemist a rich subject for exploration (Hongjie Liu *et al.,* 2021). They are also a varied prospective use due to their superior qualities in luminescence and photochemistry, extremely negative reduction potential of excited electrons, and the quick creation of electron-hole pairs (Lai *et al.,* 2012). Researchers have also concentrated more on metal sulphide owing to its enticing qualities, such as excellent bandgap properties, low cost, and ability to mix p-type and n-type semiconductors to generate a heterojunction that may be employed in several applications. There are several ways to produce metal sulphide, including the hydrothermal approach, wet chemical synthesis method, solvothermal method, and the microwave aided method.

A promising method of converting solar energy into fuels is photocatalytic water splitting to produce hydrogen; however, the recombination of charge carriers arriving from random charge movement in semiconductor photocatalysts continues to be the main obstacle to improving photocatalytic quantum efficiency. The inclusion of cocatalysts to create the co-catalyst/photocatalyst interface is one efficient method for obtaining high quantum efficiency because it not only makes charge separation and transfer easier but also creates many active sites for H_2O adsorption and activation. WS_2 have received a lot of interest recently because of their superior optical characteristics, adaptable electrical structure, inexpensive price, and high aspect ratio. Furthermore, atomic-layer WS_2 has a characteristic 2D layered structure with more exposed edges and surfaces as well as highly active basal-plane sites, making it the perfect co-catalyst for creating a 2D/2D atomic-thin co-catalyst/photocatalyst shell/core system.

Furthermore, ZnS and CdS are two green metal sulphides, that were chosen as a photocatalyst for photocatalytic activity by the previous study. Munyai & Hintsho-Mbita in 2021 reviewed that the ability of these two metal sulphides to remove contaminants is why they were chosen. Table 2.2 showed the previous study of photocatalyst from the researcher to degrade the organic pollutant.

Table 2.2
Synthesized Metal Sulphide Nanostructures Using Plants Extract for Photocatalytic Activity.

Photocatalyst	**Source of light**	**Target water pollutant**	**Efficiency (%)**	**References**
Calotropis gigantean/CdS	UV irridation	Methyl Blue (MB) and Eosin Yellow (EY)	MB with 85% and EY with 91% were degraded	(Ayodhya & Veerabhadram, 2017)
Citrus limetta/ZnS	Sunlight irridation	Rhodamine Blue (RhB)	RhB with 83% were degraded	(Samanta *et al.,* 2017)
Corymbia citriodora/ZnS	UV illumination	Methyl Blue (MB)	MB with 96% were degraded	(Chen *et al.,* 2016)
Tridax procumbens/ZnS, Phyllanthusniruri, and Syzygium aromaticum	UV irridation	Methyl Blue (MB) and Methyl Orange (MO)	Methyl Blue with 81% and MO with 99% were degraded	(Sathishkumar *et al.,* 2018)

2.4 Tungsten Disulphide (WS_2)

A solid lubricant with a layered structure and a crystal structure similar to molybdenum disulphide (MoS_2) is WS_2. Additionally, it is projected to have identical properties of the composites, such as a super lubricity state or nearly no resistance. The electronic properties of transition metal dichalcogenides (TMDs), particularly WS_2, encompass charge density waves, superconductivity, and semi conductivity. Two-dimensional (2D) layered TMDs, in especially WS_2, have drawn a lot of research interest because of their peculiar physical properties and fascinating potential for a variety of applications.

As per Mutlu *et al.,* (2016), the layered semiconductor WS_2 shows adjustable electronic characteristics that make it possible to create state-of-the-art transistors, valley polarisation devices, and other optoelectronic devices. In monolayer form, it has a direct band gap of 1.94 eV, whereas in bulk form, it has an indirect band gap of 1.48 eV. According to Mutlu *et al.,* (2016) photoluminescence (PL) analysis, WS_2 exhibits a transition from an indirect band gap semiconductor in the form of bulk to a direct band gap semiconductor in monolayers that is equivalent to MoS_2 as illustrated in Figure 2.2. In monolayer WS_2, a strong and distinct PL peak at 1.94 eV was discovered indicating a change from an indirect to a direct band gap. On bulk WS_2, the PL intensity was discovered to be incredibly poor, which is compatible with an indirect band gap semiconductor. Ab-initio DFT was used to compute the electronic band structures of monolayer and bulk WS_2 to get further understanding. The calculations (Figure 2.2(c), (d)) show that monolayer WS_2 has a direct band gap of 1.90 eV and bulk WS_2 has an indirect band gap of 1.48 eV, which agrees with other research that have been published on the electronic structure of WS_2 and our PL findings on monolayer WS_2.

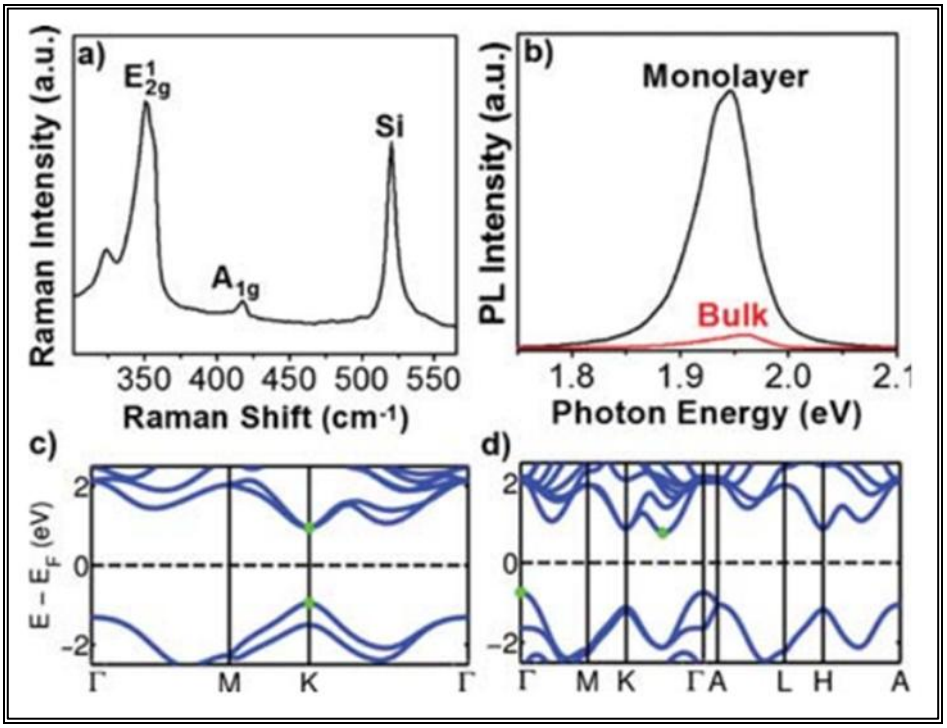

Figure 2.2 Raman of (a) Monolayer WS_2 and (b) PL (Monolayer and Bulk) Spectra WS_2. Monolayer (c) and Bulk (d) DFT-Calculated Energy Band Structures (Mutlu *et al.,* 2016).

2.4.1 Synthesis Method of WS_2

The most crucial stage in materials science and solid-state chemistry research is synthesis. The synthesis, characterisation, and assessment of the photocatalytic activity of both undoped and doped materials have been the subject of several investigations (metal or nonmetal). By using a variety of synthetic techniques, such as the sol-gel process, hydrothermal and solvothermal methods, Spray pyrolysis, flame synthesis, sonochemistry, mechanochemistry, chemical and physical vapour deposition, and photocatalytic semiconductor semiconductors can be made into powders, fibres, and films (García-López & Marcì, 2021). Figure 2.3 depicts the synthesis method for photocatalyst in schematic form.

In a prior work, Khataee *et al.,* (2018) showed that WS_2 nanosheets produced using a sonochemical approach had a high efficiency and sonocatalyst activity for the elimination of BV10 from water solution. Additionally, previous studies by Nagaraju *et al.,* 2018, have produced WS_2 utilising a simple one-step hydrothermal method and used them as electroactive materials for high-performance supercapacitors. The WS_2 electrode has an outstanding cycling stability with 77.4% retention after 3000 cycles

and a high Cs of 1439.5 F/gL at 5 mA cm^{-2}. Therefore, to produce good properties in the photocatalyst, a suitable method for its synthesis is required.

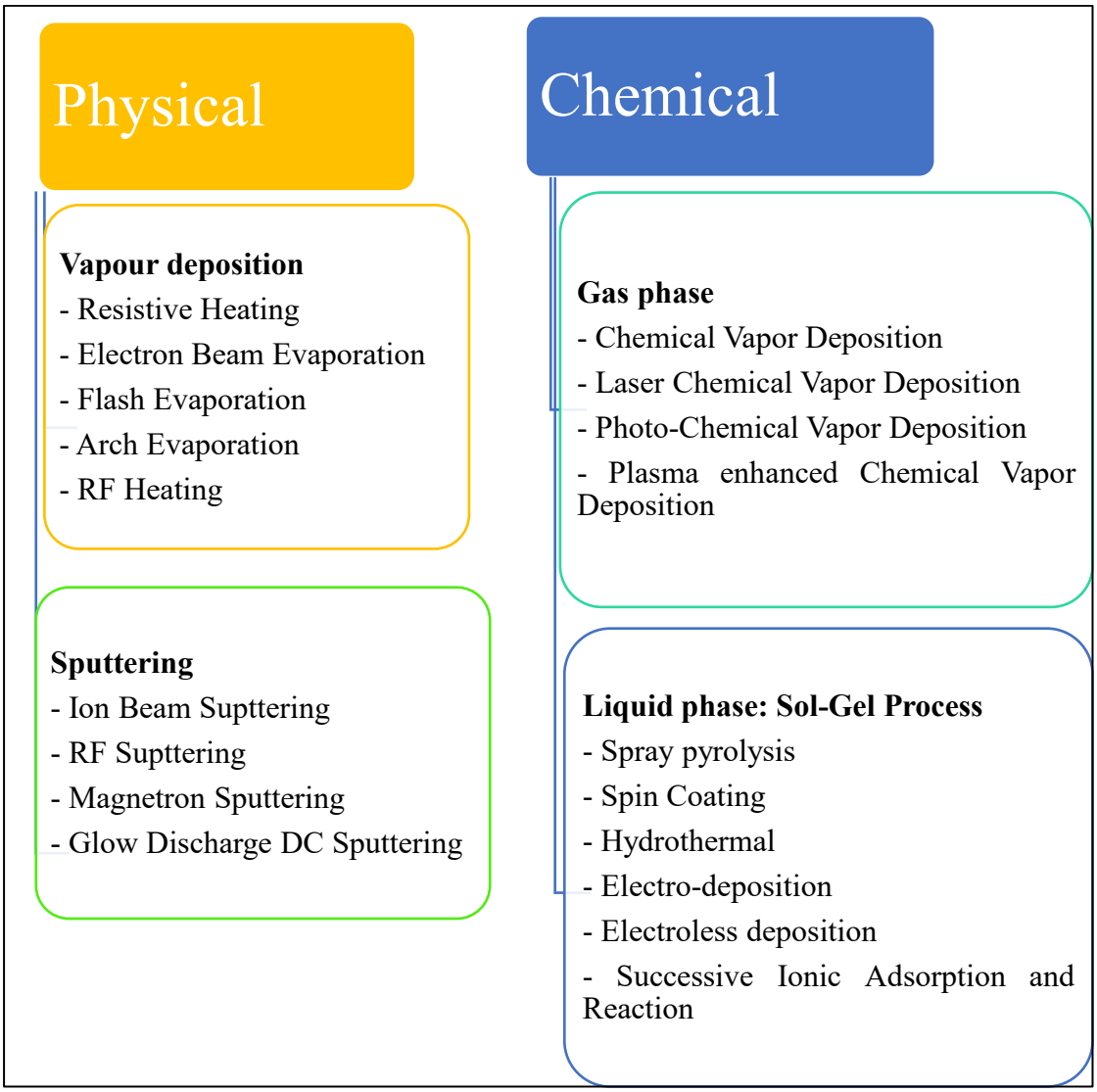

Figure 2.3 Synthesis Method for Photocatalysis.

2.4.1.1 Hydrothermal Method

One of the most popular and distinctive methods for creating nanomaterials is the hydrothermal process. The British geologist Sir Roderick Impey Murchison (1792-1871), coined the term "hydrothermal," which has geological roots, to describe the mineral production caused by hot water solutions rising from cooling magma (Feng & Li, 2017). Generally, the production of nanomaterials is essentially a solution-based process in which water is used as the solvent and may take place across a wide temperature range, from ambient temperature to extremely high temperatures. By

applying low-pressure or high-pressure settings depending on the vapour pressure of the primary component in the reaction, we may regulate the morphology of the materials to be created using the hydrothermal process.

Additionally, hydrothermal synthesis is a process for creating single crystals that relies on the solubility of minerals in hot, high-pressure water (Kafle, 2020). Figure 2.4 illustrates an apparatus for performing crystal formation that consists of an autoclave, a steel pressure vessel that can withstand temperatures as high as 600 to 700 °C (Kaur *et al.,* 2020). In addition, it is an inexpensive, uniform, high-purity, easy-to-manufacture, and environmentally friendly method of producing metal sulphides (Cao *et al.,* 2014), (Wu *et al.,* 2018). The development of nanostructure composites, particularly for WS_2, with different morphologies and more WS_2 layers exposed to the environment with greater chemical activity, is possible by hydrothermal synthesis (Cao *et al.,* 2014).

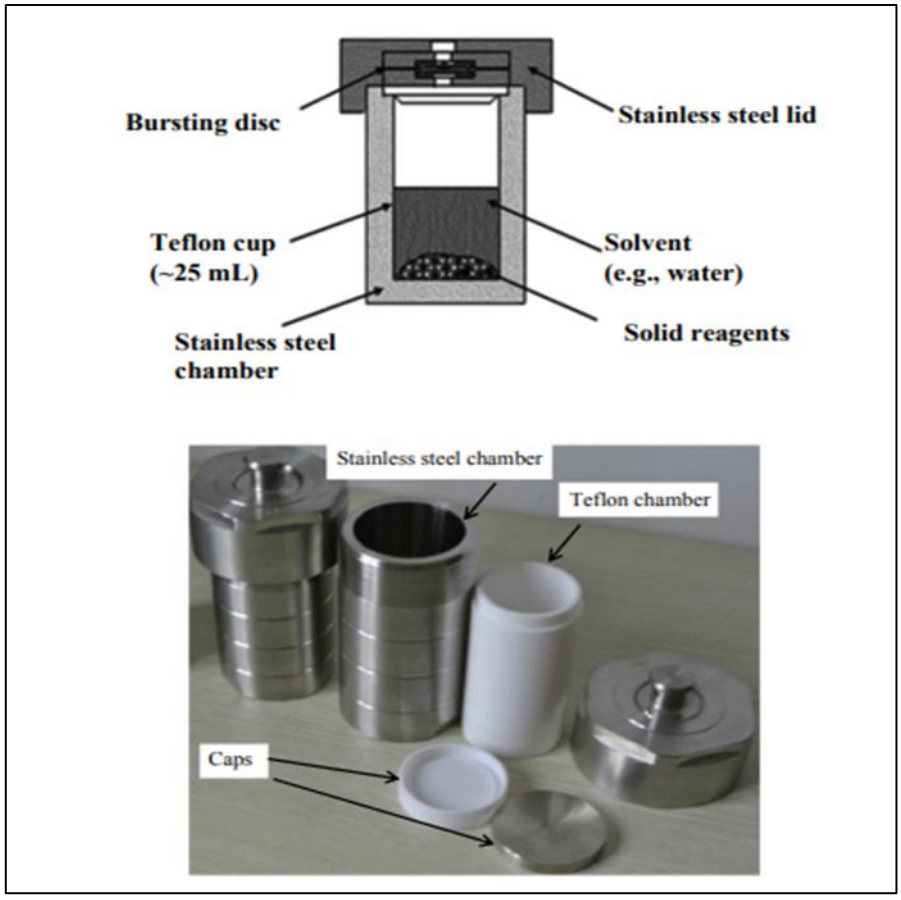

Figure 2.4 Picture of Stainless-Steel Autoclaves with Teflon Lining and Internal Parts (Upper). The Reaction Chamber, Which Is Made of Stainless Steel, Contains the Teflon Chamber. The Stainless-Steel Chamber in the Lower Picture Is Lined with Teflon and Is Commercially Available (Kafle, 2020).

A study by Cao *et al.,* 2014 examined the morphologies, structures, and possible formation mechanism of WS_2 which were prepared by hydrothermal process. WS_2 samples with four different morphologies, broccoli-like WS_2 (A-WS_2), the rod-like WS_2 (B-WS_2), flower-like WS_2 (C-WS_2) and fibre-like WS_2 (D-WS_2) were analysed through SEM. Figure 2.5 (a) reveals the A-WS_2 morphology with irregular and accumulation WS_2 nanoparticles with diameters ranging from 100 to 200 nm. Figure 2.5 (b) shows the B-WS_2 approximately 300 nm in diameter. The WS_2 surface consists of a large scale of nanorods with length of several micrometres. Figure 2.5 (c) is C-WS_2 demonstrates the aggregates of WS_2 nanosheets that are perfect open-pore alveolate structure with approximately uniform 200 nm in diameter. Figure 2.5 (d) displayed the D-WS_2 with a large quantity of fibre-like WS_2 nanostructures with a mean diameter of 100-150 nm.

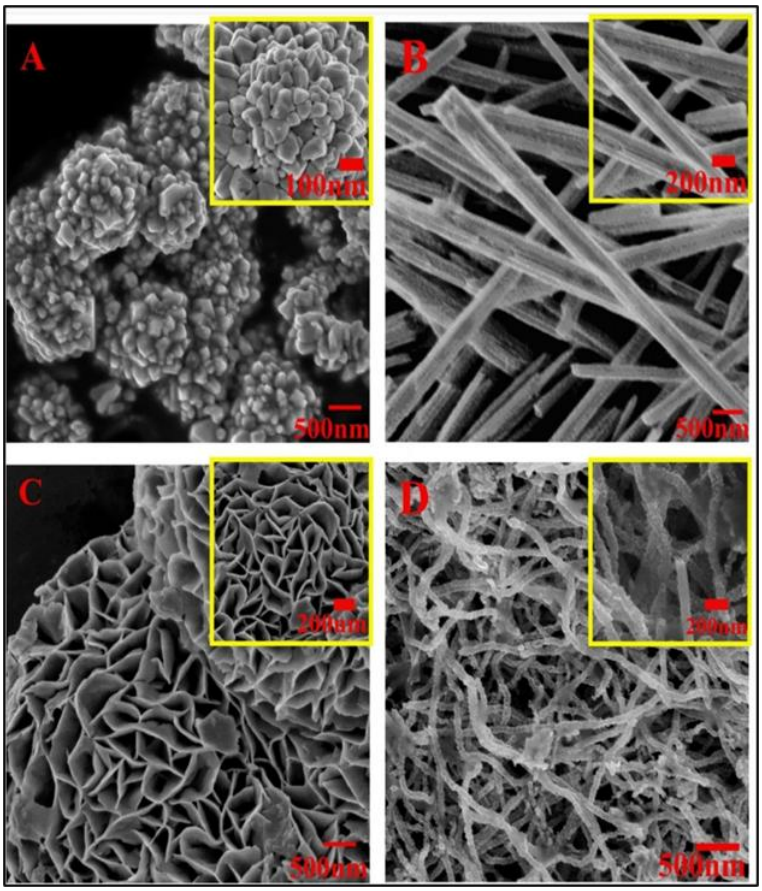

Figure 2.5 SEM Images of (A) Sample A-WS_2, (B) Sample B-WS_2, (C) Sample C-WS_2 and (D) Sample D-WS_2 (Cao *et el.,* 2014).

2.4.1.2 Solvothermal Method

Solvothermal synthesis requires a synthesis by chemical reactions at relatively high temperatures in an autoclave, just like hydrothermal synthesis does. Just that the synthesis in the solvothermal approach takes place in a nonaqueous solution. Another distinction between the hydrothermal and solvothermal methods is that the latter uses an organic solvent in place of water for preparation (Wu *et al.,* 2018). Different than hydrothermal method, the solvothermal method utilizing a solvent at moderate to high temperature that promotes precursor contact during synthesis which typically between 1 atm and 10,000 atm for pressure and 100 °C to 1000 °C for temperature where the method includes the interaction of a solvent (Feng & Li, 2017). Metals, semiconductors, ceramics, and polymers may all be produced using the solvothermal synthesis technique.

A study by Yan *et al,* (2018) produced a successful metal sulphide and transition metal dichalcogenides (TMDs) alloy nanostructures in CS_2. The hydrothermal treatment used by Huang's team to combine $(NH_2)10W_{12}O_4$ x H_2O with thiourea enhanced the fabrication of WS_2 nanosheets. However, creating WS_2 nanosheets with regulated morphologies and few contaminants, such as tungsten oxides, remains a difficult task. A simple and efficient microwave-assisted solvothermal approach for the synthesis of high-quality WS nanomaterials with adjustable sizes and morphologies is described in the research. N-methyl-2-pyrrolidone (NMP) was utilised as the synthesis medium by (Yan *et al.,* 2018), and tungsten hexachloride (WCl_6) and sublimed sulphur (S) were the starting reactants. Since WCl_6 dissolves efficiently in NMP, non-reducible WO_x may be avoided. This property is particularly advantageous to produce WS_2 nanomaterials that are homogenous and of excellent quality. NMP has a high boiling point and is a polar solvent.

Moreover, Yan *et al.* 2018, examined the product structure by stopping the reaction at various intervals with various reactant concentrations to see how the structure of the products varied with reaction time. According to the SEM investigation, WS_2 nanoworms and nanosheets developed at 240°C in less than 6 hours (Figure 2.6 (a) and (d)). 7 hours of reaction time results in the production of homogenous WS_2 nanoworms and nanosheets (Figure 2.6 (b) and (e)). The morphologies of the WS_2 nanostructures changed very little when the reaction time was increased (Figure 2.6 (c) and (f)). Therefore, for this reaction, 7 hours is the optimal reaction time. This

microwave-assisted solvothermal reaction is significantly quicker than the lengthy synthesis period of the conventional hydrothermal approach (more than 48 h), and the produced products are homogeneous because of the uniformly dispersed microwave heating.

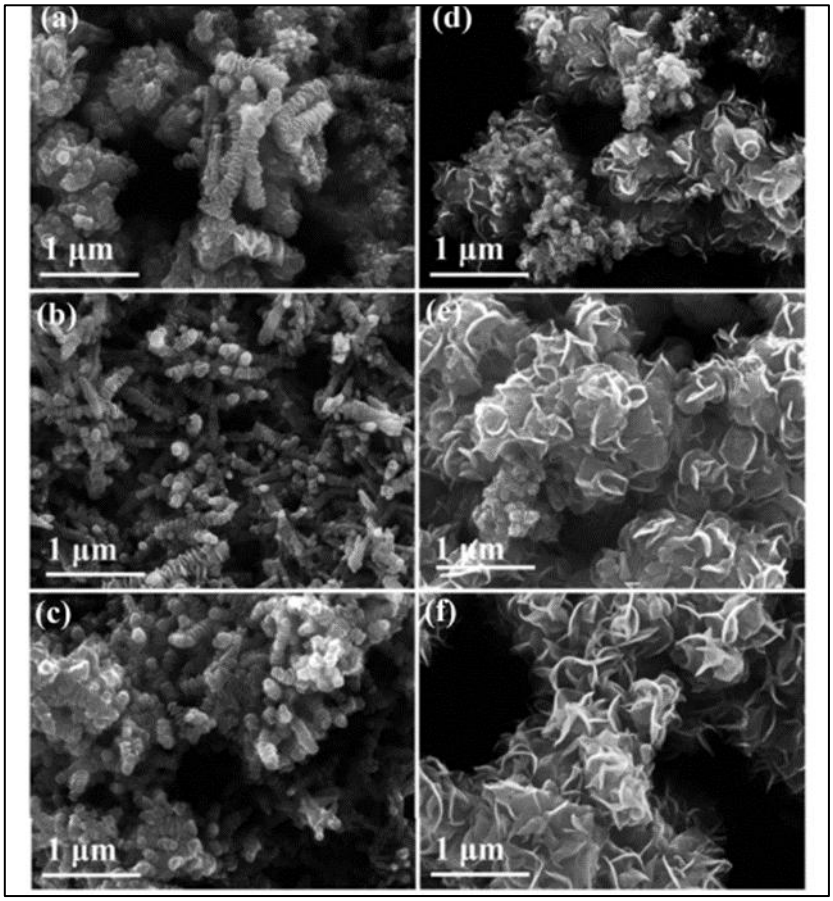

Figure 2.6 $WC1_6$ (0.112 g, 0.282 mmol), S (0.18 g, 5.625 mmol), and S (0.446 g, 1.125 mmol). Reactant Concentrations for the WS_2 Products at 240°C are Shown in the SEM Pictures in (a) Through (f) (0.72 g, 22.5 mmol). A and D: 6 hours; B and E: 7 hours; C and F: 8 hours (Yan *et al.* 2018).

2.4.1.3 Exfoliation Method

Exfoliation is often a process in which materials expand along a certain axis by factors of up to hundreds, producing puffed-up materials with low density and strong temperature resistance (Desai *et al.,* 2019). According to the report, when WS_2 is thinned to its monolayer form, its indirect bandgap changes to a direct bandgap of 2.1 eV, which makes it desirable for high-performance optoelectronics and photodetectors working in the visible range. As they transform light into electrical signals, photodetectors are utilised in a variety of applications, including optical communication and imaging. Moreover, numerous research has also been conducted on liquid-phase or chemical exfoliation since it has several benefits over other processes, including cheap cost, low temperature (as low as room temperature) processing, appealing scalability towards big sizes, and its material preserving nature.

Traditional semiconductors used in photodetectors, such Si and GaAs, are often opaque and can only be employed on stiff substrates due to their brittle nature. However, WS_2 nanosheets are transparent and exhibit significant light-matter interactions thanks to the band gap in the visible region of the electromagnetic spectrum and the existence of Van Hove singularities in the electronic density of states. Additionally, they have shown excellent performance on flexible substrates with bending curvatures as low as 5 mm (Desai *et al.,* 2019). These exceptional characteristics encourage the use of WS_2 in transparent and flexible photodetector systems by enabling it to get around some of the drawbacks associated with traditional semiconducting channel materials (such as Si, GaAs).

According to Desai *et al.* (2019), magnetic stirrer (MS) (low) and magnetic stirrer (MS) (high) correspond to 24 hours of magnetic stirring at 100 rpm and 1500 rpm, respectively. Shear mixing (SM) at 2500 rpm and 6000 rpm for 5 hours is referred to as SM (low) and SM (high), respectively, whilst horn-tip sonication (HT) sonication is referred to as HT (low) and HT (high), respectively. Figure 2.7 (a) shows the I-V response for drop-casted, annealed MS (low) and MS (high) samples, whereas Figure 2.7 (b) displays the I-V characteristic for drop-casted, annealed SM (low) and SM (high) samples (b). Current data on an extended scale for the MS (low) case are shown in the inset of Figure 2.7 (a). Similar to this, Figure 2.7 (c) shows the I-V behaviour for HT (low) and HT (high) samples that have been drop-casted and annealed. As seen in Figure 2.7 (a) to (c), all drop-casted samples exhibited non-ohmic behaviour, which is

suggestive of the WS_2 nanosheets' strong semiconducting properties. The higher electrical conductivity is obtained when WS_2 is exfoliated at a higher speed of MS (Figure 2.7 (a)), higher speed of SM (Figure 2.7 (b)), and at a higher amplitude of HT sonication (Figure 2.7 (c)), when the time is kept fixed, according to the electronic transport data. This suggests that when the net power applied to the solution is greater, a higher exfoliation rate occurs in all three of the exfoliation routes examined.

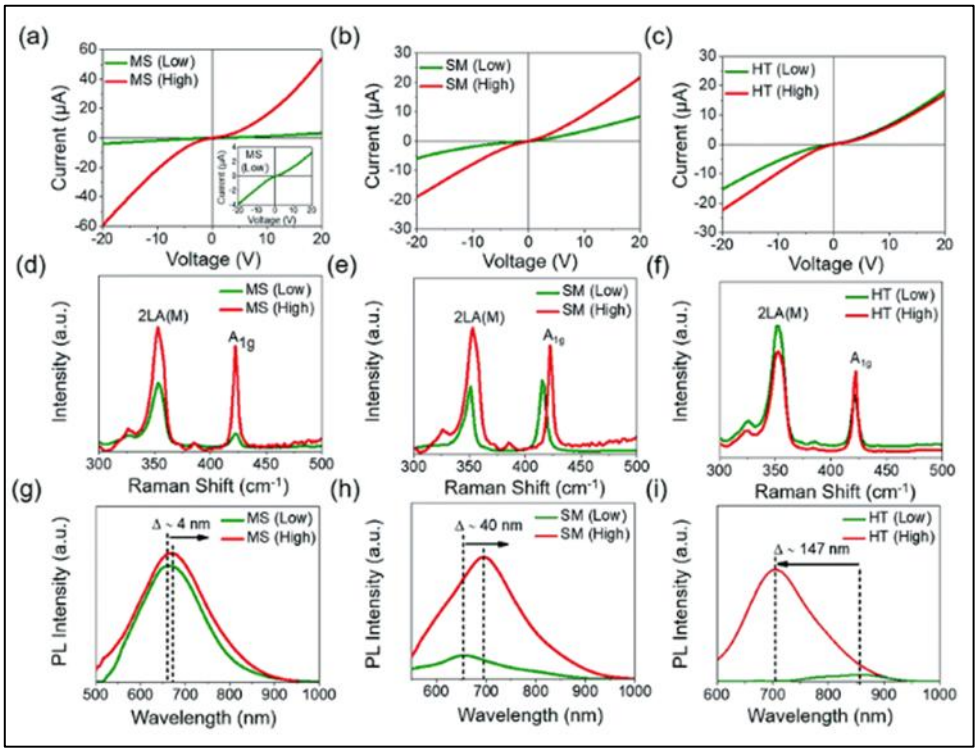

Figure 2.7 Drop-Casted Samples for WS_2 In Terms of Current (a), (b), and (c), Intensity (d), (e), and (f), and Photoluminescence Intensity (g), (h), and (i) (Desai *et. al.,* 2019).

2.5 WS_2 as Photocatalyst

Tungsten disulfide (WS_2) is an intriguing, layered semiconductor with a small bandgap (1.7 eV) among the many TMDs. WS_2 is an excellent choice for photocatalytic applications due to its straightforward manufacturing method, high stability, and adaptable few layered structures. However, the bulk WS_2 catalyst has a low small quantum efficiency, a small specific surface area, and quick photoexcited electron-hole pair recombination, which reduces its photocatalytic activity. As a result, great efforts have been made to improve the photocatalytic activity of bulk WS_2. For instance, the photocatalytic H_2 evolution activity of the WS_2/WO_3 hybrid is significantly greater than

that of the naked WS_2, for example. In aqueous solutions, the photocatalytic H_2 generation rate of the WS_2/CdS catalyst is greater than that of the single-phase WS_2 and CdS catalysts.

A composite photocatalyst is made up of just one component. For example, it may be WS_2, MoS_2, or other metal sulphides or oxides. Since their band gaps match the frequency range of visible light between red and violet (1.5 eV gap 2.6 eV), one-dimensional tungsten disulfide (WS_2) single walled nanotubes (NTs) with either achiral, i.e., armchair (n, n) and zigzag-type (n, 0), or chiral (2n, n) configuration have been found to be suitable for photocatalytic (Piskunov *et al.,* 2019).

Reported by Chen *et al.,* (2020), a bulk WS_2 which is a hexagonal structure (1.552 eV band gap) and rhombohedral structure (1.448 eV band gap) are thermodynamically stable exhibits a good adsorption effect in the ultraviolet region as shown in Figure 2.8.

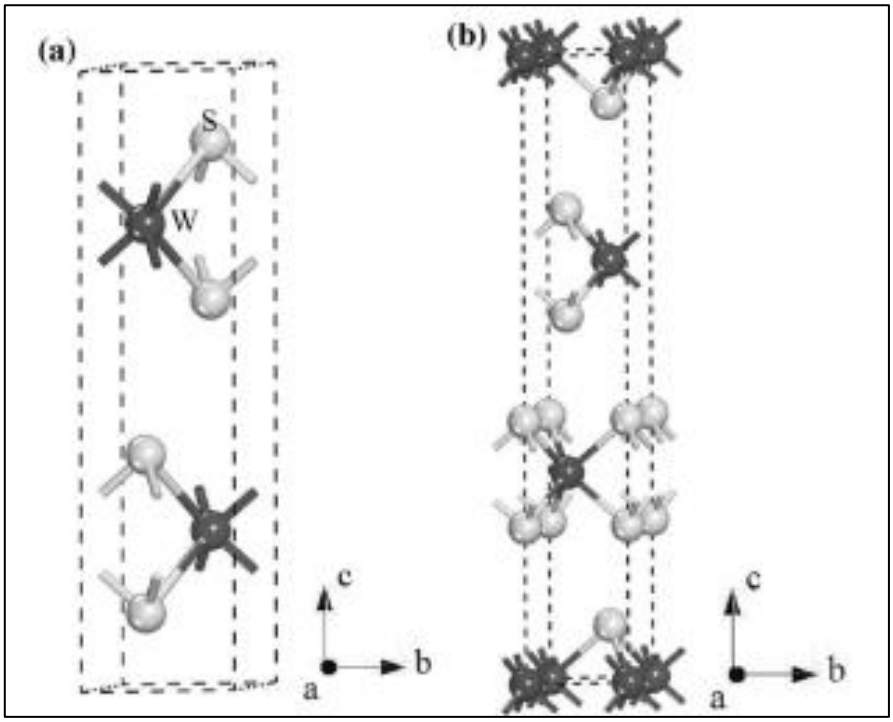

Figure 2.8 Structural Model of WS_2 (a) the Hexagonal WS_2 and (b) the Rhombohedral WS_2 (Chen *et al.,* 2020).

Moreover, the UV-vis diffuse reflectance spectra of the MoS_2 and WS_2 nanocluster sensitised TiO_2 show prolonged absorption down to 700 and 620 nm, respectively, as reported by Ho *et al.* in 2004 (Figure 2.9). It was mentioned that WS_2 had 920 nm absorption (1.35 eV band gap). The substantial quantum confinement effect

in the novel photocatalysts is indicated by the massive blue shifts. This confinement causes the band gaps of WS_2 nanoclusters to widen, which in turn affects how redox potentials are affected.

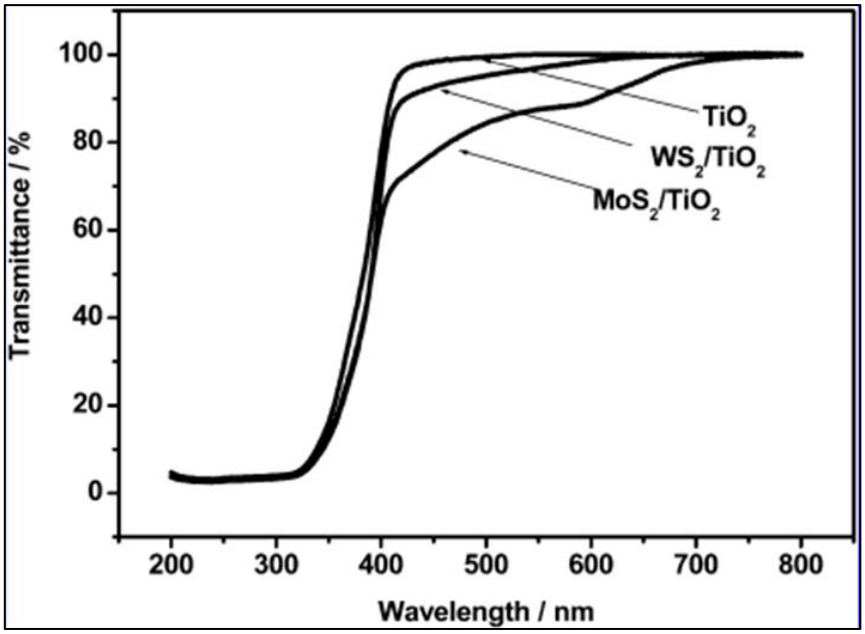

Figure 2.9 A Comparison of the UV-Visible Diffuse Reflectance Spectra of Pure TiO_2, WS_2/Tio_2, and MoS_2/TiO_2 (Ho *et al.* in 2004).

A successful method for constructing Pd nanoparticles (NPs) on exfoliated 2H-WS_2 nanosheets (WS_2/PdNPs) was described by Raza *et al.,* in 2017. This method produced hybrids with exceptional photocatalytic activity in Suzuki reactions under visible light. By using a sonic wave-assisted nucleation approach without any reductants at room temperature, Pd NPs of various sizes and densities, which can control the photocatalytic activity of the prepared WS_2/PdNPs, were successfully constructed on the basal plane of $2HWS_2$ nanosheets.

Patel *et al.,* (2020) showed that nanostructured WS_2 has improved photocatalytic activity for breaking down ternary dye mixtures which the combination of Methylene blue (MB), Congo red (CR), and Methyl orange (MO). To prevent reflection loss, photocatalytic studies were conducted utilising a 250 W halogen light enclosed in aluminium reflectors. In a typical experiment, three different dyes which are MB, CR, and MO that were combined in a 1:1:1 volume ratio to create the dye solution. The reaction solution's catalyst loading was adjusted to three different concentrations which are 0.5 g/L, 1 g/L, and 1.2 g/L respectively, while the dye content was held constant at

7 mg/L. Additionally, the pH of the dye mixture was adjusted from 2 to 8 points. WS_2 nanosheets were also added to the 100 mL solution as a photo catalyst, and the mixture was mixed in the dark for 30 minutes prior to being exposed to light. The initial sample was obtained at 0 min, and the 2mL solution was removed at intervals of 20 min for 40 min. The temperature was kept at ambient levels throughout the experiment. The sample was centrifuged for 15 minutes at 7000 rpm, and the supernatant was collected for examination.

The sample's optical characteristics, which were determined using UV-vis transmission spectra (Figure 2.10) with a range of 200-800 nm, were demonstrated by the findings in Figure 2.11. The visible spectrum of the dyes MB, OR, and CR displays absorption maxima at 665 nm, 465 nm, and 245 nm, respectively. The MD dye is superoxide (O_2), hydroxyl radical (˙OH), and H_2 under mild irritation. However, some of the valence band holes react with the adsorbed water and OH^- in the MD dye solution to create the hydroxyl radical (˙OH), while other holes destroy the dye molecules, including CO_2 and H_2O.

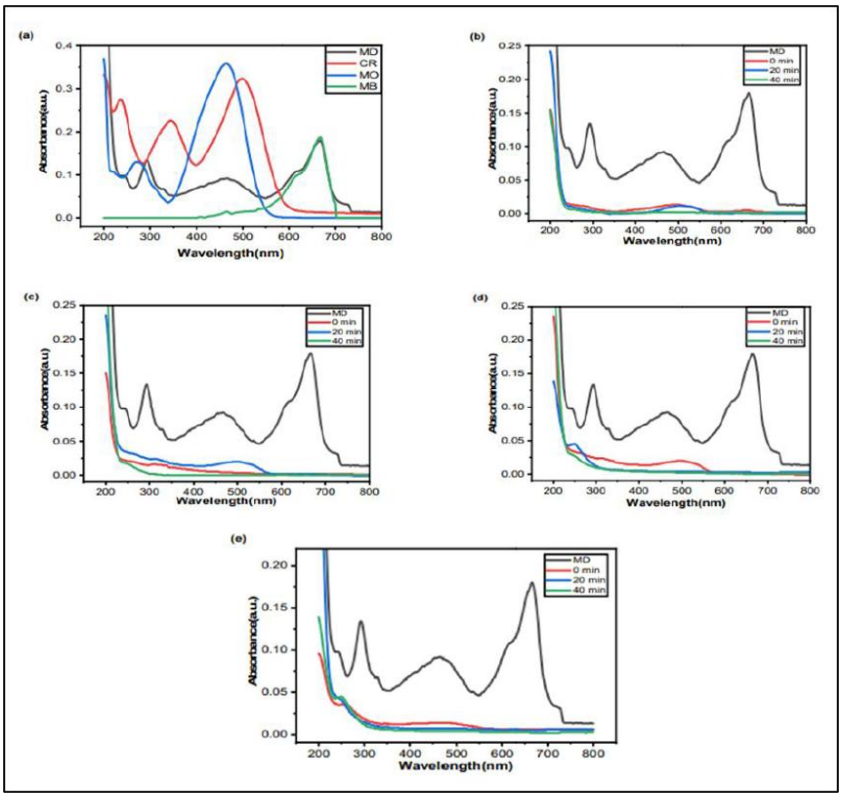

Figure 2.10 With a Catalyst Loading of 1.2g/L and a Dye Concentration of 7mg/L, the Graphs Show the Photocatalytic Degradation of MD Dye (a) Comparison of the Peak Location of the MD Dye's Absorption Spectra with Specific MB, MO, and Degradation of the MD Dye with pH Variation (b) pH2 (c), pH4 (d), pH6 (e), and pH8 (Patel *et al.,* (2020).

The performance of a semiconductor photocatalyst is harmed by the interaction between the electron and the hole, according to the fundamental theories of semiconductor photocatalysis. The electron-hole pairs must be properly separated, and charges must be swiftly transported over the surface or interface to prevent recombination, to maximise the effectiveness of photocatalytic degradation. The strategy that has often been used is to couple a semiconductor with a secondary material to create a semiconductor heterojunction, which improves the photocatalytic activity. Overall, there are four main types of heterojunction photocatalysts: the semiconductor-semiconductor heterojunction (abbreviated as S-S), the semiconductor-metal heterojunction (abbreviated as S-M), the semiconductor-carbon group heterojunction (abbreviated as S-C), and the multicomponent heterostructure (H. Wang *et al.,* 2014).

2.5.1 WS_2 Based Photocatalyst in Environmental Studies

In environmental remediation, tungsten disulfide (WS_2) has shown great promise as a photocatalyst, especially for the breakdown of organic contaminants, the removal of heavy metal ions, and the disinfection of waterborne pathogens. Its excellent photocatalytic activities under visible light irradiation are attributed to its unique two-dimensional layered structure, large surface area, and appropriate bandgap (~1.9 eV).

The effectiveness of WS_2-based composites in breaking down organic contaminants has been shown in recent investigations. For example, in visible light, WS_2/TiO_2 nanofibers produced by electrospinning demonstrated improved photocatalytic degradation of phenol, with an 83% degradation efficiency (Nada *et al.,* 2022). This increase is ascribed to the synergistic interaction between the photocatalytic activity of TiO_2 and the visible light absorption of WS_2, which improve charge separation and lower recombination rates. Similarly, in visible light, a Z-scheme WS_2/In_2S_3 composite showed notable photocatalytic activity, degrading 90% of TC hydrochloride in 60 minutes (Guo *et al.,* 2022). Effective charge separation and a bi-layered sheet-like structure that shortens the charge transfer distance are the causes of the improved performance.

Apart from degrading organic pollutants, materials based on WS_2 have demonstrated efficiency in lowering harmful heavy metal ions. Research by Yousef *et*

al., in 2022 on CdS/WS_2 heterojunctions showed improved charge separation and stability across several cycles, along with a high photoreduction rate for Cr (VI). The Z-scheme design improves photocatalytic efficacy by facilitating effective electron transport. Moreover, water disinfection has also been investigated using WS_2-based photocatalysts' antibacterial qualities. Because piezoelectric polarization increases the formation of reactive oxygen species, chemically vapor-deposited WS_2 monolayers showed strong antibacterial activity against Escherichia coli (Yousef *et al.,* 2022). Additionally, peroxymonosulfate (PMS) electrochemical activation aided by WS_2 has been used to effectively remove organic contaminants such as Acid Orange 7 from water. Within 30 minutes, the electro-assisted WS_2-activated PMS system achieved a removal efficiency of 95.8%, with singlet oxygen and hydroxyl radicals being detected as the main reactive species (Du *et al.,* 2024).

The potential of WS_2-based photocatalysts in environmental applications is highlighted by these investigations. To successfully address environmental pollution concerns, future research should concentrate on improving photocatalyst stability, optimizing synthesis techniques, and incorporating these materials into workable water treatment systems.

2.6 Graphene Oxide (GO)

Graphene is a single layer of carbon atoms bounded tightly into a hexagonal configuration. Due of its extreme thinness, graphene is regarded as two dimensional. The strongest substance known to man is regarded as graphene, which is also one of the most electrically and thermally conductive substances. On the other hand, GO, formerly known as graphitic oxide or graphitic acid, is a single-atomic layered compound of carbon, oxygen, and hydrogen in varying ratios that is created when powerful oxidizers and acids are used to treat graphite to remove excess metals. The fact that graphene oxide disperses in water is one of its key benefits. This enables the use of solution-based methods. The ability to be converted into graphene through chemical, thermal, or electrochemical processes is another advantage of graphene oxide. The resultant substance is known as reduced graphene oxide (rGO).

The surface-to-volume (STV) ratio of a traditional catalyst may frequently be used to regulate performance. Because of its 2D structure and single-atom thickness and extraordinarily high STV ratio, graphene might be appealing in catalytic applications.

Moreover, its high electrical conductivity makes it excellent for electrochemical operations, while its strong chemical stability and ultrahigh thermal conductivity may help with the high loading of catalytically active sites. Because to these characteristics, graphene able to maintain its integrity and resistance to deterioration despite challenging working circumstances, such as high temperatures, the use of high bias voltages, and extremely acidic or alkaline environments. If expensive noble metals are employed, they are often simple to recover by burning the carbon support.

2.7 Tungsten Disulphide/Graphene Oxide (WS_2/GO)

WS_2 is chosen because of its superior optical absorption qualities, strong stability, affordable price, and environmental friendliness (Sridharan & Maiyalagan, 2021). However, a single photocatalyst was difficult to degrade the TC due to rapid recombination of photogenerated electron-hole pair and tend to agglomerate between the nanosheets. Therefore, a semiconductor heterojunction is formed where WS_2 is modified by adding GO to enhance the photocatalytic activity. This incorporation of WS_2/GO can improve each element and chemical properties to degrade TC since GO will act as an efficient cocatalyst for photocatalytic reactions due to its larger specific surface area and good electron transfer abilities (Li *et al.,* 2021). Wu *et al.,* 2019, reported that the combination of WS_2/GO enhancing the photocatalytic properties and improving the dispersion of photocatalyst during the degradation of rhodamine B (RhB) under visible light.

2.8 Antibiotics

The widespread use of antibiotics has transformed contemporary medicine, but it has also resulted in their widespread presence in aquatic ecosystems, generating concerns about ecological effects and the spread of bacteria resistant to antibiotics. These persistent pharmaceutical chemicals are sometimes difficult to remove using traditional wastewater treatment methods. As a result, the potential of advanced oxidation processes (AOPs), especially photocatalysis, to break down antibiotics in water systems has attracted a lot of attention (Chen *et al.,* 2021).

In photocatalysis, a photoreaction is accelerated when a catalyst is present. Reactive oxygen species (ROS) such superoxide anions ($\cdot O_2^-$) and hydroxyl radicals ($\cdot OH$) can be produced by photocatalysts when they are exposed to light, usually in the visible or ultraviolet spectrum (Huang *et al.,* 2017). Because of their high reactivity, these ROS may oxidize a variety of organic contaminants, including antibiotics, without discriminating, causing them to mineralize into innocuous byproducts like CO_2 and H_2O.

Numerous photocatalytic materials have been investigated recently for the breakdown of antibiotics. For example, Hassan Mohamed *et al.* (2022) used zinc ferrite immobilized on chitosan under visible light to study the degradation of ciprofloxacin, ampicillin, and erythromycin. According to the study, the photocatalyst and the support material worked in concert to provide notable degradation efficiencies. In a similar vein, Tarannum *et al.* (2024) created sodium-doped hydroxyapatite (Na-HAp) and showed that it was effective in breaking down ciprofloxacin and amoxicillin when exposed to sunlight, with corresponding degradation percentages of 41.59% and 60%.

According to Tian *et al.,* (2023), multiple reactive species are frequently involved in the processes underlying the photocatalytic breakdown of antibiotics. For instance, research has indicated that photogenerated holes and hydroxyl radicals are essential components of the degradation process (Tarannum *et al.,* 2024). Increased ROS production and higher charge separation efficiency were credited with the increased photocatalytic activity in the amoxicillin degradation employing Mn-doped CuO under solar radiation (Gaim *et al.,* 2022).

Moreover, photocatalysts' performance is greatly influenced by their structural characteristics. Dopants, heterojunctions, and support materials may all be used to increase surface area, charge carrier mobility, and light absorption, all of which improve photocatalytic efficiency. For example, it has been demonstrated that TiO_2–carbon composites may efficiently break down ciprofloxacin and TC; the processes of degradation include different reactive species and are dependent on the pH and other operating factors (Tian *et al.,* 2023).

Apart from studies conducted at the laboratory level, research has also concentrated on the real-world uses of photocatalytic devices. Through studies from Zulfiqar *et al.,* (2024), photocatalysts may now be easily recovered and reused thanks to the invention of magnetic nanocomposites like magnetite/SCB biochar, which makes the process more economically and environmentally friendly.

To sum up, the breakdown of antibiotics by photocatalysis offers a viable strategy to reduce pharmaceutical contamination in aquatic ecosystems. For this technique to be used in wastewater treatment facilities, improvements in photocatalyst design, comprehension of degradation mechanisms, and optimization of system are essential. This approach aims to minimize the long-term ecological impact and reduce the risk of resistance development.

2.9 Tetracycline Antibiotic (TC)

TC antibiotics are a class of broad-spectrum antimicrobial agents widely used to treat various bacterial infections in both humans and animals (Singhal *et al.,* 2023). Discovered in the late 1940s, TC revolutionized medicine due to their ability to target a wide range of Gram-positive and Gram-negative bacteria, as well as atypical organisms like chlamydia, mycoplasma, and rickettsia. Their broad-spectrum activity, along with relatively low toxicity, made them one of the most prescribed antibiotics during the 20th century. However, their extensive use has also contributed to the growing issue of antibiotic resistance and environmental pollution.

TC inhibit bacterial growth by targeting the bacterial ribosome, specifically the 30S subunit, preventing the attachment of aminoacyl-tRNA to the mRNA-ribosome complex (Krawczyk *et al.,* 2024). This blocks the addition of new amino acids to the growing peptide chain, effectively halting protein synthesis in bacteria. By being bacteriostatic rather than bactericidal, TC do not kill the bacteria directly but inhibit their reproduction, allowing the immune system to clear the infection. The broad efficacy of TC stems from their ability to penetrate bacterial cells through both passive diffusion and active transport, which allows them to act on a wide variety of bacterial species (Singhal *et al.,* 2023). However, this same broad activity can disrupt the body's natural microbiome, potentially leading to side effects such as gastrointestinal disturbances and secondary infections.

TC antibiotics are used to treat a wide array of infections, including respiratory tract infections, urinary tract infections, skin conditions like acne, and sexually transmitted diseases such as chlamydia (Hamilton & Guarascio, 2019). They are also employed in the treatment of more specialized infections, such as Lyme disease, Rocky Mountain spotted fever, and brucellosis. In veterinary medicine, TC are commonly used for the treatment of infections in livestock and poultry, as well as for promoting growth

in animals, although this practice has come under scrutiny due to its contribution to antibiotic resistance.

Over time, the extensive use of TC has led to the development of bacterial resistance. Bacteria have evolved several mechanisms to evade the action of TC, one of the most common being the expression of efflux pumps. These pumps actively expel the antibiotic from the bacterial cell before it can exert its effect, reducing the concentration of the drug to sub-lethal levels. Another mechanism involves the modification of the ribosomal binding site, making it less susceptible to TC binding. Additionally, some bacteria produce enzymes that inactivate TC, rendering the drug ineffective.

The rise of TC resistance is a major public health concern, particularly in developing countries where TC is still widely used and often overprescribed. Resistant strains of bacteria, such as methicillin-resistant *Staphylococcus aureus* (MRSA) and multidrug-resistant *Escherichia coli*, have emerged, limiting the effectiveness of TC and other antibiotics in treating infections (Terreni *et al.,* 2021).

In addition to its clinical and agricultural uses, TC poses significant environmental concerns. Large quantities of TC are excreted unmetabolized by humans and animals, entering wastewater systems and agricultural runoff. These antibiotics then persist in water bodies, soils, and sediments, contributing to the proliferation of antibiotic-resistant bacteria in the environment. Wastewater treatment plants are often unable to completely remove pharmaceutical residues like TC, leading to their accumulation in natural ecosystems.

The presence of TC in aquatic environments is particularly concerning as it can affect microbial communities, disrupt the ecological balance and contribute to the emergence of resistant bacteria. These resistant strains can transfer resistance genes to other bacterial populations, further complicating efforts to manage antibiotic resistance. This highlights the need for innovative water treatment technologies capable of effectively degrading TC and other antibiotics before they reach the environment.

TC antibiotics have played a crucial role in combating bacterial infections for decades, but their widespread use has led to significant challenges, including antibiotic resistance and environmental contamination. As bacterial resistance to TC grows, and as these antibiotics accumulate in the environment, there is an urgent need for alternative solutions to mitigate their impact. Photocatalytic degradation using advanced materials under LED light presents a promising avenue for addressing TC

contamination in water systems, offering a sustainable and effective approach to reducing the ecological and health risks associated with this widely used antibiotic.

2.9.1 Photocatalytic Degradation of TC

Antibiotics called tetracycline (TC) are often used in both human and veterinary medicine. However, due to their widespread usage, they are now persistent in aquatic ecosystems, which presents serious threats to human health and the environment. These substances are frequently difficult to remove using traditional wastewater treatment techniques, which calls for the creation of sophisticated treatment technologies. The effectiveness and environmental friendliness of photocatalysis, a sophisticated oxidation process, have made it a viable method for the breakdown of TC antibiotics.

One promising solution to address TC contamination is the use of AOPs, such as photocatalysis, for the degradation of antibiotics in water systems. Photodegradation involves the use of light-activated catalysts to generate reactive oxygen species (ROS), which break down TC into less harmful compounds. Materials such as WS_2 and GO have shown potential as photocatalysts due to their high surface area and ability to absorb visible light, making them suitable for environmental applications.

Photodegradation under visible light, particularly using energy-efficient light sources like LEDs, offers a sustainable and effective approach to removing TC from water systems. By investigating the photodegradation of TC with WS_2/GO composites, researchers can explore new ways to tackle the environmental persistence of this antibiotic, contributing to the broader effort to mitigate the impact of pharmaceutical pollutants.

Recent research as shown in Table 2.3, has concentrated on creating new photocatalysts that exhibit increased activity when exposed to visible light. For example, a lanthanum-doped TiO_2@g-C_3N_4 composite activated by persulfate was produced, and after four cycles under visible light, the degradation efficiency of TC hydrochloride was 97.68% (Wang *et al.,* 2023). Both the existence of non-radical species like e^- and h^+ and the production of reactive species like $SO_4^{\cdot -}$, $^{\cdot}OH$, and $^{\cdot}O_2^-$ were credited with the improved performance.

Similarly, hollow nanofiber Ag@$ZnGaO_4$/ZnO photocatalysts were created, utilizing S-scheme interface engineering and localized surface plasmon resonance (LSPR) to their mutual benefit (Phakathi *et al.,* 2022). The improved photocatalyst outperformed the self-degradation rate of TCH by 22 times, achieving a degradation

rate constant of 0.0708 min^{-1}. Effective charge separation and greater light absorption were the causes of the improved performance. Additionally, graphitic carbon nitride (g-C_3N_4) has been investigated as a photocatalyst driven by visible light. shown that, after just two hours, porous g-C_3N_4 nanosheets degraded TC by 76.7% when exposed to visible light. For optimal degradation efficiency, the study emphasized the significance of pH adjustment and catalyst loading.

Other noteworthy photocatalysts that exhibit substantial degrading efficiencies and offer insights into the processes involved are $NiFeO_4/CeO_2$/GO nanocomposites, SiC/CdS composites, and MoS_2/TiO_2 composites (Latif *et al.,* 2024).

Among all previous studies based on Table 2.3, a study by Oluwole & Olatunji (2022), resulted as the best photocatalyst in degrading the TC. It has been demonstrated that the creation of heterojunctions greatly increases photocatalytic activity. produced needle-shaped SnO_2 nanoparticles that were anchored to exfoliated g-C_3N_4, resulting in a 95.90% TC breakdown efficiency when exposed to visible light. The enhanced performance was ascribed to the synergistic interaction between g-C_3N_4 and SnO_2, which reduces recombination and promotes charge separation.

In conclusion, considerable progress has been made in the photocatalytic breakdown of TC antibiotics. It has been crucial to create new photocatalysts with improved visible-light activity, effective charge separation, and high stability. Future studies must concentrate on expanding these technologies' use and investigating how they may be applied in actual wastewater treatment situations.

Table 2.3
Degradation of TC with Different Photocatalyst.

Photocatalyst	**Light source**	**Concentration (mg/L)**	**Degradation Efficiency (%)**	**References**
Porous g-C_3N_4 nanosheets	Visible light	10	76.7%	(Phakathi *et al.,* 2022)
SnO_2/g-C_3N_4	Visible light	30	95.90%	(Oluwole and Olatunji, 2022)
SiC/CdS-0.5	Visible light	20	78%	(Qian *et al.,* 2022)
$NiFe_2O_4$/CeO_2/GO	Visible light	Not specified	95%	(Latif *et al.,* 2024)
CDs/g-C_3N_4/$BiPO_4$	Visible light	10	75.50%	(W. Qian *et al.,* 2022)
La/TiO_2@g-C_3N_4	Visible light	20	97%	(Wang *et al.,* 2023)

2.10 Research Gap

The greatest photocatalyst must be available to accomplish TC's photocatalytic degradation since TC is affecting all living things. Here, it is suggested that WS_2/GO serve as a photocatalyst for the TC's breakdown. Theoretical band gaps can be used to demonstrate the complement of the components, in addition to the positive characteristics of each element.

Additionally, the performance of the photocatalyst is strongly influenced by the light source. Here, we reported a hybrid WS_2/GO nanocomposite that was used for the first time to breakdown TC using light from an LED. Compared to halogen lamp and fluorescent lamp, LED are the most energy efficient and long lasting. Moreover, according to Wasylaschuk *et al.,* (2020), LED effectively can degrade TC better than fluorescent lamp. Moreover, LED sources benefits in the elimination of the need for a separate water-cooling facility to maintain a constant temperature and the flexibility of LED source placement in the designed reaction system and the addition of co-catalyst securing the enhancement of photocatalytic activity under visible-light region. Considering this, the current study concluded that WS_2/GO photocatalysts effectively reduce TC using inexpensive light emitting diodes. Therefore, WS_2/GO has the potential to get beyond the drawbacks of currently available photocatalytic materials and offer the best option for removing TC from wastewater for reasonably priced water filtration.

CHAPTER 3
RESEARCH METHODOLOGY

3.1 Introduction

This study focused on four main components which is synthesizing, characterizing, optimizing, and investigating as mentioned as in the objectives of the research. Therefore, to complete this research smooth and accordingly, a framework of research needs to be made, and it is shown as in Figure 3.1.

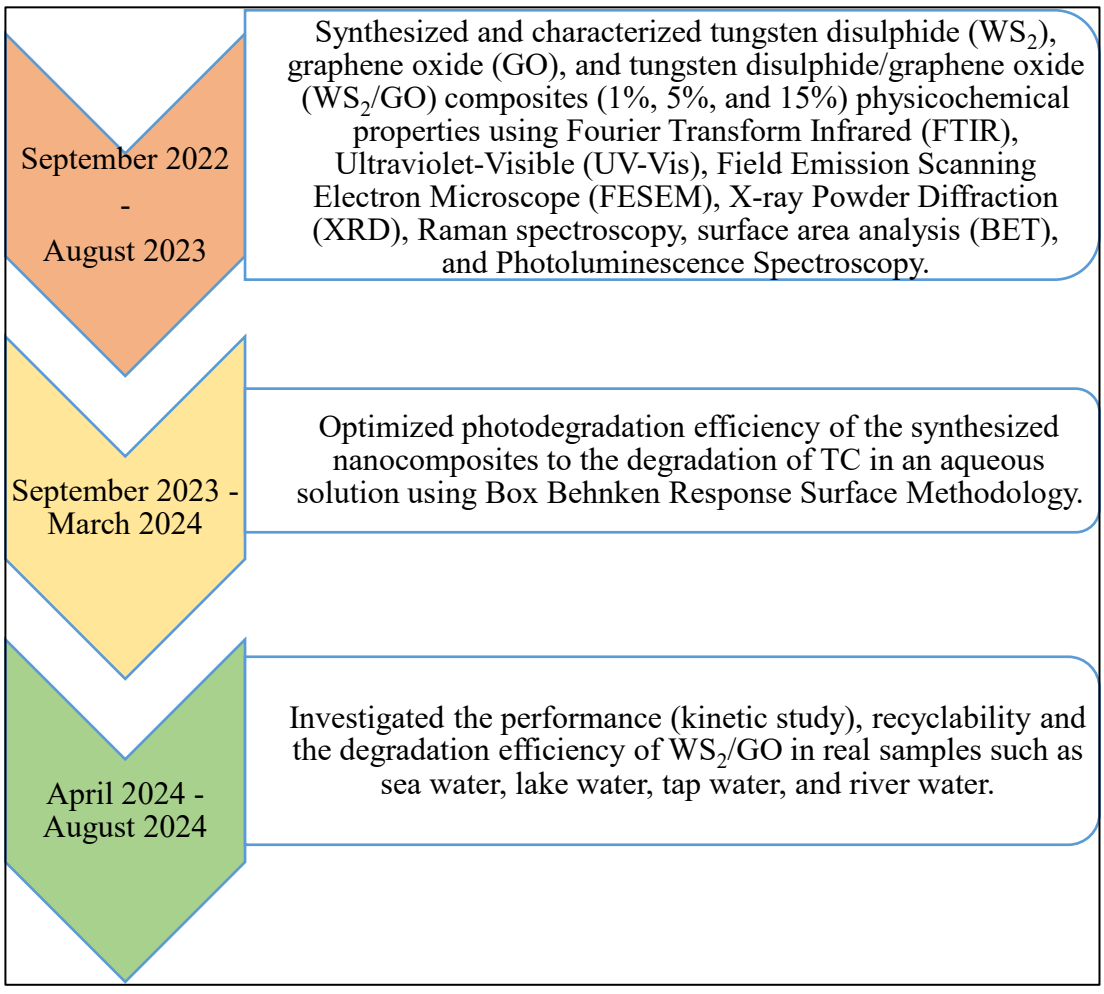

Figure 3.1 Flowchart of Research.

3.2 Materials

3.2.1 Apparatus

250 ml of round bottom flask, 25 ml and 50 ml beaker, 5 ml, 10 ml and 25 ml of measuring cylinder, 10 ml and 50 ml of conical flask, 5 ml, 10 ml and 50 ml volumetric flask, 15 ml of centrifuge tube, micropipette tips (1- 1000 µl) magnetic stirrer, glass rod, dropper, Styrofoam box, Buchner funnel, water bath, hot plate, thermometer, filter paper, weighing boat, Teflon stainless steel and analytical balance.

3.2.2 Chemicals

In this research hydrochloric acid (HCl, 37%, R&M brand, Malaysia), tungstic acid (H_2WO_4, 98%, Sigma Aldrich, Malaysia), thiourea (CH_4N_2S, ≥99.0%), graphene, sodium nitrate ($NaNO_3$), sulfuric acid (H_2SO4, 98%), acetone, methanol and potassium permanganate ($KMnO_4$, 99%) were purchased from Sigma Aldrich. Lastly, the TC (98%) were purchased from LabChem Sdn Bhd.

3.3 Method

3.3.1 Synthesis of WS_2 (Hydrothermal Method)

WS_2 materials were synthesized via a simple hydrothermal method under acid condition using the tungstic acid (H_2WO_4) and sulfourea as starting materials. 0.003 mol of H_2WO_4 and 0.008 mol of thiourea was dissolved in 60ml of deionized water and then sonicated for 30 minutes. Then, the pH value of the solution was adjusted to 6.0 by adding 1 mol/L HCl solution, and then the solution was stirred for another 30 min. After that, the mixed solution was transferred into a 100 mL Teflon-lined stainless-steel autoclave for hydrothermal treatment at 180°C for 10 hours and cooled to room temperature. WS_2 was centrifuged at 4000 rpm for 10 min, then was washed with deionized water and ethanol several times and was dried in the vacuum oven at 60°C for 12 hours. The final product WS_2 formed in a fine black powder.

3.3.2 Synthesis of GO (Modified Hummer's Method)

Graphene oxide (GO) was prepared by modified Hummer's method. 1g of graphite flakes, 0.5 g of sodium nitrate ($NaNO_3$) and 23 mL of concentrated sulfuric acid (H_2SO_4) were added into a 250ml, three necked round-bottom (RB) flask, stirred at room temperature for 1 hour and kept in an ice bath. 3 g of potassium permanganate ($KMnO_4$) were added slowly for 1 hour and stirred vigorously. The ice bath was removed and stirred further for 4 hours. Then the mixture temperature was raised up to 35°C using a water bath and stirred for another half an hour. The suspension was poured into 250 mL of deionized water and heated up to 70°C. Then, the suspension was stirred for 15 minutes. The unreacted compounds were removed by the addition of a 30% hydrogen peroxide solution. The GO obtained through repeated centrifugation and washing with a 5% HCl solution. Finally, the slurry was dried in a vacuum oven at 70°C overnight (Appavu *et al.,* 2016).

3.3.3 Synthesis of WS_2/GO

The 1 g of GO was added into the 40 mL deionized water in the beaker. The GO dispersion was then ultrasonicated for 10 minutes. Next, 40 mL deionized water was poured into the 0.5 g WS_2. Then, the dispersion solution was ultrasonicated for 10 minutes. The mixed solution was poured into 100 mL Teflon-line stainless steel and heated with high pressure at 120°C for 24 hours. Lastly, the precursor was centrifuged, rinsed with water, and was dried in a vacuum oven at 80°C for 24 hours (Song *et al.,* 2018). The synthesized composite was labelled as WS_2/GO-15. The experiment was repeated with different calculation and labelled as WS_2/GO-1 and WS_2/GO-5.

3.4 Characterization of Tungsten Disulphide/Graphene Oxide Photocatalyst (WS_2/GO)

3.4.1 Fourier Transform Infrared Spectroscopy (FTIR)

ATR-FTIR of Perkin Elmer model 100 spectrometer was used to show the functional group present in synthesis of WS_2, GO and WS_2/GO composite. The wavenumbers that were used 650 cm^{-1} to 4000 cm^{-1}.

3.4.2 Ultraviolet-Visible Solid Spectroscopy (UV-vis Spectroscopy)

The ultraviolet-visible spectroscopy solid Perkin Elmer model Lambda 750 was used to elucidate the effect of crystal structure of polymer with 275 to 380 nm of scanning wavelength. To estimate the optical band gaps, Tauc plots were constructed based on the equation:

$$(\alpha h\nu)^{n} = A(h\nu - E_g) \tag{3.1}$$

where α is the absorption coefficient, hν is the photon energy, A is a constant, E_g is the band gap energy, and n depends on the type of electronic transition. For allowed direct transitions, n=2n, which was applied in this study based on literature precedent for similar materials (Kumar *et al.,* 2019). Extrapolation of the linear portion of the *Tauc* plot to the energy axis (i.e., $(\alpha h\nu)^2 = 0$) yielded the band gap energies.

3.4.3 X-ray Diffractometer (XRD)

The crystallographic structure of WS_2, GO and WS_2/rGO composites was determined by using Empyrean X-ray diffractometer by keeping 2θ = 10° - 90° Cu Kσ

radiation (λ = 1.5418 A°). The crystallite size was then calculated by using Schererr equation as 3.2:

$$D = \frac{0.9\,\lambda}{\beta\,cos\,\theta} \tag{3.2}$$

where D is the crystallite mean size (nm), K is the crystallite form factor (a fair approximation is 0.9), λ is the X-ray wavelength, B is the X-ray diffraction peak's full width at half maximum (FWHM) in radians, and θ is the Braggs' angle (deg.) (Ingham & Toney, 2013).

3.4.4 Field Emission Scanning Electron Microscopy (FESEM)

FESEM technology was utilized to get a high-resolution surface morphology characterization of WS_2, GO, and WS_2/GO materials at the nanoscale. Using the FEI Nova NanoSEM 230 instrument, Field Emission Scanning Electron Microscopy (FESEM) was used to analyze the surface morphology of the synthesized photocatalysts. The samples were oven-dried at 60°C to eliminate any remaining moisture and guarantee sample stability during imaging. The preparation method allowed for high-resolution imaging of the surface morphology and structural features of the photocatalyst by carefully spreading a small amount of the dried sample onto carbon adhesive tape, which was affixed to an aluminium sample stub to provide a stable and conductive surface. A thin layer of gold (Au) or platinum (Pt) was applied using a sputter coater for about 30 to 60 seconds, creating a uniform conductive coating. The coated samples were then placed into the FESEM chamber, and imaging was conducted under high vacuum conditions, with the accelerating voltage set between 5 and 15 kV and the working distance maintained between 5 and 10 mm, depending on the desired magnification and resolution.

3.4.5 Raman Analysis

Raman spectroscopy analysis was carried out by using a Horiba Scientific to determine the vibrational and rotational analyses of the solid-state catalyst. In this investigation, the Jobin Yvon HR-800 Raman spectrometer was used to perform the Raman spectroscopy analysis. By combining this high-resolution equipment with a combination Photoluminescence (PL)-Raman system, it is possible to thoroughly characterize the electrical and vibrational characteristics of materials in a single benchtop setup. With sub-micron spatial resolution and sophisticated confocal mapping capabilities, the device enables accurate surface feature imaging and analysis. Its wide range of excitation wavelengths, which span from the ultraviolet (UV) to the near-infrared (NIR) spectrum, enables the depth of penetration into the sample to be adjusted according to the material's optical absorption properties.

3.4.6 Brunauer–Emmett–Teller (BET) Surface Area Analysis

The specific surface area and the pore distribution of prepared materials under different synthesis conditions was measured by using TriS-tar II 3020 surface area measurement instruments (Micromerit-ics Inc. USA) at 77 K following the BET method. The photocatalyst samples were degassed before being submitted to BET surface area analysis to remove any physically deposited gases and moisture that can compromise the precision of nitrogen adsorption measurements. Each powdered sample weighed between 0.1 and 0.2 grams, which were then transferred to a dry, clean sample tube. After that, the samples were degassed using a degassing apparatus for 12 hours at 150°C under vacuum. In addition to providing a clean surface for gas adsorption, this pre-treatment procedure guaranteed the removal of all volatile pollutants. To avoid exposure to outside air, the samples were promptly moved to the BET instrument's analysis port after degassing. To ascertain the photocatalyst's specific surface area, pore volume, and pore size distribution, nitrogen adsorption–desorption isotherms were subsequently examined at liquid nitrogen temperature (77 K). The BET equation was

used to determine the surface area, and the Barrett–Joyner–Halenda (BJH) method was used to estimate the distribution of pore sizes.

3.4.7 Photoluminescene Spectroscopy

Photoluminescence Spectroscopy (PL) is a contactless characterization technique that was quantified Shockley-Reed-Hall (SRH) lifetimes and recombination velocities in direct band gap experimental semiconductor materials and devices. The samples were sent to Universiti Teknologi Malaysia (UTM) for the PL analysis of GO, WS_2, and WS_2/GO-15.

3.5 Photocatalytic Measurement

3.5.1 Photocatalytic Degradation of TC Analysis

The photocatalytic performance of WS_2/GO-1, WS_2/GO-5 and WS_2/GO-15 were tested by degrading TC under the irradiation of 18-watt light emitting diode. All photocatalytic experiments were carried out in a photoreactor equipped with multiple quartz tube reactors. In a typical photocatalytic experiment, 10 mL from 20 mg/L stock solution was added into a beaker that contained 0.02 g of WS_2/GO (different percent (%) value, which are 1%, 5% and 15%) composites. Then, it was continuously stirred in the dark for 30 minutes to ensure the establishment of adsorption/desorption equilibrium, 10 mL, 20 mg/L (C_o) of each solution was pipetted out and put in a UV photoreactor at the starting point (t = 0) which the maximum wavelength (λmax) 210nm. Lastly, the solutions were centrifuged and filtered to remove the nanocomposites. During the photocatalytic degradation reaction, the concentration of TC was monitored by measuring the absorbance of the solution samples using UV-Vis Spectroscopy. From the measured absorption of TC for each sample, the C/C_o ratio was calculated where C_o is the concentration of TC at t = 0 and C is the concentration of TC at a specified time.

3.5.2 Screening Study

All the synthesized composites were screened to determine the suitable conditions source of light and the optimum weight of photocatalyst for the degradation of TC. The 10 mL of 20 mg/L TC was added into beakers that contain 0.02 g of different weight ratios of WS_2/GO under dark and visible light conditions (LED, fluorescent, and UV light irradiation). In another beaker, 10 mL of TC was added and act as a blank or control. All the solution were stirred in the dark for 30 minutes to reach adsorption – desorption equilibrium before being exposed with light emitting diode (LED) for 1 hour in visible light. Next, all the solution was centrifuged, filtered and analysed by using UV-Vis spectroscopy in UV region ranges of TC from 275 until 380 nm.

3.5.3 Response Surface Methodology (RSM) with Box-Behnken Design (BBD)

Response Surface Methodology (RSM) was used in this work to maximize the photocatalytic breakdown of TC utilizing a WS_2/GO-15 nanocomposite when exposed to visible light from LED. When a response is influenced by several independent factors, RSM are noted as a potent statistical tool for modelling and analysis particularly for process optimization with fewer experimental trials. Because it fits quadratic models well and doesn't need extreme combinations of component values, a Box-Behnken Design (BBD) was utilized for this investigation. For photocatalytic optimization studies, BBD is perfect since it is rotatable (or almost rotatable) and need less runs than a central composite design as the number of components rises. Design-Expert software (version 13, Stat-Ease Inc., Minneapolis, USA) was used to create the design as shown in Figure 3.2, which had three independent variables that varied at three coded levels (-1, 0, +1):

A: Amount of dosage (g)
B: Potential of hydrogen (pH)
C: Initial concentration (ppm)

The response variable was the percentage of TC under LED irradiation, as measured by UV–Vis spectrophotometric measurement at the maximum absorbance wavelength (λ_{max} = 380 nm).

Analysis of Variance (ANOVA) was used to assess the model's and its terms' significance. Using the coefficient of determination (R^2), adjusted R^2, projected R^2, and lack-of-fit test, the model's adequacy was evaluated. Surface plots and contour plots in three dimensions were created to show how the factors affected the answer. Using the WS_2/GO-15 photocatalyst, this method made it easier to identify the ideal conditions for maximal TC degradation and gave a thorough knowledge of how factors interact.

Table 3.1
Table Design of RSM with BBD

Standard	Run	Space Type	Factor 1 A: Amounts of dosage (g)	Factor 2 B: Potential of hydrogen (pH)	Factor 3 C: Initial concentration (ppm)	Response 1 Degradation (%)
4	1	IBFact	0.04	9	12.50	58.93
11	2	IBFact	0.03	3	20.00	10.32
5	3	IBFact	0.02	6	5.00	96.05
13	4	Center	0.03	6	12.50	60.82
10	5	IBFact	0.03	9	5.00	95.92
1	6	IBFact	0.02	3	12.50	42.01
6	7	IBFact	0.04	6	5.00	96.77
7	8	IBFact	0.02	6	20.00	33.80
15	9	Center	0.03	6	12.50	60.82
8	10	IBFact	0.04	6	20.00	41.63
9	11	IBFact	0.03	3	5.00	80.90
2	12	IBFact	0.04	3	12.50	43.14
17	13	Center	0.03	6	12.50	60.82
16	14	Center	0.03	6	12.50	60.82
14	15	Center	0.03	6	12.50	60.82
3	16	IBFact	0.02	9	12.50	51.48
12	17	IBFact	0.03	9	20.0	12.34

3.5.4 Effect of pH

The pH value of the solution, which can change the net charge of the photocatalyst and the target pollutant, is one of the most critical parameters to investigate. The effect of pH value on the TC removal ratios was studied with an initial TC concentration of 20 mg/L in a pH range of 2.0-10.0 and adjust by HCl or NaOH at 25°C. Then, each composite was added to the adjusted pH solution and sonicated for 30 minutes. Then, the mixture solution was poured into a glass cuvette and put in UV photoreactor for the photocatalytic degradation process. Lastly, the solutions were centrifuged, and the absorbance of clear supernatant solution (clear liquid) were measured using UV-Vis spectroscopy in UV region ranges from 275 until 380 nm.

3.5.5 Amount of Loading

Firstly, 20 mg of all the composites was weighed by using analytical balance. After that, 20 mg/L of TC was produced via direct dilution from stock solution and 10 ml of the TC was poured into three beakers. Each beaker was contained 10 ml of TC, and the pH was adjusted to the best pH by adding some NaOH or HCl. Then, the composites that have been weighted before it was added into each beaker and sonicated for 30 minutes. Next, the mixture solution was poured into a glass cuvette and stored in UV photoreactor for the photocatalytic degradation process. Lastly, the solutions were filtered using centrifuged to remove out the composites and absorbance of clear supernatant solution (clear liquid) was measured using UV-Vis spectroscopy in UV region ranges from 275 until 380 nm. The photocatalyst was evaluated for its photocatalytic activity by using different amounts of it and 50 mg/L of TC was added into.

3.5.6 Effect of Contact Time

The effect of contact time on the degradation of TC was investigated in the time range of 0-180 minutes. Firstly, 10 mL from 20 mg/L stock solution was added into a

beaker that contains the best pH and amount of loading of WS_2/GO (different percent (%) value, which is 1%, 5% and 15%) composites. The solution was placed in the UV photoreactor for the photocatalytic degradation process. After each 30 minutes interval, the solutions were filtered by using a syringe filter and the absorbance was measured by using UV-Vis detection in the UV region that are ranges between 275 to 380 nm.

Extensive studies on heterogeneous photocatalysts in organic pollutants photodegradation have demonstrated that the result is consistent with the Langmuir-Hinshelwood (L-H) kinetic model (Eq. 3.3):

$$ro = -\frac{dC}{dt} = \frac{kKC}{1 + KC} \tag{3.3}$$

where C is the reactant's concentration, ro is the reactant's degradation rate, k is the reaction rate constant, and K is the adsorption equilibrium constant. Given the low concentration of TC antibiotics used in the experiment, Kc < < 1 in the L-H equilibrium may be reduced to a pseudo-first-order kinetic model (Eq. 3.4):

$$-\frac{dC}{dt} = kKc = k_{obs}C \tag{3.4}$$

Further set the limit of C = GO at t = 0, the Eq. 3.4 can be integrated, which results in (Eq. 3.5):

$$-Ln\ \frac{C}{C_o} = k_{obs}t \tag{3.5}$$

3.5.7 The Photodegradation Efficiency

The absorption of TC was observed and measured for each sample and the degradation of TC of each sample was calculated by using the formula:

$$\text{Degradation of TC (\%)} = 1\text{-}C/(C_{\circ}) \times 100 \tag{3.6}$$

where $C_{\circ}$ is the concentration of TC at t = 0 and C is the concentration of TC at t.

3.5.8 Analytical Procedure

TC antibiotic concentration has been measured in this study utilizing ultraviolet-visible (UV-Vis) spectroscopy, which is based on the antibiotics' distinctive absorbance in the UV region, which typically ranges between 275 to 380 nm. This procedure entails serially diluting a TC stock solution (20 mg/L) with distilled water to create a number of standard solutions. Solid samples must be dissolved in the proper solvent, filtered through a 0.45 µm membrane filter, and the absorbance must be within the calibration curve's linear range. Absorbance measurements of standard and sample solutions are taken at the chosen wavelength, usually close to 360 nm, after a UV-Vis spectrophotometer has been calibrated using a blank solution. The sample concentrations are calculated using interpolation and plotting of a calibration curve. Assuring linearity ($R^2 > 0.99$), checking for recovery rates (90–110%) in spiked samples, and verifying repeatability (relative standard deviation <5%) are examples of quality control procedures. Recovery studies, repeated measurements, and blank sample analysis are used to confirm the approach and guarantee accuracy. Environmental rules are followed while disposing of garbage, and appropriate safety measures are followed, such as using gloves and safety eyewear. TC quantification using this UV-Vis spectroscopic technique is dependable and repeatable, which makes it appropriate for analytical uses in environmental and pharmaceutical research.

3.5.9 Reusability Study

Reusability studies were conducted to determine the possibilities for reutilizing and regeneration of photocatalysts. The photocatalyst (0.02g) was recycled after being washed with methanol and water and then dried in the oven at 70˚C for 12 hours. The recycled photocatalyst was further confirmed the changes on the surface area by using FTIR analysis.

3.5.10 Real Sample Analysis

Real sample analysis was conducted to determine the efficiency of the optimization photocatalysts to degrade TC. The real samples were collected from the river, sea, lake, and tap water that are near to the industrial effluents around Negeri Sembilan. The real sample water such as river, sea, lake and tap water was spiked with 20 mg/L of TC. Then, the mixture was poured into a glass cuvette and stored in UV photoreactor for the photocatalytic degradation process. Lastly, the solutions were centrifuged and filtered to remove out the nanocomposite and the absorbance of clear supernatant solution (clear liquid) was measured using UV detection at the maximum wavelength (λ_{max}) of 210 nm.

CHAPTER 4
RESULTS AND DISCUSSION

4.1 Characterization of Photocatalysts

Figure 4.1 displays the FTIR spectra for GO, WS_2, and WS_2/GO composites. The O-H stretching vibrations, which are indicative of the hydroxyl groups frequently found in graphene oxide, are shown by the conspicuous peak in the GO spectrum at 3328 cm^{-1}. Furthermore, carbonyl (C=O) stretching, C=C stretching of the graphitic domains, and C-O stretching are responsible for the distinctive absorption bands at 1732 cm^{-1}, 1583 cm^{-1}, and 1044 cm^{-1}, respectively. These bands demonstrate graphene's oxidation, which produces a variety of functional groups that include oxygen. The in-plane vibrations of sulphur atoms (S-S bonds) inside the WS_2 layers, on the other hand, are linked to the notable peaks at 657 cm^{-1} and 739 cm^{-1} in the FTIR spectrum of WS_2 (Figure 4.1 (b)). These peaks reveal information about the structural integrity of WS_2 and are typical of its hexagonal phase.

The effective integration of WS_2 onto the GO sheets is demonstrated by the WS_2/GO composite spectrum (Figure 4.1(c) - 4.1(e)), which displays a mixture of the peaks seen in both GO and WS_2. In particular, the sulphur-related peaks from WS_2 and the O-H (3200-3600 cm^{-1}), C=O (1741 cm^{-1}), and C-O (1047 cm^{-1}) extending from GO show that the WS_2/GO hybrid material is effectively formed. This implies that both the structural characteristics of WS_2 and the functional groups of GO are retained in the composite material, which is essential for improving its photocatalytic capabilities. Between WS_2/GO-1, WS_2/GO-5 and WS_2/GO-15, WS_2/GO-1 and WS_2/GO-5 showed a smooth and broad characteristics of O-H than WS_2/GO-15. Therefore, these photocatalysts were study thoroughly in order to conclude whether having a smooth and broad O-H characteristic does impact towards its degradation performances and efficiency.

In addition, several peaks of S-S bonds (739 cm^{-1}), C=O stretching (1741 cm^{-1}), and O-H (3200-3600 cm^{-1}) in the WS_2/GO spectrum may have shifted or broadened in comparison to their original components, which may indicate substantial interactions between the WS_2 and GO layers which possibly via chemical bonding or van der Waals

forces. These interactions enhance the efficiency of electron transfer and charge separation when exposed to visible light.

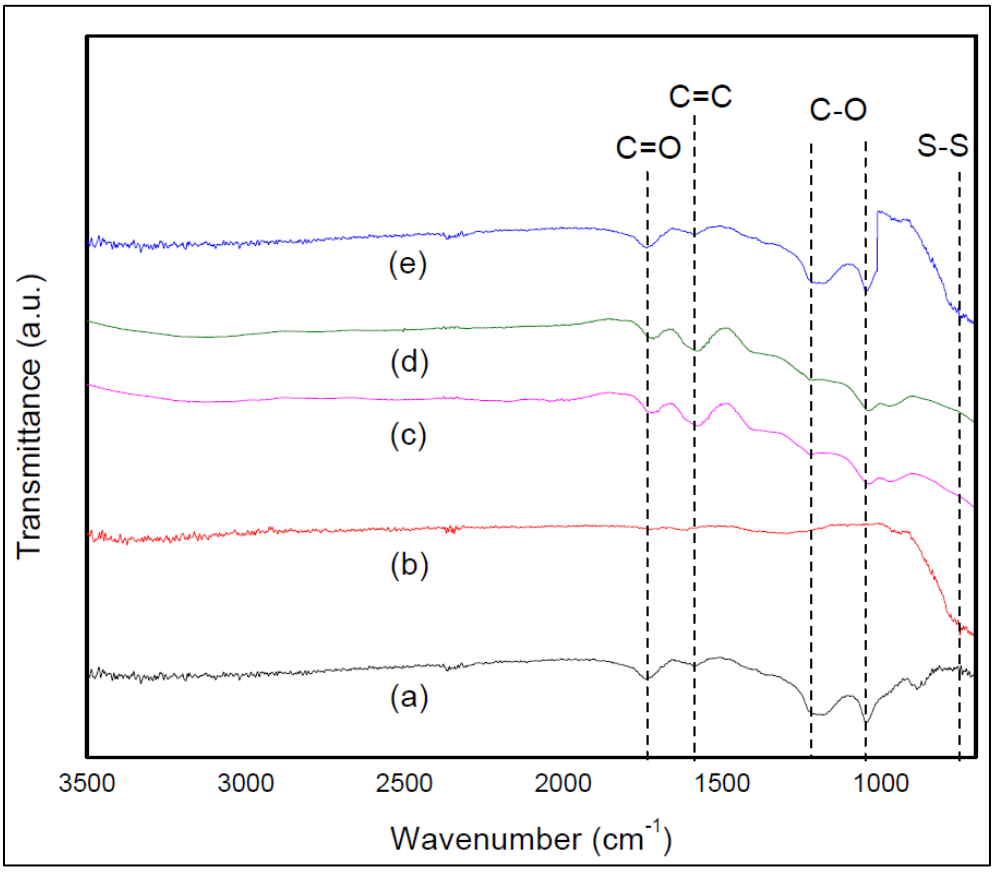

Figure 4.1 FTIR Spectrum for (a) Graphene Oxide (GO), (b) Tungsten Disulphide (WS_2), (c) 1% Tungsten Disulphide/Graphene Oxide (WS_2/GO-1), (d) 5% Tungsten Disulphide/Graphene Oxide (WS_2/GO-5), and (e) 15% Tungsten Disulphide/Graphene Oxide (WS_2/GO-15).

4.1.1 XRD

XRD patterns displays in Figure 4.2, provide the atomic arrangement and phase composition on the crystalline structures of GO, WS_2, and WS_2/GO composites. Because graphene oxide has an uneven layer stacking and disorder brought on by oxidation (Yadav *et al.,* 2022), the wide peak in its XRD pattern indicates an amorphous structure. WS_2, on the other hand, exhibits distinct crystalline peaks at 2θ values of 14.3˚, 15.5˚, 23.8˚, 28.5˚, 37.2˚, and 43.2˚, which correspond to the (002), (002), (004), (100), and (103) planes individually. The WS_2 present is in its hexagonal phase is confirmed by the fact that these peaks correspond well with the standard JCPDS Card No. 08-0237.

In addition, WS_2/GO-5 (Figure 4.2 (d)) showed an additional peak at 38.5˚ which correspond to the (103) plane. This peak indicated that the WS_2 nanoparticles may be well distributed and sufficiently crystalline and allowing the (103) plane to diffract clearly. While the WS_2/GO-1 and WS_2/GO-15 missing this diffract peak could be due to 1% of WS_2 amount of loading is too little that make the diffraction intensity is below the detection limit and 15% of WS_2 amount of loading may be too much and making the WS_2 nanoparticles to aggregate and reduce its visibility of specific relations.

Good crystallinity and layered development are reflected in the (002) peak at 15.5˚, which is very sharp and shows that WS_2 produces well-ordered layers along the c-axis (Shin *et al.,* 2020). A characteristic of WS_2 layers, the interlayer spacing (D-spacing) for the (002) plane is determined to be 2.24 nm. The WS_2/GO composite likewise exhibits this clear peak, indicating that WS_2 was successfully incorporated into the GO matrix and that single or few-layer WS_2 nanosheets were present in the composite. Additionally, the (002) plane of GO, which represents its layered structure, corresponds to the typical GO peak at $2\theta = 10.1°$. The GO peaks' prominence in the WS_2/GO composite's XRD pattern suggests that the hybrid material has a greater GO to WS_2 ratio. The fact that both materials maintain their structural identities in the composite, is confirmed by the presence of the characteristic WS_2 peaks.

In contrast to pure WS_2, which has a crystallite size of 8.34 nm, the addition of GO to the WS_2 matrix causes the crystallite size to decrease to 3.6 nm, as shown by the wider XRD peaks in the WS_2/GO pattern. The entire dispersion of GO sheets inside the composite is responsible for this drop in crystallinity because it disrupts the normal stacking of WS_2 layers and decreases the size of the crystallites overall. The crystallite size (D) was calculated using the Scherrer equation (Eq.4).

The reduced crystallinity of WS_2/GO composite should boost its photocatalytic activity by improving charge separation and the interaction between light-induced carriers and the target molecules. This will ultimately increase the production of reactive oxygen species, which will aid in the effective degradation of pollutants (Zhang *et al.,* 2016).

In addition, the crystallite size, structural order, and photocatalytic performance of the final material are all significantly influenced by the composition ratio of WS_2 in WS_2/GO composites. It has been demonstrated that variations in WS_2 loading, such as 1%, 5%, and 15% of WS_2 amount of loading, affected the degree of WS_2 layer stacking, crystallinity, and dispersion on the GO surface. Better interaction and electrical

connection between the two components are encouraged by WS_2's tendency to spread more evenly throughout the GO sheets at lower concentrations for example with 1% of WS_2. This can increase defect density and improve photocatalytic reactivity by decreasing crystallite size because of hindered crystal development (Jiang *et al.,* 2020). According to Zhang *et. al.,* (2021), larger crystallites and less surface area accessible for photocatalytic interactions might arise from agglomeration, which is more likely to occur when the WS_2 concentration rises. Moreover, there is an ideal WS_2 content, which is typically around a 1:1 or 2:1 weight ratio with GO. At this content, enhanced electron transfer and light-induced charge separation are accomplished without sacrificing material dispersion and surface exposure (Adewuyi *et al.,* 2022).

Additionally, research has shown that too much WS_2 can cause layers to restack or re-crystallize, which lowers interfacial contact and limits light penetration, which reduces photocatalytic activity (Wang *et al.,* 2023). Overall, as it directly affects crystallite size, structural strength, and efficiency in applications like photocatalytic pollution degradation, managing the WS_2/GO ratio is essential for customizing the composite's physicochemical features.

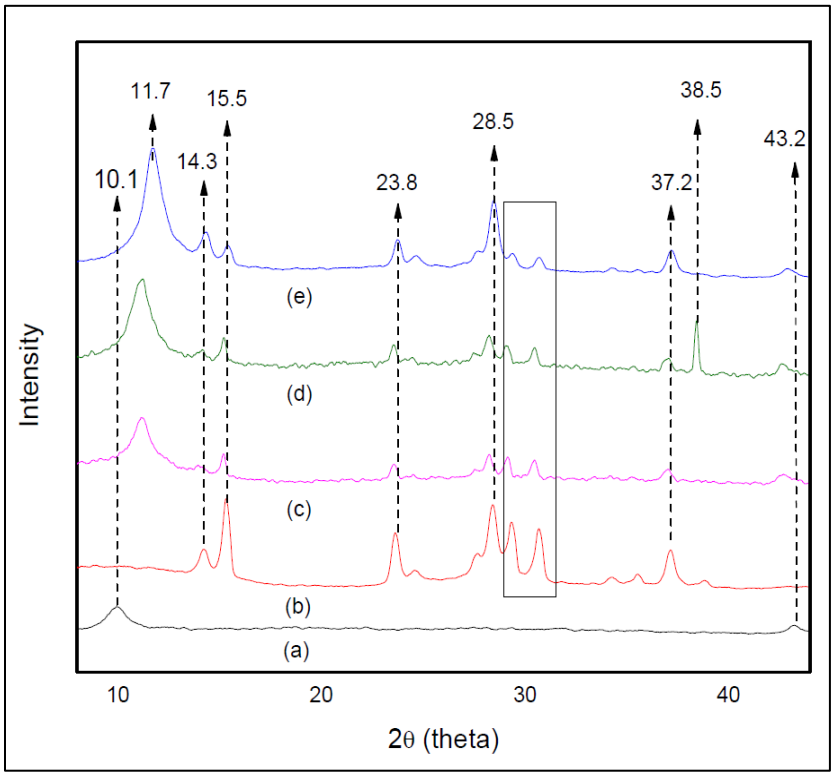

Figure 4.2 XRD Spectrum of (a) GO, (b) WS_2 (c) WS_2/GO-1, (d) WS_2/GO-5, and (e) WS_2/GO-15 Composites.

4.1.2 Photoluminescence (PL)

The optical and electrical characteristics of GO, WS_2, and the WS_2/GO-15 composite are significantly revealed by their photoluminescence (PL) spectra. Photons with energies exceeding the band gap move electrons from the valence band (VB) to the conduction band (CB), leaving holes in the VB. This process is known as photoluminescence (PL). Both radiative and non-radiative relaxation of these excited electrons in the CB can result in energy output or dissipation.

Since the photon energy emitted during radiative recombination is closely connected to the band gap energy of the material, it provides a clear indication of the electronic structure. Details on the material's fault density and structural quality may be found in the PL spectrum's intensity, line edge, and full width at half maximum (FWHM) of the emission peak. A greater FWHM indicates less crystallinity or structural integrity, while a higher PL intensity indicates fewer defects. A larger density of defect states is often indicated by a wider emission peak in the PL spectrum. These states can serve as charge trapping centres and lower the recombination rate, both of which are critical for enhancing photocatalytic performance (Zhang *et al.,* 2021).

The PL peak in Figure 4.3 for GO is located at 565 nm (2.21 eV) and is associated with radiative recombination of electron-hole pairs (Ikram *et al.,* 2020). The energy of the photons that are released is near the band gap energy. Oxygen-containing functional groups contribute to the high energy emission by introducing localized band gap energies and defect states. Given the importance of these oxygen functional groups in the recombination process, the comparatively high intensity of the PL signal indicates that GO has a moderate density of deficiencies (Das *et al.,* 2024).

Meanwhile, as seen in Figure 4.3, WS_2 displays a PL peak at 587 nm (2.08 eV), which is characteristic of its semiconducting nature with a direct band gap. Radiative recombination, in which the excitons (bound electron-hole pairs) in WS_2 relax and release photons, is indicated by the high PL emission. A low defect density and well-ordered crystalline structure in WS_2 are suggested by the sharp and strong peak. Depending on the defect density and crystallinity of the material, the rapid relaxation of electrons in the CB (within 15–25 ps) might happen non-radiatively through phonon interactions or radiatively, producing photons.

Furthermore, in between the peaks of pure WS_2 and GO, the WS_2/GO-15 composite exhibits a PL peak at 581 nm (2.13 eV) as shown in Figure 4.3. A significant

interaction between WS_2 and GO, which promotes charge transfer between the two materials, is shown by this shift in emission energy. The lower energy in comparison to GO implies that the band structure is altered by the electrical connection between WS_2 and GO, improving charge separation and electron mobility.

Compared to pure WS_2, the PL intensity of the WS_2/GO-15 composite is lower, suggesting a larger defect density or photogenerated electron-hole pairs recombine without emitting photons (Yu *et al.,* 2023). This can be explained by the dispersion of GO in the composite, which might provide more non-radiative recombination routes, like phonon emission-based SRH recombination. Additionally, because GO interferes with the normal stacking of WS_2 layers, the FWHM of the WS_2/GO-15 composite may expand in comparison to pure WS_2, revealing a more disordered structure. Because of the electron transport between WS_2 and GO, the WS_2/GO-15 composite has lower recombination rates and effective charge separation, which are advantageous for photocatalytic applications. Pollutant degradation under visible light is made possible by the composite structure's improved migration of photo-induced carriers to the material's surface, which improves photocatalytic activity.

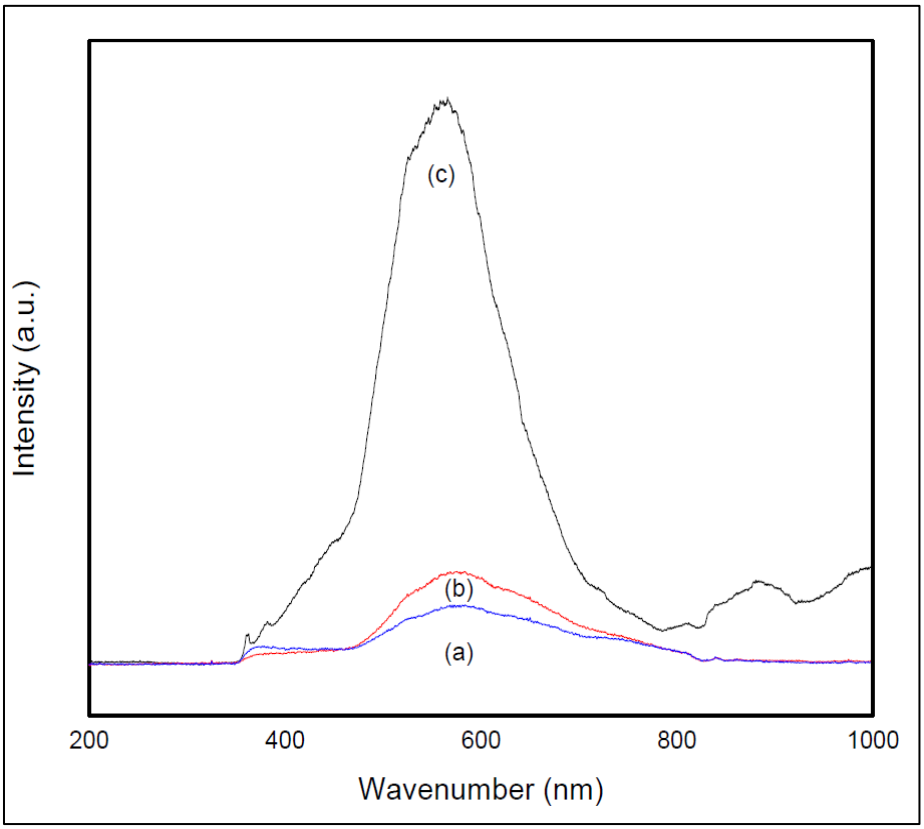

Figure 4.3 Photoluminescence (PL) Peaks of (a) WS_2/GO-15 (581 nm), (b) WS_2/GO (587 nm), and (c) GO (567 nm).

4.1.3 Raman Spectroscopy

The Raman spectra shown in Figure 4.4 give important information on the structural and vibrational characteristics of WS_2 and GO, emphasizing their salient characteristics and their relationship to the quality and behaviour of the material.

The most noticeable peak in the Raman spectra for WS_2 is located at around 355 cm^{-1} is associated with the $E^1{}_2g$ mode, which deals with the in-plane vibrations of sulphur atoms in relation to tungsten atoms (Rajeswaran *et al.,* 2023). This peak is a key sign of the material's structural integrity and is typical of WS_2's crystalline, layered structure. In addition, usually seen around 425 cm^{-1}, the A_1g mode is another prominent peak in the Raman spectra. This mode, which is a crucial indicator of the material's stacking and layer thickness, displays the out-of-plane vibrations of sulphur atoms. Because the vibrational characteristics vary as material thickness rises, the A_1g mode tends to shift with the number of layers in WS_2, with thicker samples exhibiting a little redshift in comparison to thinner layers or monolayers.

Two further peaks in WS_2 composite can be seen in the Raman spectra at about 823 cm^{-1} and 955 cm^{-1}. These are probably connected to the layer breathing modes of WS_2. These modes, which include the collective vibrations of the tungsten disulfide layers, offer important insights on the material's overall stacking order and interlayer interactions. W-S bond stretching vibrations may also be present in these peaks, suggesting both symmetric and asymmetric stretching modes. Comprehending these vibrations aids in evaluating the bonding properties and layered structure of the material, both of which are critical to its performance in a variety of applications, including as catalysis and optoelectronics.

Next, as can be seen in Figure 4.4, the Raman spectra of GO also show significant peaks. The D band appears at around 1352 cm^{-1}, while the G band appears at 1597 cm^{-1}. When assessing the defect density and structural quality of materials generated from graphene, these bands are essential. The E_2g phonon mode of sp^2 carbon atoms, which is linked to the G band, is responsible for the in-plane stretching of carbon-carbon bonds in graphene's hexagonal lattice. A larger concentration of sp^2 carbon atoms and a more organized graphitic structure are indicated by a more intense and well-defined G band, which gives information on the degree of graphitization of GO (Sim *et al.,* 2022).

Conversely, the D band is linked to chaos and structural flaws in the graphene lattice. It originates from the breathing mode of A_1g symmetric k-point phonons, which is triggered by sp^3-hybridized carbon atoms, edges, and vacancies. The degree of disorder in the GO is reflected in the D band's intensity; a higher D band intensity denotes a higher defect density. A popular criterion for evaluating the quality of GO is the ratio of the D and G band intensities; a greater ratio denotes more structural flaws and less graphitization. Further information about the structural order may also be gleaned from the full width at half maximum (FWHM) of the D and G bands; a wider FWHM indicates a higher degree of disorder and a less crystalline material.

Key characteristics of GO and WS_2 are combined in the Raman spectrum of the WS_2/GO-15 composite, indicating a good integration of the two materials. However, the presence of distinctive WS_2 peaks, of A_1g and E^1_2g modes which is associated with the out-of-plane vibration of sulfur atoms were much reduced or entirely vanished in the WS_2/GO composite. This phenomenon happens could be due to low Raman activity or a change in vibrational modes that might result from the strong interfacial contact between WS_2 and GO, which includes van der Waals forces and potential charge transfer (Sahu *et al.,* 2016). According to Staiger *et al.* (2015), the addition of GO may also cause strain, exfoliation, or structural instability in WS_2 layers, which would disturb the periodic lattice arrangement and diminish or eliminate the Raman-active modes. In addition, the D and G bands, located at 1352 cm^{-1} and 1597 cm^{-1}, respectively, would dominate the Raman spectra of GO itself. Particularly if the composite's WS_2 content is very low, these strong and wide signals may obscure the lower WS_2 peaks (Kumar *et al.,* 2020).

Any alteration in the I_D/I_G ratio or widening of the D and G bands in the composite material may indicate more disorder brought on by WS_2 and GO interactions (Goldie *et al.,* 2020). When creating such a composite, some increase in defects is anticipated since the functionalization of GO, which improves its interaction with WS_2, inherently creates certain structural flaws. Nonetheless, because it can promote charge transfer, which is advantageous for processes like photocatalysis, this degree of disorder is usually tolerated. It indicates that the faults stay within a suitable range, allowing the composite to maintain its functional qualities, provided that the D band intensity isn't too high. The WS_2/GO-15 composite has been effectively synthesized with a balance of structure and defectiveness, according to the Raman data, which suggests that it would

likely perform well in applications that depend on effective light absorption and charge transfer.

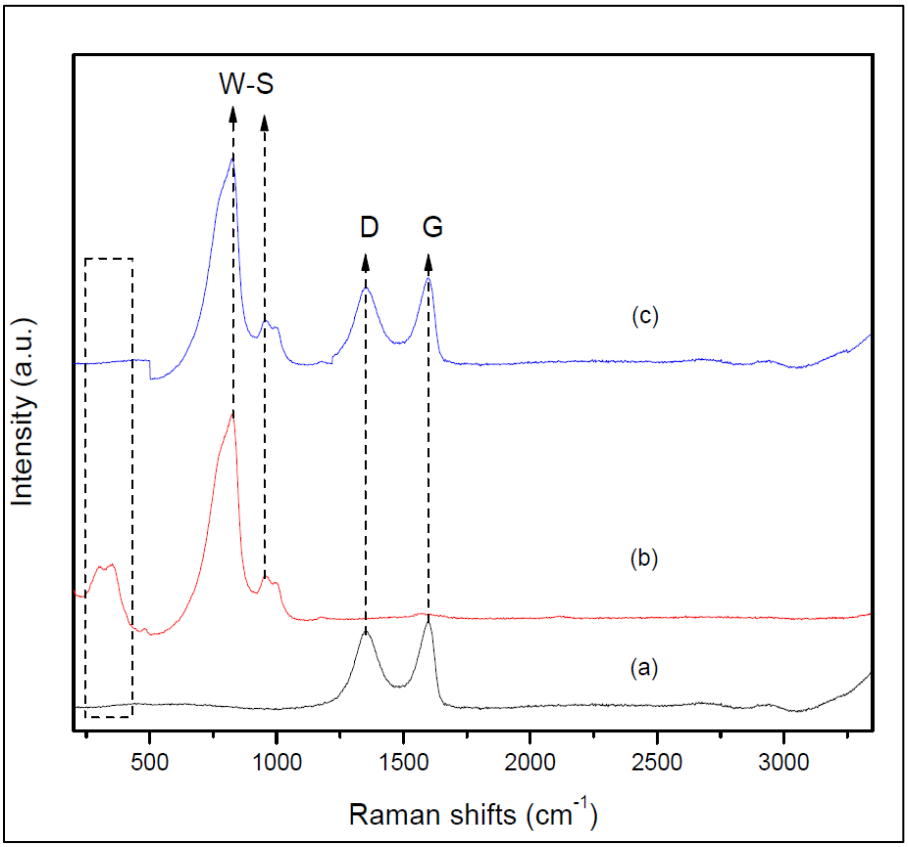

Figure 4.4 Raman Spectroscopy of (a) GO, (b) WS_2, and (c) WS_2/GO-15.

4.1.4 Field Emission Scanning Electron Microscopy (FESEM)

The morphological features of GO, WS_2, and WS_2/GO-15 that are crucial to their functional capabilities are revealed by the Field Emission Scanning Electron Microscopy (FESEM) investigation. Successful exfoliation and the presence of oxygen-containing functional groups are indicated by the characteristic sheet-like structure and crumpled and wrinkled morphologies seen in the Figure 4.5 (a) and (b). According to Kröner & Hirsch, (2020), these wrinkled structures result from oxygen functions disrupting the sp^2 hybridized carbon network, which prevents GO sheets from completely restacking and increases their surface area. Since the thin, transparent sheets that have been found attest to GO's nanoscale nature, it can be used in energy storage, catalysis, and sensing applications.

Next, the layered architecture of transition metal dichalcogenides (TMDs), is characterized by ultrathin, sheet-like structures with distinct edges, as shown in the Figure 4.5 (c). Since van der Waals interactions between layers are a frequent characteristic in TMDs, the high-resolution micrographs show a rather uniform dispersion of WS_2 nanosheets with some degree of aggregation (Chhowalla *et al.,* 2013).

In addition, as shown in Figure 4. 5 (a) and (b), WS_2 and GO are successfully integrated throughout the synthesis process of the WS_2/GO-15 nanocomposite. The micrographs corroborate the strong contacts between the two materials by showing a well-distributed mixture of WS_2 nanosheets scattered throughout the GO matrix. While the WS_2 nanosheets look equally fastened onto the GO sheets, limiting considerable restacking, the GO sheets maintain their distinctive wrinkled and layered architecture. Wrinkled and layered nanosheets indicate WS_2's flexibility, which is advantageous for its uses in tribology and flexible electronics. Both GO and WS_2's unique morphological characteristics attest to their applicability for a variety of uses, such as energy conversion, storage, and catalysis, where large surface area and nanoscale roughness are essential for improving performance (Wang *et al.,* 2012).

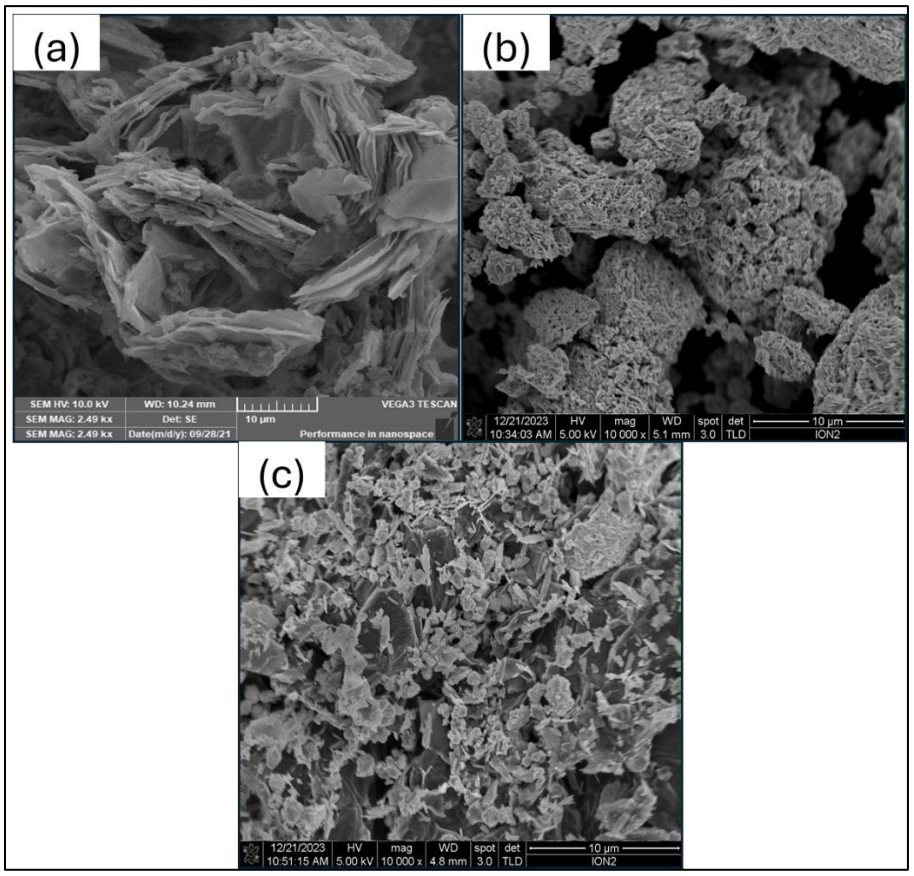

Figure 4.5 Morphology of (a) GO, (b) WS_2, and (c) WS_2/GO-15.

4.1.5 Brunauer-Emmett-Teller (BET) Surface Area Analysis

Brunauer-Emmett-Teller (BET) analysis was used to determine the surface area of the photocatalysts GO, WS_2, and WS_2/GO-15 composites using adsorption and desorption isotherms with nitrogen as the analytical gas. According to the BET classification, the adsorption-desorption isotherms for WS_2 and WS_2/GO-15 composites that were produced were categorized as TYPE H4, as illustrated in Figure 4.6. This kind of isotherm is convex in relation to the x-axis across its whole range and shows hysteresis, which is a characteristic of mesoporous materials with pore diameters between 2 and 50 nm.

Table 4.1 provides a summary of the surface area analysis properties of GO, WS_2, and WS_2/GO-15. It was discovered that GO's specific surface area varied between 2 and 1000 m^2/g (S. Zhang *et al.,* 2019). This large variation is explained by GO's propensity to group together when it dries, which results in a substantially smaller surface area than would be expected theoretically. Nonetheless, it is known that GO may be completely exfoliated and distributed uniformly, which is essential for

optimizing its performance in composite materials. The specific surface area of WS_2, according to the research that is currently accessible, ranges from 5.00 to 20.00 m^2/g (Dai *et al.,* 2017). The results demonstrate that the specific surface area of WS_2/GO-15 is larger than that of either GO or WS_2 alone, indicating that the combination of WS_2 and GO efficiently decreases the restacking of WS_2 layers and the graphene layers.

The specific surface area of the composite rises after WS_2 is intercalated into the GO matrix, despite the tendency of GO and WS_2 nanoparticles to combine, which normally reduces their total surface area. By increasing the number of active sites and enhancing the reactant adsorption transport route, this surface area boosts photocatalytic activity. A more compact and synergistic interaction between WS_2 and GO is suggested by the observed decrease in pore size of the WS_2/GO-15 composites, which also shows that the pores between the materials are filled and integrated. This, in turn, leads to improved material properties for photocatalytic applications.

According to these BET results, the WS_2/GO-15 composite enhances its photocatalytic activity by offering the ideal ratio of surface area to porosity. Better pollutant adsorption is encouraged by the larger surface area, and more effective charge carrier movement within the photocatalyst structure may result from the smaller pore size and volume. Additionally, the compact structure of WS_2/GO-15 could enhance electron mobility, lower recombination rates, and eventually boost TC photocatalytic degradation.

The necessity to assess the extreme instances within the series of synthesized materials led to the choice to perform BET analysis exclusively on GO, WS_2, and WS_2/GO-15. While GO and WS_2 are used as reference materials to comprehend their respective contributions, the WS_2/GO-15 composite shows the greatest WS_2 loading and sheds light on how WS_2 integration affects the composite's surface characteristics. Their BET characterisation was not given priority in this investigation since lesser WS_2 loadings (1% and 5%) are anticipated to show intermediate surface properties between GO and WS_2/GO-15 (Liu *et al.,* 2020).

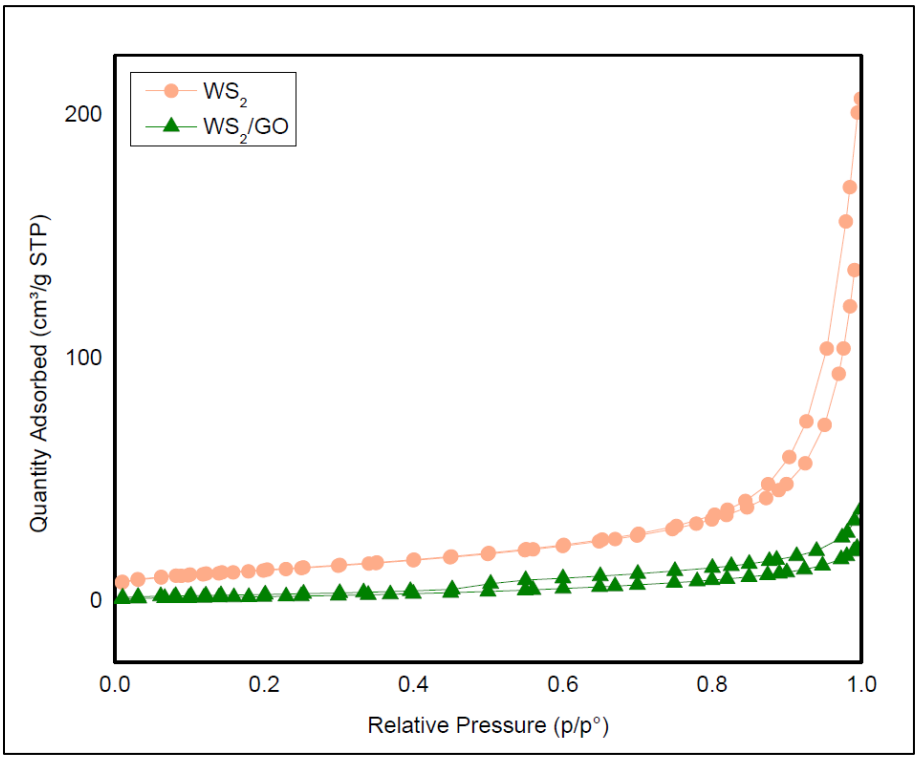

Figure 4.6 Hysteresis Loop of Nitrogen Adsorption Isotherm of WS_2 and WS_2/GO-15 Nanocomposite.

Table 4.1
Surface Area Analysis of GO, WS_2, and WS_2/GO-15 Composites.

Materials	**BET Surface Area (m^2g^{-1})**	**Pore size (nm)**	**Pore Volume (cm^3/g)**
GO	2.5090	15.6349	0.0122
WS_2	1.2119	6.0231	0.0122
WS_2/GO-15	7.8637	5.6977	0.0018

4.1.6 Ultraviolet-visible (UV-Vis) Analysis

The UV-Visible (UV-Vis) spectroscopy is frequently used to examine the optical characteristics and electronic transitions in nanomaterials. GO, WS_2, and WS_2/GO-15 composite were evaluated for light absorption behaviour and optical band gap energies by using UV-Vis spectroscopy. To assess a material's photocatalytic efficiency, it is essential to comprehend its band gap, which establishes the minimal energy needed to excite an electron from the valence band to the conduction band and start photocatalytic reactions when exposed to light (Suyuan *et al.,* 2022).

Figure 4.7 presents the UV-Vis absorption spectra of GO, WS_2, and WS_2/GO-15. With a sharp peak at about 230 nm and a shoulder at about 300 nm, graphene oxide showed a noticeable absorption peak in the UV range. These peak and shoulder correspond to $\pi \rightarrow \pi^*$ transitions of aromatic C=C bonds and $n \rightarrow \pi^*$ transitions of C=O bonds, respectively (Zhang *et al.,* 2010). Strong absorption was seen in both the visible and UV spectrums for WS_2, with a discernible absorption edge suggesting that it is semiconducting.

The determined optical band gaps for GO, WS_2, and the WS_2/GO-15 composite were 3.26 eV, 3.27 eV, and 3.19 eV, respectively. The comparatively broad band gap of pure WS_2 (3.27 eV) is consistent with previous findings for exfoliated or few-layered WS_2 nanosheets, which, as a result of quantum confinement phenomena, often show wider band gaps than bulk WS_2 (Chhowalla *et al.,* 2013). In its highly oxidized form, when the sp^2 carbon lattice is disrupted and electronic delocalization is lost, the band gap of graphene oxide (3.26 eV) similarly reflects this condition (Eda *et al.,* 2010).

Crucially, the band gap of the WS_2/GO-15 composite was somewhat less (3.19 eV) than that of its constituent parts. The development of a heterostructure that promotes charge transfer between WS_2 and GO is responsible for this decrease. In order to improve visible light absorption and decrease the energy threshold for excitation, the interaction between the layered structure of WS_2 and the π-electron system of GO probably encourages greater separation of photo-generated charge carriers (Zhou *et al.,* 2020). The reduction of the band gap suggests an enhancement in the light-harvesting capabilities of the composite, which is useful for photocatalytic applications such as the destruction of organic contaminants.

Because a reduced band gap not only permits absorption of a wider spectrum of visible light but also improves the production and mobility of charge carriers, this

synergistic interaction is crucial for enhancing the photocatalytic performance of the WS_2/GO-15 composite (Liu *et al.,* 2021). These results are in line with other studies that found improved optical and electrical characteristics when transition metal dichalcogenides (TMDs) were integrated with graphene-based materials (Wang *et al.,* 2015).

In conclusion, the WS_2/GO-15 composite's enhanced light absorption and narrowed band gap were validated by UV-Vis analysis, underscoring its promise as an effective visible-light-driven photocatalyst. It is anticipated that these optical advancements would be crucial in raising the photodegradation effectiveness of TC when exposed to LED light.

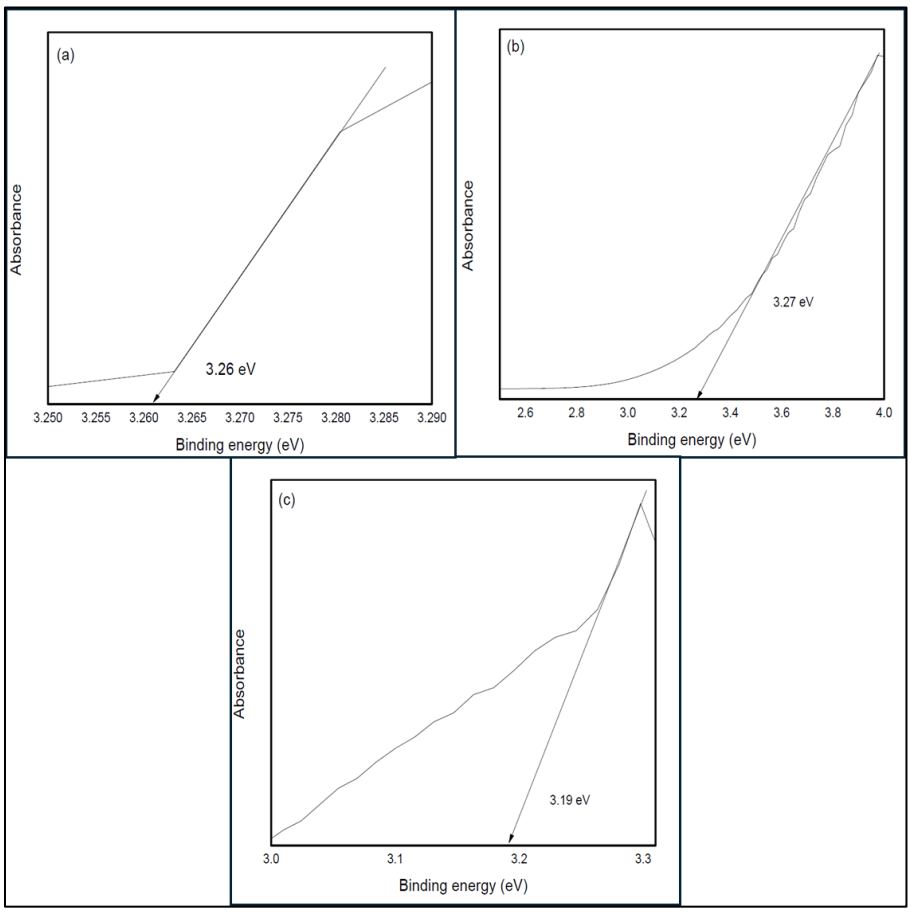

Figure 4.7 Binding Energy of (a) GO, (b) WS_2, and (c) WS_2/GO-15.

4.2 Photocatalytic Degradation of Tetracycline

Through this study, WS_2, GO, and WS_2/GO-1, WS_2/GO-5, and WS_2/GO-15 composites was used to degrade the water-soluble TC antibiotic solution in order to evaluate their photocatalytic performance. The purpose of the light source effect study was to establish a connection between the characterisation analysis of composites and their capacity to break down the antibiotic TC. This study assessed four distinct irradiation settings for 180 minutes: dark, LED, UV, and fluorescent. The C/C_o ratios of GO, WS_2, WS_2/GO-1, WS_2/GO-5, and WS_2/GO-15 under the specified irradiations are shown in Fig. 4.8, According to C/C_o, a low C/C_o ratio denotes a high degradation efficiency.

Thus, the figure revealed that all photocatalysts perform poorly at degradation under dark settings, with physisorption playing a major role in controlling degradation. In contrast, WS_2/GO-15 outperformed other photocatalysts in terms of degrading performance when light emitting diodes (LEDs) were present. This is because there is enough WS_2, or visible active photocatalyst. Moreover, the separation efficiency of photogenerated electron pairs in WS_2/GO-15 composites was significantly enhanced by the addition of GO.

In addition, since only WS_2/GO-15 outperformed WS_2/GO-1 and WS_2/GO-5, WS_2/GO-15 photocatalyst was selected as the representative photocatalyst for further physicochemical analysis where these analyses were conducted to better understand the optical properties, surface characteristics, charge recombination behaviour, structural defects, and morphology responsible for the enhanced photocatalytic performance.

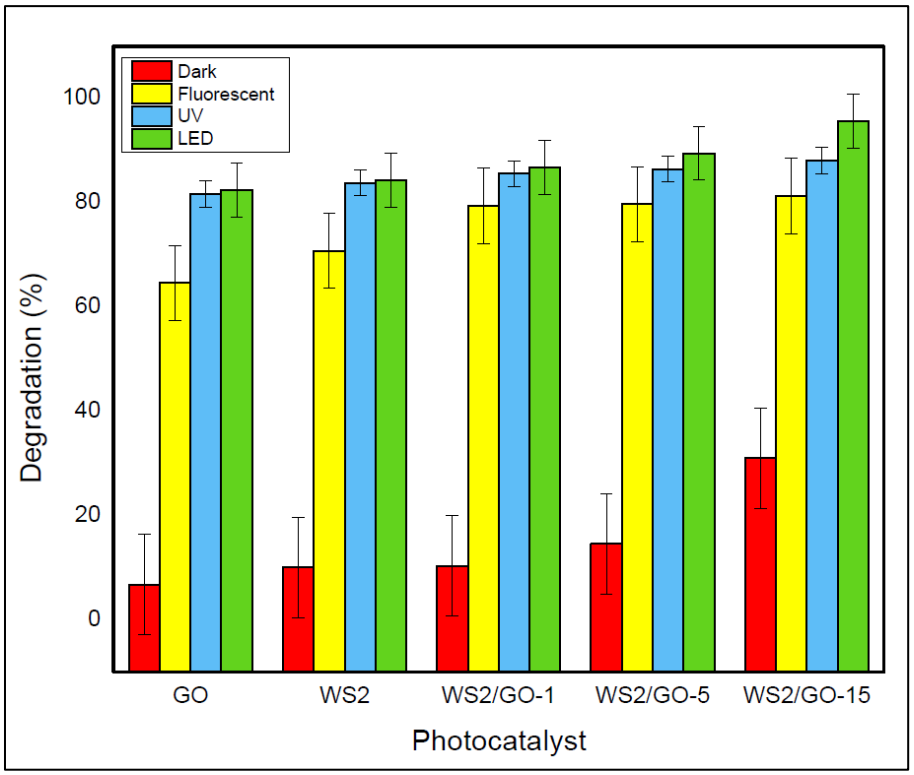

Figure 4.8 Degradation of TC with Different Type of Light Sources with Different Amount of Photocatalyst Loading.

4.2.1 Box Behnken Design (BBD) and Response Surface Methodology (RSM)

Figure 4.9 illustrates the relationship between the experimental (actual) values and the values that the quadratic model produced using the Box-Behnken Design (BBD) and Response Surface Methodology (RSM) projected. In this work, the response is the photocatalytic degradation efficiency of TC using WS_2/GO-15 composites under LED irradiation. This graphical tool is a crucial diagnostic that evaluates the precision and suitability of the established model for predicting the reaction.

A full agreement between the expected and experimental values is shown when all of the data points in a predicted vs. real plot fall exactly on the 45° diagonal line (y = x) (Montgomery, 2017). A substantial connection between the expected and actual responses is shown by the plot's close clustering of the majority of the data points around the diagonal line. This suggests that the connection between the independent variables (i.e., starting TC concentration, photocatalyst dose, and irradiation period) and the response (degradation efficiency) is well captured by the Box-Behnken Design model.

Only a few deviations at higher levels (such as red and yellow points above 80%) indicate that the data points are spread out around the line, which might indicate

that, under some experimental conditions, the predictions were somewhat over or under. These variations, however, are small and fall within reasonable bounds, demonstrating how well the second-order polynomial model predicts the behaviour of the system.

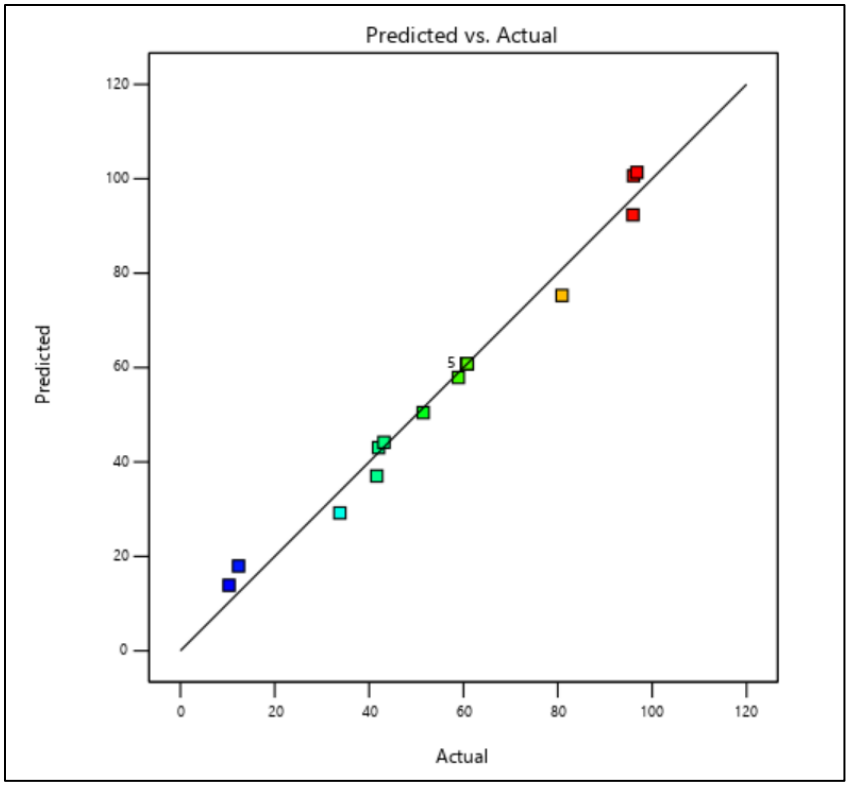

Figure 4.9 The Predicted Against Actual Results in Response to BBD and RSM.

The three-dimensional (3D) response surface plots in Figure 4.10 (a-c) show the interaction effects of operational parameters, specifically photocatalyst dosage, solution pH, and initial TC concentration, on the degradation efficiency. These effects were examined using the Box-Behnken Design (BBD) approach. Critical information on the behaviour of the WS_2/GO photocatalyst system under various conditions may be gained from these graphs, which show how paired variables impact the response while holding the third variable constant.

The relationship between the photocatalyst dose (g) and solution pH and the percentage of TC degradation is shown in Figure 4.10 (a). As demonstrated, a considerable improvement in degradation efficiency was obtained by increasing the dose of photocatalyst from 0.02 to 0.04 g. This suggests that a greater quantity of photocatalyst offers more reactive sites and active surface area for photogenerated electron-hole pairs to start redox processes. The effect of pH, however, was nonlinear, which is an acidic (pH 3) to slightly neutral range (pH 6), and subsequently decreased

when in alkaline condition (pH 9). This conduct is in line with earlier research showing that at lower pH levels, acidic conditions promote the production of reactive oxygen species (ROS), including hydroxyl radicals (•OH), and strengthen the electrostatic attraction between the negatively charged TC molecules and the positively charged catalyst surface (Rajiv *et al.,* 2018). The repulsion between negatively charged catalyst surfaces and TC molecules may prevent adsorption and hence lower photocatalytic performance in alkaline environments (Lu *et al.,* 2022).

The combined effects of the initial TC's concentration and photocatalyst dose on the degradation efficiency are shown in Figure 4.10 (b). The findings show that, independent of photocatalyst dose, degradation is continuously high when the initial TC's concentration is kept within a lower range (5-11 ppm). However, once the concentration crosses 14 ppm, a considerable drop in degradation efficiency is seen, especially at decreasing photocatalyst doses. This decrease is explained by the photocatalyst surface's active sites becoming saturated, which restricts the quantity of TC molecules that can be adsorbed and then broken down. The total degradation efficiency is decreased because more TC molecules remain unreacted when the surface gets saturated. Furthermore, a significant amount of incoming light may be absorbed by TC molecules at high pollutant concentrations, which would reduce the number of photons available for catalytic activation. Reactive oxygen species (ROS), which are essential for the photocatalytic process, and photogenerated electron–hole pairs are reduced because of this impact (Kumar *et al.,* 2023; Zhang *et al.,* 2021). Photocatalytic efficacy is further hampered by such restrictions at high concentrations, which further encourage charge carrier recombination (Chen *et al.,* 2022). To enhance degradation efficiency in real-world applications, these findings highlight the need of adjusting initial pollutant concentrations and photocatalyst loading.

The correlation between initial TC levels and pH is seen in Figure 4.10(c). Lower TC concentrations (5–11 ppm) and acidic conditions (pH 4–6) resulted in the maximum degradation. Particularly at high pH and high concentration, the degradation efficiency decreased as both parameters rose. This pattern confirms previous findings that the photocatalyst's surface chemistry and the contaminant's behaviour in various pH ranges both have an impact on photocatalysis efficiency. Higher pH is anticipated to inhibit photocatalytic activity due to the increased recombination of photogenerated electron-hole pairs and the reduced production of •OH radicals (Wang *et al.,* 2015).

Furthermore, inadequate light penetration and competing absorption lower the

quantity of active species generated at increasing pollution concentrations. In contrast to pH and beginning TC concentration, which show nonlinear and interacting effects, photocatalyst dose has a substantial positive linear effect on degradation, as confirmed by these three surface plots taken together. The BBD study revealed that optimal pH values is 5, photocatalyst doses at 0.02 g, and TC concentrations at 10 ppm were the ideal operating window for optimizing degradation efficiency. In wastewater treatment applications, our research offers helpful recommendations for enhancing WS_2/GO-based photocatalytic systems, allowing for the effective and economical removal of pharmaceutical pollutants.

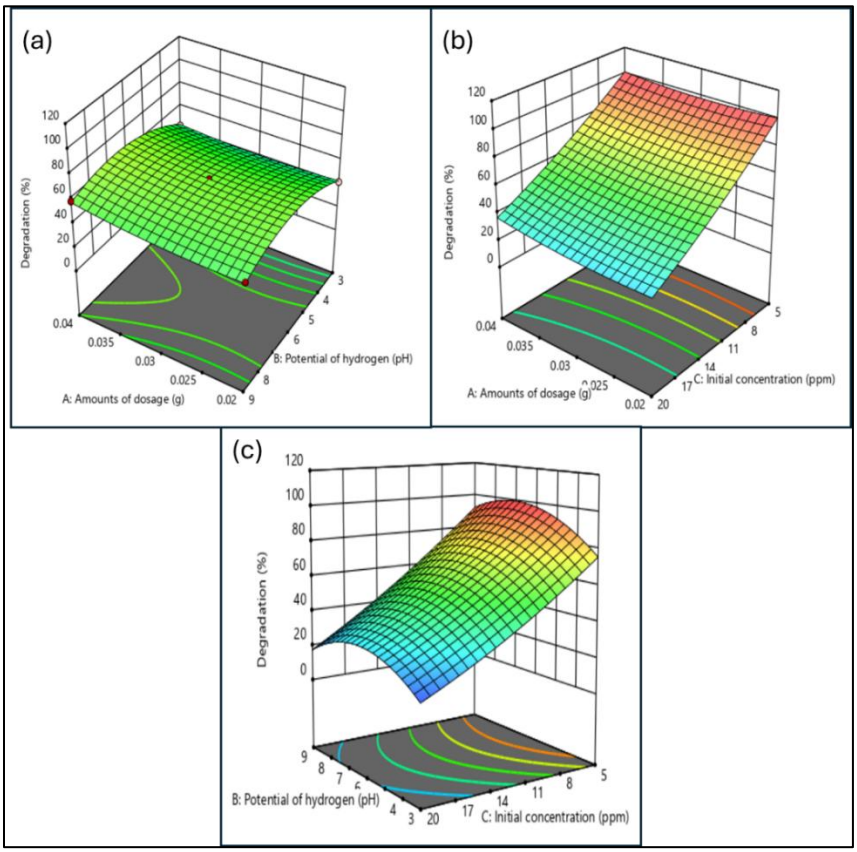

Figure 4.10 (a) Amount of Dosage Against (g) Potential of Hydrogen (pH), (b) Amounts of Dosage Against (g) Initial Concentration (ppm), and (c) Potential of Hydrogen (pH) Against Initial Concentration (ppm).

The quadratic model in Table 4.2 shown the analysis of variance (ANOVA) response for degradation demonstrates the model's overall significance with a high F-value of 45.95 and a p-value of less than 0.0001, indicating that the model is statistically significant at the 95% confidence level. With a very high F-value of 363.47 and a p-value < 0.0001, among the individual components, the starting concentration of TC

(Factor C) shows the most significant influence on the degradation process, suggesting a major contribution to the response's variability. Factor B, the hydrogen potential (pH), is equally statistically significant ($F = 8.82$, $p = 0.0208$), while Factor A, the catalyst dosage, has no discernible effect on the response ($p = 0.2681$). Furthermore, a non-linear relationship between pH and degradation efficiency is shown by the statistical significance of the quadratic term B2 ($F = 35.21$, $p = 0.0006$). However, based on their individual p-values being more than 0.05, the quadratic terms (A^2 and C^2) and other interaction terms (AB, AC, and BC) do not significantly affect the degradation outcome.

The model fits the data well, as evidenced by the little residual error (Sum of Squares = 177.52) and significant lack of fit. According to Myers *et al.* (2016), these results are consistent with Response Surface Methodology (RSM) standard procedures, which use quadratic models to assess the interaction and curvature impacts of process parameters to optimize photocatalytic degradation processes. The initial concentration's dominance as the most important component is in line with other studies that show that contaminant load has a significant impact on photocatalytic degradation rates because of active site competition and restrictions in photon absorption (Gupta & Garg, 2020; Sahu *et al.,* 2021). The quadratic model's applicability for process optimization is thus validated by the ANOVA results, which also show that pH and beginning concentration have a substantial impact on the degrading efficiency.

Table 4.2
The Analysis of Variance (ANOVA) for Quadratic Model.

Source	**Sum of Squares**	**of**	**Mean Square**	**F-value**	**p-value**	
Model	10487.25	9	1165.25	45.95	< 0.0001	significant
A-Amounts of dosage	36.70	1	36.70	1.45	0.2681	
B-Potential of hydrogen	223.64	1	223.64	8.82	0.0208	
C-Initial concentration	9217.63	1	9217.63	363.47	< 0.0001	
AB	9.96	1	9.96	0.3929	0.5507	
AC	12.63	1	12.63	0.4982	0.5031	
BC	42.28	1	42.28	1.67	0.2376	
A^2	29.15	1	29.15	1.15	0.3193	
B^2	892.95	1	892.95	35.21	0.0006	
C^2	54.86	1	54.86	2.16	0.1848	
Residual	177.52	7	25.36			
Lack of Fit	177.52	3	59.17			
Pure Error	0.0000	4	0.0000			
Cor Total	10664.77	16				

4.2.2 Effect of Time and Kinetic Study

The materials were evaluated for 30 minutes in the dark and then for 0 to 180 minutes under LED irradiation to further examine the impact of contact time on the kinetic behaviour of the photodegradation process. Figure 4.11 illustrates, there was very little degradation in the dark, and the variations suggested that an equilibrium between adsorption and desorption had been established. From 0 to 30 minutes, there was rapid degradation; from 150 to 180 minutes, there was a progressive drop and final standstill. TC degraded quickly at first because the photocatalyst's active sites were still empty, enabling quick degradation. TC's rate of degradation was slowed down when more active sites were filled since this lessened the possibility of electron-hole recombination.

A plot of Ln (C/Co) against time (min) under different lights displayed in Figure 4.12, revealed the kinetic constants for the measured parameters pseudo-first-order L-H model. Among these types of light sources, LED-irradiated system had the greatest rate constant ($k = 0.4658\ min^{-1}$) among the three light sources. It also had a good correlation coefficient ($R^2 = 0.986$) and a matching half-life of 1.4878 minutes. This confirms good agreement with the L-H model and shows a strong linear link between time and the logarithmic concentration ratio. In Zhao et. el., (2020) study says that its narrow emission spectrum and effective photon utilization, which match the absorption capabilities of the WS_2/GO-15 photocatalyst utilized in this investigation and may also be the reason for the higher performance under LED illumination.

Next, a slower kinetic profile under UV light was observed with $k = 0.2256\ min^{-1}$, half-life of 3.072 minutes, and $R^2 = 0.8826$. Wang *et al.* (2019) suggested that although UV light contains photons with higher energy, its inferior performance when compared to LEDs indicates inadequate overlap with the catalyst's bandgap and potential charge carrier recombination. Compared to UV light, fluorescent had comparatively high R^2 value with 0.9555. However, it has the lowest deterioration rate ($k = 0.135\ min^{-1}$) with half-life of 5.133 minutes. This result might be due to fluorescent light's wider emission profile and lower intensity which decreased the photocatalytic activity (Li *et al.,* 2018).

Through these findings it is support the effectiveness of the first-order Langmuir–Hinshelwood equation in modelling the photocatalytic degradation of TC under visible and UV light. The superior kinetic performance from LED irradiation

confirmed its feasibility as an effective and energy-efficient light source for photocatalytic applications (Ahmed *et al.,* 2022).

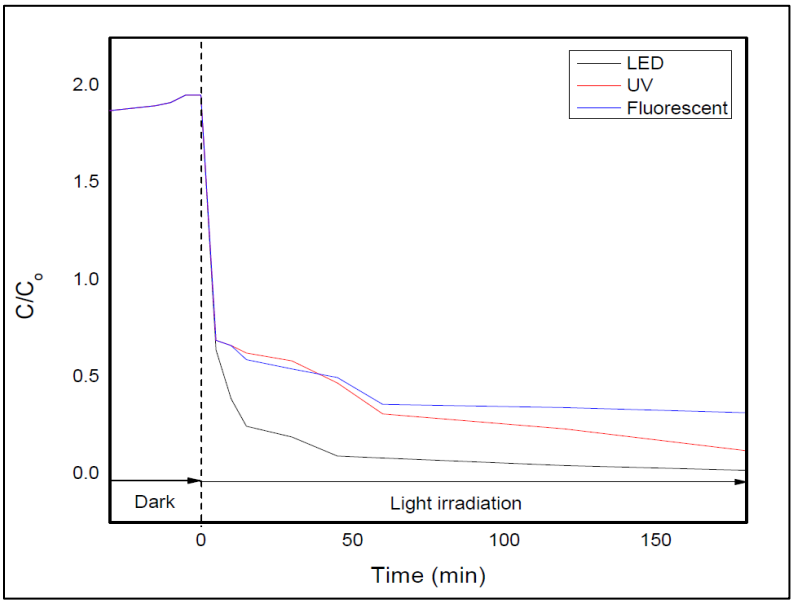

Figure 4.11 Effect of Contact Time in Different Types of Light Sources for Photocatalytic Degradation of TC Antibiotic (20 mg/L TC Antibiotic, 0.02 g/L of WS_2/GO-15 Photocatalyst Loading).

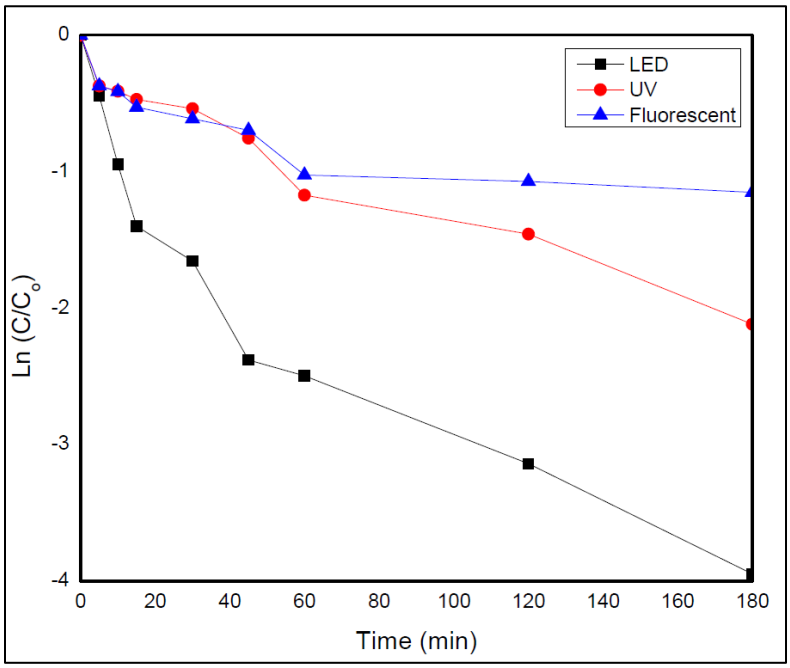

Figure 4.12 Kinetic Plot of Ln (C/C_o) Against Irradiation Time for the Photocatalytic Degradation of TC Antibiotics.

4.2.3 Effect of pH

In the photocatalytic breakdown of TC, pH is essential because it affects the photocatalyst's surface charge, TC speciation, and reactive oxygen species (ROS) production. The ability of GO, WS_2, and WS_2/GO-15 composite to degrade TC under various pH settings was examined (Figure 4.13); degradation efficiencies varied considerably depending on the pH range. According to the degradation data at various pH values, the WS_2/GO-15 composite demonstrated greater photocatalytic activity, with a maximum degradation of 95.7% at pH 5 and somewhat lower degradation efficiencies at neutral and alkaline pH levels.

The degradation efficiency of GO (10.32%) and WS_2 (17.51%) was comparatively lower in very acidic conditions (pH 2), but WS_2/GO-15 showed noticeably greater degradation (75.34%). Protonation actions that change the surface charge and decrease contact with TC molecules are the cause of GO and WS_2's decreased efficiency in acidic environments (Zhao *et al.,* 2022). However, because of better charge separation and increased ROS production in acidic environments, WS_2/GO demonstrated greater degrading efficiency.

At pH 5, WS_2/GO-15 demonstrated the maximum degradation, with 95.7%, followed by GO and WS_2 with 15.75% and 59.05%, respectively. The surface charge of WS_2/GO-15 is tuned for improved TC adsorption under slightly acidic circumstances, which leads to effective electron-hole separation and ROS generation. According to Wang *et al.* (2023), the production of superoxide radicals ($O_2^{\bullet -}$) and hydroxyl radicals (•OH) is preferred in this pH range and is crucial to the degradation process.

While WS_2 and GO both exhibited diminishing trends, the degrading efficiency of WS_2/GO dropped to 90.75% and 80.9%, respectively, at alkaline circumstances (pH 9 and 12). Because OH^- ions can function as scavengers for ROS, lowering their availability for TC breakdown, the reduced efficiency at high pH is probably caused by their excessive presence (Chen *et al.,* 2020). Additionally, the very alkaline pH of WS_2/GO may cause electrostatic repulsion between negatively charged TC species and the catalyst surface, reducing the efficacy of adsorption and subsequent degradation.

In summary, pH has a significant impact on the photocatalytic degradation of TC utilizing WS_2/GO under LED irradiation. At slightly acidic pH levels (pH 5), charge interactions, ROS production, and charge separation processes are increased, making this the ideal pH for degradation. Degradation efficiency is reduced in very acidic or

alkaline environments because of variations in surface charge and ROS dynamics. For environmental applications, our results emphasize how crucial pH adjustment is to be improving WS_2/GO-15's photocatalytic activity.

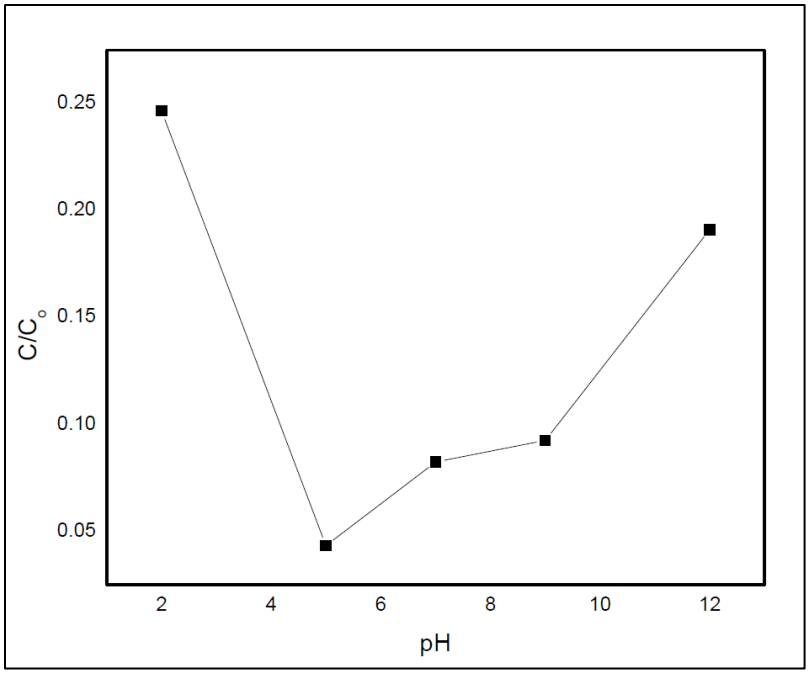

Figure 4.13 Effect of pH on Photocatalytic Degradation of TC (20 mg/L TC, 12-watt of LED Light and 0.02 g/L of WS_2/GO-15 Loading Catalyst).

A crucial factor in photocatalysis, the point of zero charge (pH_{zpc}) establishes the surface charge of the photocatalyst at various pH values, which affects the adsorption of contaminants and the effectiveness of degradation. The pH_{zpc} findings as reveal in Figure 4.14 obtained before and after TC breakdown using WS_2/GO-15 under LED irradiation show notable differences in surface charge properties. The surface charge of WS_2/GO-15 changes from positive in acidic circumstances to negative in neutral and alkaline situations, as indicated by the pH_{zpc} values, which varied from 0.33 at pH 2 to -3.1 at pH 9. The interaction between WS_2/GO-15 and TC molecules, which take on various ionic forms based on the pH of the solution, is significantly impacted by this change (Zhao *et al.,* 2023).

The WS_2/GO photocatalyst shows a strongly positive surface charge at pH 2 with a pH_{zpc} of 0.33. Lower degradation rates can result from electrostatic repulsion between the catalyst and the pollutant, which can decrease adsorption effectiveness since TC is mostly cationic in extremely acidic environments. But following degradation, the pH rose from 2.07 to 2.4, indicating that protons were used up during

the photocatalytic process. This was probably caused by the oxidation of water molecules and the creation of hydroxyl radicals (•OH) (Li *et al.,* 2022).

The values of pH_{zpc} are 0.7 and 0.46, respectively, in the somewhat acidic range, especially at pH 4 and 5. Because WS_2/GO-15 maintains a little positive charge at these pH levels, it interacts more easily with partly deprotonated TC molecules. Degradation performance is high at pH 5, indicating that this setting increases adsorption and degradation efficiency. Further evidence for the function of photogenerated holes (h^+) in oxidizing TC, which results in enhanced hydroxyl radical production and proton release, comes from the pH rise following degradation (from 5.04 to 5.5) (Wang *et al.,* 2021).

The pH_{zpc} values turn negative at neutral and alkaline pH levels (-2.98 at pH 7 and -3.1 at pH 9), suggesting that WS_2/GO-15 has a mostly negative surface charge. In this pH range, TC is mostly found in its anionic form, which causes the pollutant and the photocatalyst surface to repel one another electrostatically. This repulsion lowers the rates of photocatalytic degradation by decreasing the adsorption effectiveness. The substantial pH reduction following degradation at pH 7 (from 7.18 to 4.2) and pH 9 (from 9.1 to 6) further implies the formation of acidic byproducts or intermediate species during the process, which may have contributed to the decline in solution pH (Chen *et al.,* 2020).

In the slightly acidic range (pH 4-5), where advantageous electrostatic interactions between the catalyst and TC promote adsorption and degradation, WS_2/GO-15 shows the best photocatalytic activity, according to the pHzpc study. Pollutant removal effectiveness is limited by repulsive forces at very acidic or alkaline pH levels. The observed pH variations during degradation point to active photocatalytic processes that include intermediate production, charge transfer, and ROS creation. These results emphasize how crucial it is to adjust pH levels to optimize WS_2/GO-15's efficacy in wastewater treatment applications.

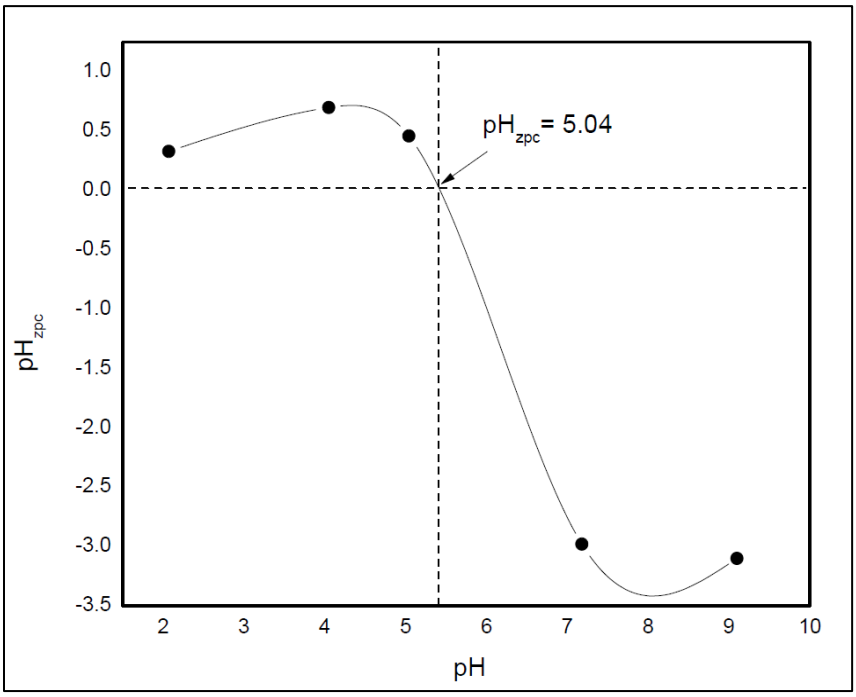

Figure 4.14 Point of Zero Charge (pHzpc).

4.3 Scavenging Study

Trapping experiments, often referred to as scavenging investigations, are essential for determining which reactive oxygen species (ROS) are in charge of the photocatalytic breakdown of TC. According to Wang *et al.* (2021), the breakdown process of TC antibiotics includes photogenerated electrons (e^-), holes (h^+), and ROS such hydroxyl radicals (•OH), superoxide radicals ($O_2•^-$), and singlet oxygen ($^1O_2$). By knowing which species control the reaction pathway, scientists may adjust photocatalytic devices to achieve the best degradation efficiency (Huang *et al.,* 2022).

The activation of the photocatalyst under LED irradiation results in the generation of numerous important reactive oxygen species (ROS) throughout the photocatalytic process. As a result of photogenerated holes oxidizing water, one of the most reactive species that is created is the hydroxyl radical (•OH). The tremendous oxidative potential of these radicals makes them essential for the breakdown of organic contaminants. Moreover, photogenerated electrons that decrease molecular oxygen produce superoxide radicals ($O_2•^-$), which aid in the degradation process by starting additional oxidation events. Energy transfer between excited oxygen molecules and other ROS produces singlet oxygen ($^1O_2$), another important ROS that contributes to the degradation efficiency. Additionally, photogenerated holes (h^+) themselves are potent

oxidizers that prey on and break down organic pollutants. The efficient breakdown of TC antibiotics in photocatalytic devices is facilitated by the combined action of these ROS (Zhang *et al.,* 2023).

The main reaction pathway of the photocatalytic system may be inferred by examining the effects of various scavengers on the breakdown of TC. Figure 4.15 reveals scavenging investigations for p-benzoquinone (-16.71%), IPA (-12.03%), EDTA (58.67%), and $K_2Cr_2O_7$ (-149.15%) revealed percentage degradation, which offers important information about the mechanism of WS_2/GO-15 photocatalysis shown in Figure 4.15.

In addition to inhibiting ROS, the negative degradation percentages for BQ, IPA, and $K_2Cr_2O_7$ indicate that these scavengers also helped stabilize or recombine charge carriers, which decreased photocatalytic activity. Electron transfer is essential for producing ROS for efficient TC breakdown, as seen by the substantial negative impact of $K_2Cr_2O_7$ (-149.15%). The considerable contribution of electron-driven ROS, especially superoxide radicals ($O_2•^-$), to the degradation mechanism is confirmed by the strong inhibitory action of $K_2Cr_2O_7$, which efficiently catches photogenerated electrons (Zhang *et al.,* 2023).

Conversely, EDTA markedly increased degradation (58.67%), indicating that hole-mediated oxidation is not the main mechanism at work in this system. In contrast to ROS like •OH and $O_2•^-$, this data suggests that although h^+ may play a part in degradation, its contribution is less substantial (Huang *et al.,* 2022). Although hydroxyl radicals are not the predominant species, their involvement is suggested by the modest inhibitory impact of IPA (-12.03%).

In conclusion, research on scavenging offers crucial information on the reactive species that contribute to photocatalytic degradation. The outcomes of using IPA, BQ, EDTA, and $K_2Cr_2O_7$ aid in determining whether electron transfer, photogenerated holes, superoxide radicals, or hydroxyl radicals are more important in the breakdown of TC antibiotics. While the enhanced deterioration in the presence of EDTA implies that hole-mediated oxidation is less important, the considerable negative effect of $K_2Cr_2O_7$ demonstrates that electron transfer is crucial. This information guarantees the efficacy of WS_2/GO-15 photocatalytic systems in actual environmental applications by allowing them to be optimized for improved performance under LED irradiation.

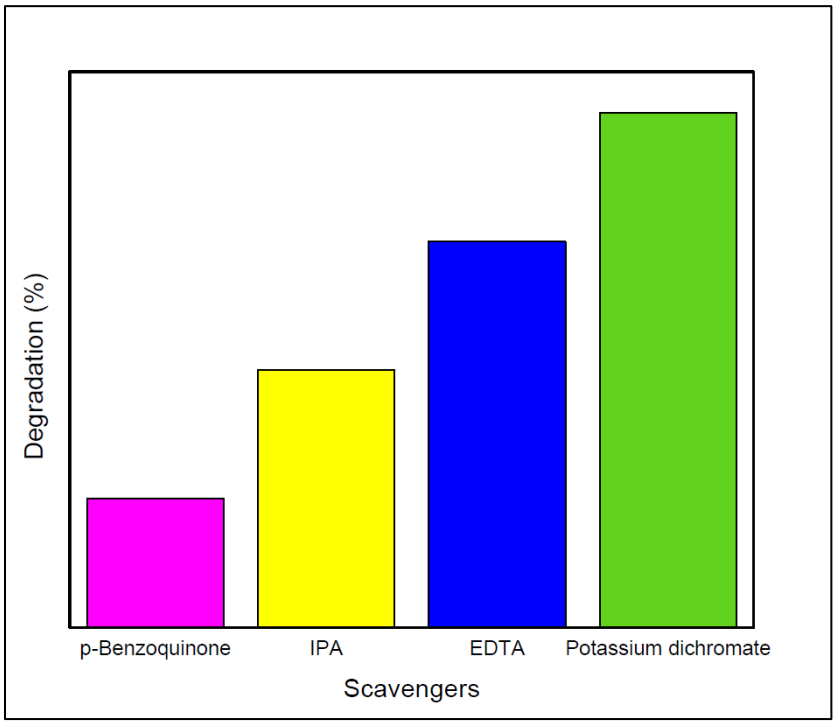

Figure 4.15 Trapping Experiment of the Active Species During Photocatalytic Degradation of TC Over Nanocomposite Alone and with the Addition of P-Benzoquinone (Quencher of $\bullet O_2^-$) and IPA (Quencher of •OH), EDTA (Quencher of h^+), and Potassium Dichromate (Quencher of e^-) Under Indoor LED Light Irradiation.

4.4 Recyclability Study

The most noteworthy aspect of photocatalytic degradation studies is a reusable, sustainable photocatalyst. After a few cycles of use, a promising photocatalyst must be able to maintain good degrading performance. The photocatalyst was cleaned with ethanol and water prior to the experiment, and it was then dried in a vacuum for two hours at 70°C. Figure 4.16 shows that after seven further experiments, the deterioration efficiency was decreased. The photocatalyst maintained relatively high in degradation efficiency of 81.67% (5^{th} cycle) and cycle 6 with 75.34% which indicating a good stability in degrading the TC. However, at 7^{th} cycle, the degradation efficiency decreased to 65.87% which is below the performance threshold of 70% degradation aimed in this study. Therefore, the recyclability study was considered only up to six cycles, where the photocatalyst still exhibited satisfactory photocatalytic activity above 70%. As a result, it was determined that the WS_2/GO-15 may be reused and renewed for up to six cycles.

The seventh cycles of photocatalyst were examined using FTIR to demonstrate the causes of WS_2/GO-15 's reduced degradation efficiency. According to Figure 4.17,

the FTIR spectrum demonstrates that the peak's intensity decreases after reusability due to lesser affinity as most active sites interact, reducing the production of free radicals and, consequently, the degradation process. They may be seen in the missing peaks at 2264 cm^{-1}, 2634 cm^{-1}, and 2788 cm^{-1} as well as the larger peak at 3038 cm^{-1} that resulted from the repeated washing and drying.

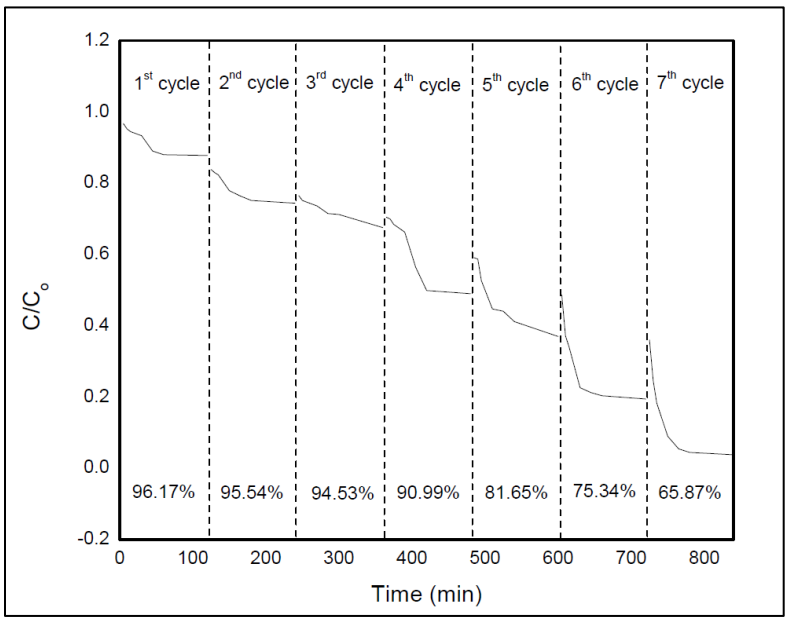

Figure 4.16 The Recyclability Study of Degradation TC Up to 7th Cycles.

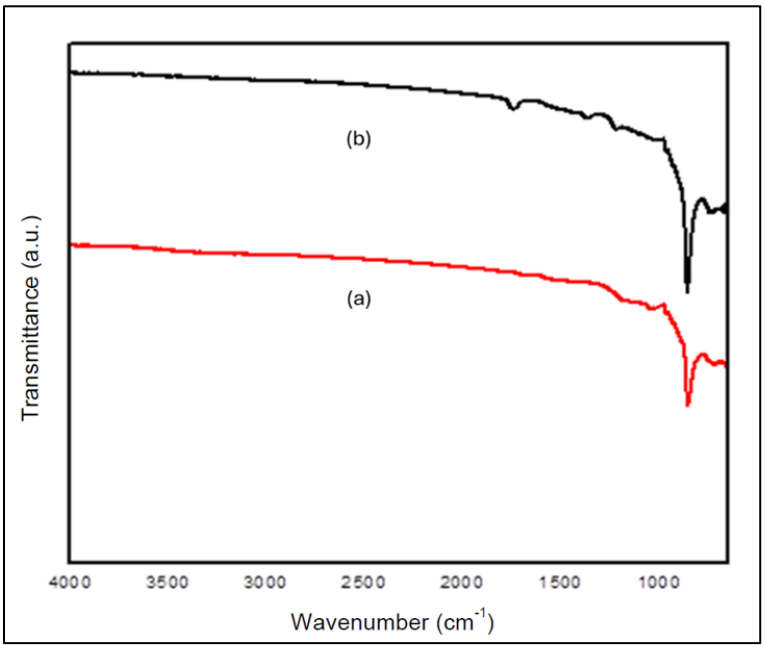

Figure 4.17 FTIR Spectrum of WS_2/GO-15 (a) After and (b) Before 7th cycle.

4.5 Real Sample

In environmental research, real sample analysis is crucial, especially when evaluating the usefulness of photocatalytic materials in real-world settings. The complexity of natural water systems is not well represented by laboratory research, even though they offer a controlled setting for assessing degrading efficiency. Environmental water sources' different organic and inorganic content can have a big impact on how well photocatalysts work (Li *et al.,* 2022). To ensure that the produced photocatalyst stays effective in a variety of environmental circumstances, researchers can bridge the gap between laboratory findings and real-world applications by doing real sample analysis.

Through this work, four distinct water sources which are seawater, river water, tap water, and lake water were exposed to LED light to assess the photocatalytic degradation of TC antibiotics utilizing tungsten disulfide-graphene oxide (WS_2/GO). Understanding how environmental factors like pH, dissolved organic matter, ionic strength, and the presence of other competing pollutants affect the WS_2/GO photocatalyst's performance requires the examination of actual samples (Zhang *et al.,* 2023). It is feasible to improve photocatalytic settings for practical wastewater treatment applications by researching these variables.

The photocatalyst's effectiveness may be enhanced or inhibited by matrix effects introduced by the complex composition of actual water samples. Photocatalyst surface sites interact with dissolved species such organic matter, metal ions, and colloidal particles to produce these effects. The degree to which matrix influences have affected photocatalytic activity is reflected in the relative standard deviation (%RSD) values that were determined for the various water samples in this investigation. The use of %RSD rather than degradation efficiency (%) because the %RSD is suitable to provide a measure of the reproducibility and stability of photocatalytic degradation across various water matrices.

Based on Table 4.3, the largest RSD, 5.11%, was found in saltwater, suggesting a higher degree of variability in the efficacy of photocatalytic degradation. It is probably because of the high ionic strength and the presence of metal ions as SO_4^{2-}, Mg^{2+}, Cl^-, and Na^+ that can compete with TC molecules for adsorption sites on the WS_2/GO photocatalyst. According to Li *et al.* (2022), an excess of salts can also result

in charge screening effects, which lowers the separation efficiency of photogenerated electron-hole pairs.

The moderate percentage RSD for river water (2.90% RSD) indicates that minerals, dissolved oxygen, and natural organic matter (NOM) had a little impact on degrading efficiency. According to Zhang *et al.* (2023), NOM can function as a radical scavenger by decreasing the availability of superoxide radicals ($O_2 \cdot^-$) and hydroxyl radicals (OH·), both of which are essential for photocatalytic degradation.

Tap water had the least amount of fluctuation (1.45% RSD), indicating a stable and regulated water matrix. According to Wang *et al.* (2021), constant photocatalytic activity results from good charge transfer and effective electron-hole separation, which are ensured by the lack of considerable organic or inorganic interference.

In comparison to tap and river water, lake water has a somewhat higher RSD (3.26%), which is explained by the presence of organic contaminants, suspended particles, and algae. These elements could absorb photons, which eventually affects photocatalytic performance by lowering the amount of light energy available for electron excitation (Liu *et al.,* 2020).

The primary mechanism (Figure 4.18) behind the breakdown of TC utilizing WS_2/GO under LED irradiation is the excitation of electrons, which leads to the production of reactive oxygen species (ROS). When photons from LED light are absorbed by WS_2, positively charged holes (h^+) are left behind as electrons (e^-) are driven from the valence band (VB) to the conduction band (CB). TC molecules are broken down by these charge carriers' interactions with oxygen and water molecules, which produce very reactive OH· and $O_2 \cdot^-$ species (Huang et al., 2021).

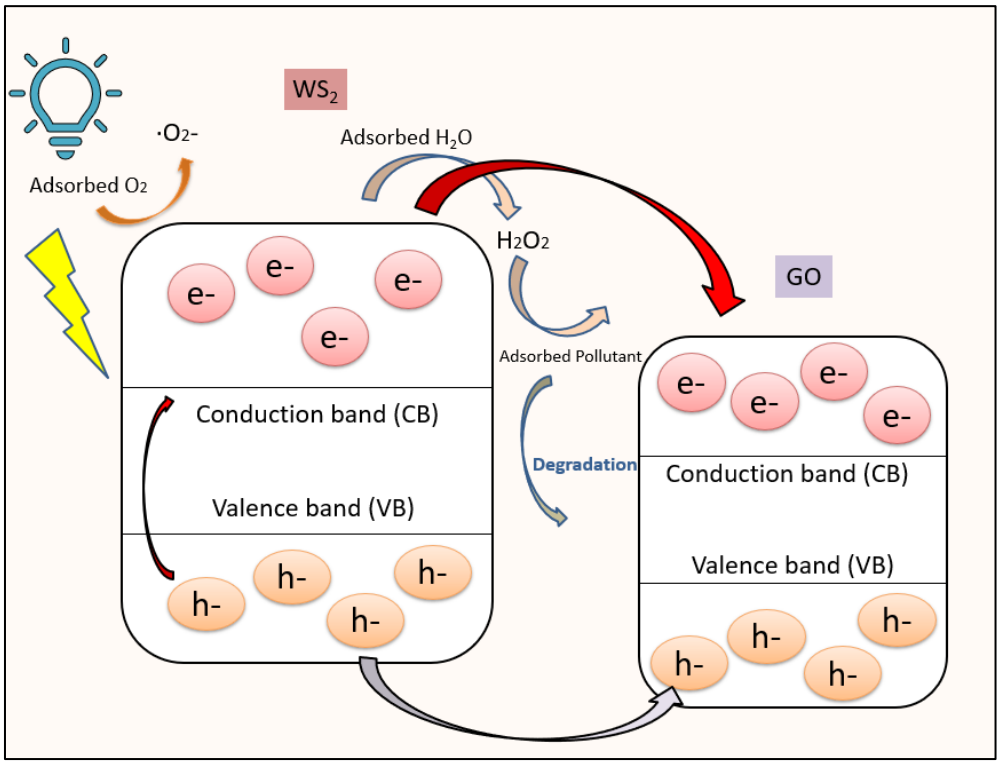

Figure 4.18 General Mechanism of Degradation Process of TC Under LED Irradiation.

Environmental influences on charge excitation and electron mobility are emphasized by the differences in %RSD across various water matrices. Higher levels of dissolved organic matter and ionic strength, found in river and seawater, can inhibit the mobility of charge carriers, decrease photocatalytic effectiveness and increase degradation rate variability (Huang *et al.,* 2021). On the other hand, tap water facilitates effective electron excitation and charge transfer due to its low levels of interfering species, which lowers the RSD percentage.

Table 4.3
The Percentage Degradation of TC in the Real Sample.

Sample	**Spike (ppm)**	**RSD (%)**	**Degradation (%)**
Sea water	20.00	5.1128	5.2399
River water	20.00	2.9019	58.8005
Tap water	20.00	1.4496	55.1389
Lake water	20.00	3.2627	51.6035

CHAPTER 5
CONCLUSION

The goal of this work was to improve the visible-light photocatalytic degradation of TC by creating a WS_2/GO composite which combining the modified Hummers' technique for graphene oxide synthesis with a hydrothermal process. This study demonstrated that the combination of GO and WS_2 resulted in a successfully combined nanocomposite with enhanced physicochemical characteristics that are advantageous for photocatalytic uses. Moreover, GO boosted the surface area and porosity of WS_2 nanosheets which improved their dispersion and fostered a significant interfacial contact between the two materials. In addition, under visible light irradiation, these structural and morphological enhancements promoted improved light absorption as well as more effective separation and transfer of photogenerated charge carriers. Consequently, the photocatalytic activity of the WS_2/GO-15 composite was much greater than that of pure WS_2 and GO.

Next, the photocatalytic degradation process is likely affected by the pH (5) and the initial concentration of TC (10ppm) where it showed the maximum degradation efficiency. Moreover, LED irradiation produced the best photocatalytic activity among the examined light sources which demonstrating the composite's response to visible light. While scavenger studies revealed that photogenerated electrons were crucial to the degradation mechanism, kinetic analysis revealed that the degradation reaction exhibited pseudo-first-order behaviour.

Furthermore, the WS_2/GO-15 showed remarkable reusability and stability, sustaining efficient photocatalytic activity up to six cycles with just a little decline in performance. In addition, the synergistic interaction between WS_2 and GO, which enhances light harvesting, charge separation, and surface reactivity, is responsible for the overall improved photocatalytic performance of the WS_2/GO-15 composite. Therefore, these results demonstrate the potential of the WS_2/GO composite as an effective visible light-driven photocatalyst for environmental remediation, especially for the treatment of wastewater polluted with antibiotics.

5.1 Recommendations

A thorough examination of the degradation by-products and intermediate chemicals produced during the photocatalytic process is strongly advised for future studies:

a. Advanced analytical methods like High-Performance Liquid Chromatography (HPLC), Gas Chromatography-Mass Spectrometry (GC-MS), or Liquid Chromatography-Mass Spectrometry (LC-MS) to identify the intermediate products created during the photocatalytic degradation process and comprehend the parent compound's (such as TC) gradual disintegration.
b. Undergoing an eco-toxicological assessment, such as in vitro cytotoxicity studies, algal toxicity tests, or microbial inhibition assays, to determine the toxicity of intermediate and ultimate breakdown products is crucial. This guarantees that the degrading process does not produce more toxic or hazardous chemicals than the initial pollutant, which is crucial for both regulatory compliance and environmental safety.
c. Using the Total Organic Carbon (TOC) or Chemical Oxygen Demand (COD) analysis to quantify the degree of mineralization in addition to pollutant removal efficiency. This aids in verifying if substantial amounts of organic residues are still present in the solution or whether the antibiotic has completely broken down into non-toxic end products (such as CO_2 and H_2O).

REFERENCES

Arunachalam, P., Nagai, K., Amer, M. S., Ghanem, M. A., Ramalingam, R. J., & Al-Mayouf, A. M. (2021). Recent developments in the use of heterogeneous semiconductor photocatalyst based materials for a visible-light-induced water-splitting system—A brief review. *Catalysts*, *11*(2), 160. https://doi.org/10.3390/catal11020160

Ayodhya, D., & Veerabhadram, G. (2017). One-pot green synthesis, characterization, photocatalytic, sensing and antimicrobial studies of Calotropis gigantea leaf extract capped cds NPS. *Materials Science and Engineering: B*, *225*, 33–44. https://doi.org/10.1016/j.mseb.2017.08.008

Bai, J., Cui, K., Xie, X., Fang, B., & Wang, F. (2022). Sepiolite-supported WS2 nanosheets for synergistically promoting photocatalytic rhodamine B degradation. *Catalysts*, *12*(11), 1400. https://doi.org/10.3390/catal12111400

Banerjee, S., Pillai, S. C., Falaras, P., O'shea, K. E., Byrne, J. A., & Dionysiou, D. D. (2014). New insights into the mechanism of visible light photocatalysis. *Journal of Physical Chemistry Letters*, *5*(15), 2543–2554. https://doi.org/10.1021/jz501030x

Byrne, C., Subramanian, G., & Pillai, S. C. (2018). Recent advances in photocatalysis for environmental applications. *Journal of Environmental Chemical Engineering*, *6*(3), 3531–3555. https://doi.org/10.1016/j.jece.2017.07.080

Chai, C. H. I. N. G., & Bong, C. W. (2022). Tetracycline resistance and prevalence of tetracycline resistance genes in bacteria from marine aquaculture farms in Peninsular Malaysia. *Sains Malaysiana*, *51*(2), 345-357. http://doi.org/10.17576/jsm-2022-5102-02

Chen, Y., Yang, J., Zeng, L., & Zhu, M. (2022). Recent progress on the removal of antibiotic pollutants using photocatalytic oxidation process. *Critical Reviews in Environmental Science and Technology*, *52*(8), 1401-1448. https://doi.org/10.1080/10643389.2020.1859289

Choi, H., Seo, J. H., & Weon, S. (2023). Visualizing indoor ozone exposures via o-dianisidine based colorimetric passive sampler. *Journal of Hazardous Materials*, *460*, 132510. https://doi.org/10.1016/j.jhazmat.2023.132510

Dai, Y., Wei, L., Chen, M., Wang, J., Ren, J., Wang, Q., Wu, Y., Wang, Y., Cheng, X., & Yan, X. (2017). Liquid exfoliation and electrochemical properties of WS2

nanosheets. *Journal of Nanoscience and Nanotechnology*, *18*(5), 3165–3170. https://doi.org/10.1166/jnn.2018.14689

Das, P., Ibrahim, S., Chakraborty, K., Ghosh, S., & Pal, T. (2024). Stepwise reduction of graphene oxide and studies on defect-controlled physical properties. *Scientific Reports*, *14*(1). https://doi.org/10.1038/s41598-023-51040-0

Dovi, E., Aryee, A. A., Kani, A. N., Mpatani, F. M., Li, J., Qu, L., & Han, R. (2022). High-capacity amino-functionalized walnut shell for efficient removal of toxic hexavalent chromium ions in batch and column mode. *Journal of Environmental Chemical Engineering*, *10*(2), 107292. https://doi.org/10.1016/j.jece.2022.107292

Du, W., Xia, X., Li, Z., Liu, F., & Xu, Y. (2024). WS2-Assisted electrochemical activation of peroxymonosulfate for eliminating organic pollutant in water. *Catalysts*, *14*(11), 763. https://doi.org/10.3390/catal14110763

Ferreira, S., Bruns, R., Ferreira, H., Matos, G., David, J., Brandão, G., Da Silva, E., Portugal, L., Reis, P. D., Souza, A., & Santos, W. D. (2007). Box-Behnken design: An alternative for the optimization of analytical methods. *Analytica Chimica Acta*, *597*(2), 179–186. https://doi.org/10.1016/j.aca.2007.07.011

Gaim, Y. T., Yimanuh, S. M., & Kidanu, Z. G. (2022). Enhanced Photocatalytic Degradation of Amoxicillin with Mn-Doped Cu2O under Sunlight Irradiation. *Journal of Composites Science*, *6*(10), 317. https://doi.org/10.3390/jcs6100317

Goldie, S. J., Bush, S., Cumming, J. A., & Coleman, K. S. (2020). A Statistical Approach to Raman Analysis of Graphene-Related Materials: Implications for Quality control. *ACS Applied Nano Materials*, *3*(11), 11229–11239. https://doi.org/10.1021/acsanm.0c02361

Guo, B., Liu, B., Wang, C., Wang, Y., Yin, S., & Han, W. (2022). WS2/In2S3 composite photocatalyst for photocatalytic H2 generation and pollutant degradation. *New Journal of Chemistry*, *46*(16), 7366–7373. https://doi.org/10.1039/d2nj00190j

Guo, G., Wang, Y., Zhang, D., & Lei, M. (2021). Source-specific ecological and health risks of potentially toxic elements in agricultural soils in Southern Yunnan Province and associated uncertainty analysis. *Journal of Hazardous Materials*, *417*, 126144. https://doi.org/10.1016/j.jhazmat.2021.126144

Hamilton, L. A., & Guarascio, A. J. (2019). Tetracycline allergy. *Pharmacy*, *7*(3), 104. https://doi.org/10.3390/pharmacy7030104

Huang, S., Xu, Y., Liu, Q., Zhou, T., Zhao, Y., Jing, L., ... & Li, H. (2017). Enhancing reactive oxygen species generation and photocatalytic performance via adding oxygen reduction reaction catalysts into the photocatalysts. *Applied Catalysis B: Environmental*, *218*, 174-185. https://doi.org/10.1016/j.apcatb.2017.06.030

Ikram, M., Raza, A., Imran, M., Ul-Hamid, A., Shahbaz, A., & Ali, S. (2020). Hydrothermal Synthesis of Silver Decorated Reduced Graphene Oxide (rGO) Nanoflakes with Effective Photocatalytic Activity for Wastewater Treatment. *Nanoscale Research Letters*, *15*(1). https://doi.org/10.1186/s11671-020-03323-y

Krawczyk, S. J., Leśniczak-Staszak, M., Gowin, E., & Szaflarski, W. (2024). Mechanistic insights into clinically relevant ribosome-targeting antibiotics. *Biomolecules*, *14*(10), 1263. https://doi.org/10.3390/biom14101263

Kröner, A., & Hirsch, T. (2020). Current trends in the optical characterization of Two-Dimensional Carbon Nanomaterials. *Frontiers in Chemistry*, *7*. https://doi.org/10.3389/fchem.2019.00927

Latif, M., Nawaz, R., Aziz, M. H., Asif, M., Noor, F., Aligayev, A., Ali, S. M., Alam, M., Papanikolaou, S., & Huang, Q. (2024). Evaluation of tetracycline photocatalytic degradation using NiFe2O4/CeO2/GO nanocomposite for environmental remediation: In silico molecular docking, antibacterial performance, degradation pathways, and DFT calculations. *Separation and Purification Technology*, *351*, 128074. https://doi.org/10.1016/j.seppur.2024.128074

Li, C., Sang, D., Ge, S., Zou, L., & Wang, Q. (2024). Recent excellent optoelectronic applications based on two-dimensional WS2 nanomaterials: a review. *Molecules*, *29*(14), 3341. https://doi.org/10.3390/molecules29143341

Li, W., Chu, X. S., Wang, F., Dang, Y. Y., Liu, X. Y., Wang, X. C., & Wang, C. Y. (2021). Enhanced cocatalyst-support interaction and promoted electron transfer of 3D porous g-C3N4/GO-M (Au, Pd, Pt) composite catalysts for hydrogen evolution. *Applied Catalysis B: Environmental*, *288*, 120034. https://doi.org/10.1016/j.apcatb.2021.120034

Lu, Y., Cai, Y., Zhang, S., Zhuang, L., Hu, B., Wang, S., ... & Wang, X. (2022). Application of biochar-based photocatalysts for adsorption-(photo) degradation/reduction of environmental contaminants: mechanism, challenges

and perspective. *Biochar*, *4*(1), 45. https://doi.org/10.1007/s42773-022-00173-y

Nada, E. A., El-Maghrabi, H. H., Raynaud, P., Ali, H. R., El-Wahab, S. A., Sabry, D. Y., Moustafa, Y. M., & Nada, A. A. (2022). Enhanced Photocatalytic Activity of WS2/TiO2 Nanofibers for Degradation of Phenol under Visible Light Irradiation. *Inorganics*, *10*(4), 54. https://doi.org/10.3390/inorganics10040054

Oluwole, A. O., & Olatunji, O. S. (2022). Photocatalytic degradation of tetracycline in aqueous systems under visible light irridiation using needle-like SnO2 nanoparticles anchored on exfoliated g-C3N4. *Environmental Sciences Europe*, *34*(1). https://doi.org/10.1186/s12302-021-00588-7

Phakathi, N. A., Tichapondwa, S. M., & Chirwa, E. M. N. (2022). Photocatalytic Degradation of Tetracycline Using Visible-light-driven Porous g- C3N4 Nanosheets Catalyst. *DOAJ (DOAJ: Directory of Open Access Journals)*. https://doi.org/10.3303/cet2296066

Qian, S., Qiao, F., Zhou, L., Liu, Y., Liu, W., Yang, J., Wang, T., & Li, H. (2022). Performance and mechanism analysis of photocatalytic degradation of tetracycline by SiC/CdS composites. *CrystEngComm*, *24*(35), 6269–6277. https://doi.org/10.1039/d2ce00906d

Qian, W., Hu, W., Jiang, Z., Wu, Y., Li, Z., Diao, Z., & Li, M. (2022). Degradation of Tetracycline Hydrochloride by a Novel CDs/g-C3N4/BiPO4 under Visible-Light Irradiation: Reactivity and Mechanism. *Catalysts*, *12*(7), 774. https://doi.org/10.3390/catal12070774

Rajeswaran, B., Konar, R., Yitzhari, R., Nessim, G. D., & Tischler, Y. R. (2023). Enhancement of the E12g and A1g Raman modes and layer identification of 2H-WS2 nanosheets with metal coatings. *Journal of Raman Spectroscopy*, *54*(9), 1030–1037. https://doi.org/10.1002/jrs.6585

Shin, Y., Kim, J., Jang, Y., Ko, E., Lee, N., Yoon, S., & Kim, M. H. (2020). Vertically-Oriented WS2 Nanosheets with a Few Layers and Its Raman Enhancements. *Nanomaterials*, *10*(9), 1847. https://doi.org/10.3390/nano10091847

Sim, H. J., Li, Z., Xiao, P., & Lu, H. (2022). The influence of lateral size and oxidation of graphene oxide on its chemical reduction and electrical conductivity of reduced graphene oxide. *Molecules*, *27*(22), 7840. https://doi.org/10.3390/molecules27227840

Singhal, M., Agrawal, M., Bhavna, K., Sethiya, N. K., Bhargava, S., Gondkar, K. S., ... & Arora, M. K. (2023). Chloramphenicol and tetracycline (broad spectrum antibiotics). In *Antibiotics-Therapeutic Spectrum and Limitations* (pp. 155-165). Academic Press. https://doi.org/10.1016/B978-0-323-95388-7.00019-X

Song, C., Li, X., Wang, L., & Shi, W. (2016). Fabrication, Characterization and Response Surface Method (RSM) Optimization for Tetracycline Photodegration by Bi3.84W0.16O6.24- graphene oxide (BWO-GO). *Scientific Reports*, *6*(1). https://doi.org/10.1038/srep37466

Tarannum, S., Hossain, M. S., Bashar, M. S., Bahadur, N. M., & Ahmed, S. (2024). Amplification of photocatalytic degradation of antibiotics (amoxicillin, ciprofloxacin) by sodium doping in nano-crystallite hydroxyapatite. *RSC Advances*, *14*(18), 12386–12396. https://doi.org/10.1039/d4ra00126e

Terreni, M., Taccani, M., & Pregnolato, M. (2021). New antibiotics for multidrug-resistant bacterial strains: latest research developments and future perspectives. *Molecules*, *26*(9), 2671. https://doi.org/10.3390/molecules26092671

Tian, C., Huang, W., Wei, Z., Liang, C., Dong, Y., Shi, J., Zhang, X., Nong, G., Wang, S., & Xu, J. (2023). Photocatalytic degradation of different antibiotics using TiO2–carbon composites: a case study of tetracycline and ciprofloxacin. *New Journal of Chemistry*, *47*(42), 19646–19656. https://doi.org/10.1039/d3nj02748a

Wang, Y., Xiu, J., Gan, T., Zou, H., & Li, F. (2023). Photocatalytic degradation of tetracycline hydrochloride by lanthanum doped TiO2@g-C3N4 activated persulfate under visible light irradiation. *RSC Advances*, *13*(12), 8383–8393. https://doi.org/10.1039/d3ra00729d

Yadav, S., Raman, A. P. S., Meena, H., Goswami, A. G., Bhawna, N., Kumar, V., Jain, P., Kumar, G., Sagar, M., Rana, D. K., Bahadur, I., & Singh, P. (2022). An update on Graphene Oxide: Applications and toxicity. *ACS Omega*, *7*(40), 35387–35445. https://doi.org/10.1021/acsomega.2c03171

Yousef, A., Thiehmed, Z., Shakoor, R. A., & Altahtamouni, T. (2022). Recent progress in WS2-Based nanomaterials employed for photocatalytic water treatment. *Catalysts*, *12*(10), 1138. https://doi.org/10.3390/catal12101138

Yu, M., Lin, Y., Wu, C., Wang, T., Cyue, J., Kikkawa, J., Ishii, S., Lu, T., & Chen, K. (2023). Role of defects in the photoluminescence and photoresponse of WS2–

graphene heterodevices. *Applied Surface Science*, *642*, 158541. https://doi.org/10.1016/j.apsusc.2023.158541

Zhang, L., Sun, L., Liu, S., Huang, Y., Xu, K., & Ma, F. (2016). Effective charge separation and enhanced photocatalytic activity by the heterointerface in MoS2/reduced graphene oxide composites. *RSC Advances*, *6*(65), 60318–60326. https://doi.org/10.1039/c6ra10923c

Zhang, S., Wang, H., Liu, J., & Bao, C. (2019). Measuring the specific surface area of monolayer graphene oxide in water. *Materials Letters*, *261*, 127098. https://doi.org/10.1016/j.matlet.2019.127098

Zulfiqar, N., Nadeem, R., & Musaimi, O. A. (2024). Photocatalytic Degradation of Antibiotics via Exploitation of a Magnetic Nanocomposite: A Green Nanotechnology Approach toward Drug-Contaminated Wastewater Reclamation. *ACS Omega*. https://doi.org/10.1021/acsomega.3c08116

AUTHOR'S PROFILE

The author, Zulhatiqah Zolekafeli, was born on 16th February 1996 in Seremban, Negeri Sembilan. She earned her Bachelor of Science (Hons.) in Chemistry with Management from Universiti Teknologi Mara (UiTM) Negeri Sembilan Kampus Kuala Pilah in 2023. Her undergraduate research focused on bibliometric analysis in sensor technology, culminating in a final year project titled *"Bibliometric Analysis on Conducting Polymer Sensors for Ammonia Gas Detection Using Scopus Database,"* which was subsequently published in the *Vietnam Journal of Chemistry*. Driven by a growing interest in environmental remediation and advanced nanomaterials, she pursued her Master of Science in Chemistry at from Universiti Teknologi Mara (UiTM) Negeri Sembilan Kampus Kuala Pilah, with a research focus on the synthesis and application of tungsten disulfide–graphene oxide (WS_2/GO) nanocomposites for photocatalytic degradation of pharmaceutical contaminants. Her master's thesis explored the material's efficiency in degrading tetracycline antibiotics under visible LED light, utilizing multiple characterization techniques such as FTIR, UV-Vis spectroscopy, XRD, BET, and FESEM. During her postgraduate studies, she published a research article titled *"Removal of Tetracycline Using Tungsten Disulphide–Graphene Oxide as Photocatalyst: Effect of Light Irradiation and Kinetic Studies"* in the *Bulletin of Chemical Reaction Engineering & Catalysis (BCREC)*. Through her academic and research journey, she has demonstrated a strong commitment to advancing sustainable environmental technologies and aspires to further her career through doctoral research in materials chemistry, particularly in the field of photocatalysis and environmental nanotechnology.

LIST OF PUBLICATION

Baharin, S. N. A., Zain, Z. M., Zolekafeli, Z., Mehmood, S., & Sambasevam, K. P. (2024). Bibliometric analysis on conducting polymer sensors for ammonia gas detection using Scopus database. *Vietnam Journal of Chemistry*, *62*(3), 399–411. https://doi.org/10.1002/vjch.202200122

Zolekafeli, Z., Sateria, S. F., Mohamed, A. H., Alias, S. H., Sambasevam, K. P., & Baharin, S. N. A. (2024). Removal of tetracycline using tungsten Disulfide/Graphene oxide as photocatalyst: Effect of light irradiation and Kinetic studies. *BULLETIN OF CHEMICAL REACTION ENGINEERING AND CATALYSIS*, *19*(3), 512–520. https://doi.org/10.9767/bcrec.20204

Zolekafeli, Z., Sambasevam, K. P., Nor, S., & Baharin, A. (2023). PHOTOCATALYTIC PERFORMANCE OF MOLYBDENUM DISULPHIDE-GRAPHENE OXIDE IN PERFLUOROOCTANOIC ACID (PFOA) DEGRADATION UNDER INDOOR LIGHT EMITTING DIODE (LED) IRRADIATION (Prestasi Fotokatalitik Molibdenum Disulfida-Grafena Oksida dalam Degradasi Asid Perfluorooktanoik (PFOA) di bawah Penyinaran Diod Pemancar Cahaya Dalaman (LED)). In *Malaysian Journal of Analytical Sciences* (Vol. 27).